Investigations on Raw Material Samples of European Deposits for the Application in Plastics

Diplomarbeit

von

Tassilo Adelsmayr

Angefertigt am Lehrstuhl für Aufbereitung und Veredelung,
eingereicht am Lehrstuhl für Geologie und Lagerstättenlehre
an der Montanuniversität Leoben

Leoben, im April 2014

EIDESSTATTLICHE ERKLÄRUNG

Ich erkläre an Eides statt, dass ich diese Arbeit selbstständig verfasst, andere als die angegebenen Quellen und Hilfsmittel nicht benutzt und mich auch sonst keiner unerlaubten Hilfsmittel bedient habe.

AFFIDAVIT

I declare in lieu of oath, that I wrote this thesis and performed the associated research myself, using only literature cited in this volume.

03/04/2014

Datum

Unterschrift

Danksagung

Mein Dank gilt allen, die mich bei der Erstellung dieser Diplomarbeit unterstützt haben. Allen voran bedanke ich mich bei Dipl.-Ing. Elke Krischey, Ao.Univ.-Prof. Dr.phil. Walter Prochaska und Univ.-Prof. Dipl.-Ing. Dr.mont. Helmut Flachberger für die gute Betreuung und die interessanten Diskussionen. Weiters danke ich Dr. Martin Huber, Dr. Alexander Schmiderer und Dr. Karl-Heinz Ohrdorf für die gute Zusammenarbeit.

Besonders möchte ich mich auch bei meinen Studienkolleginnen und Kollegen bedanken, die mir stets mit Rat und Tat zur Seite standen. Danke für die schöne Zeit.

An dieser Stelle sei auch Dank meinen Eltern und meinem Bruder ausgesprochen, die mir dieses Studium ermöglicht und mich immer unterstützt haben.

Gewidmet meiner Mutter Antonia

Abstract

Three industrial materials: bentonite, barite and pyrophyllite were investigated regarding their suitability as fillers in plastic compounds.

Two Bulgarian calcium **bentonites** had to be transformed ("alkali-activated") into sodium bentonites. The montmorillonite content, the "Swelling Index", as well as an X-Ray diffraction analysis (XRD) were chosen as suitability indicators. The montmorillonite content was 55 - 58 %, the swelling index was 21 ml / 2g and additional minerals such as albite occurred in large quantities (25 %). The low montmorillonite content in connection with the low Swelling Index indicates that the two bentonites are not suitable as active filler for plastics. For possible further applications, e.g. drilling bentonite, rheological properties were tested, resulting in a viscometer dial reading at 600 rpm R_{600} = 11 and a plastic viscosity ratio b = 2.4.

The Bosnian **barite** was characterized by mineralogical aspects and processed by optical, gravity, magnetic and electrostatic separation methods. The raw material was medium grained and intergrown with quartz and tetrahedrite. The brightness varied between 96 % and 73 %. $SrSO_4$ contents differed between the samples in the range of 0.7 – 17 %. The manual optical sorting resulted in a barite recovery of 87 %. The sink-float analysis in three particle size ranges < 1 mm showed a degree of liberation of > 99 % for barite. The shaking table test resulted in a barite grade of 98 % with a recovery of 81 %. The suitability as a filler in plastics may apply.

Two Bosnian **pyrophyllites** were mineralogically investigated and processed by attrition and flotation. The mineral processing products were characterized by acid solubility, loss on ignition (LOI), brightness measurements and XRD. As accessory minerals quartz and carbonates occurred. Heavy minerals were apatite and zircon. The least amount of acid-soluble minerals (1.29 %) and the least LOI (3.95 %) were reached by flotation. The brightness of the raw material (81 % and 72 %) could not be increased. The suitability as a filler in plastics is not given regarding these particular results, due to the high quantity of additional minerals.

Zusammenfassung

Drei Industrieminerale: Bentonit, Baryt und Pyrophyllit wurden hinsichtlich ihrer Eignung als Füllstoff in Kunststoffen geprüft.

Zwei bulgarische Kalzium-**Bentonite** wurden (alkalisch) zu Natrium-Bentonit aktiviert. Als Indikatoren für deren Eignung in Kunststoffen wurden der Montmorillonitgehalt, das Quellvolumen sowie die Ergebnisse der Röntgendiffraktometrie gewählt. Der Montmorillonitgehalt ergab 55 – 58 %, das Quellvolumen lag bei 21 ml/2g. Begleitminerale wie zum Beispiel Albit traten in großen Mengen (25 %) auf. Der niedrige Montmorillonitgehalt, verbunden mit dem geringen Quellvolumen ließ darauf schließen, dass die Bentonitproben nicht als Füllstoff für Kunststoffe geeignet sind. Um die Verwendbarkeit für andere Anwendungen, zum Beispiel Bohrbentonit, zu prüfen, wurden die rheologischen Eigenschaften getestet. Der Viscometer Skalenwert ergab R_{600} = 11 bei 600 min^{-1} und das Verhältnis der plastischen Viskosität b = 2,4.

Die **Barytproben** aus Bosnien Herzegowina wurde mineralogisch charakterisiert und mittels optischer, gravimetrischer, magnetischer und elektrischer Sortiermethoden aufbereitet. Die Kristalle des Rohgutes waren mittelkörnig und mit Quarz und Tetraedrit verwachsen. Die Weiße lag zwischen 96 % und 73 %. Der Gehalt an $SrSO_4$ variierte zwischen 0.7 – 17 %. Mit der optischen Trennung durch Handklaubung wurde ein Konzentrat aus unverwachsenen $BaSO_4$-Körnern mit einem Inhaltsausbringen von 87 % erreicht. Auch die Schwimm-Sink Analysen in den Korngrößenklassen 0,71/1 mm, 05/0,71 mm und 0,315/0,5 mm ergaben Aufschlussgrade von > 99 %. So konnten mittels Herdarbeit $BaSO_4$-Gehalte von 98 % bei einem Inhaltsausbringen von 81 % erreicht werden. Die Eignung als Füllstoff könnte gegeben sein.

Zwei **Pyrophyllit** Proben aus Bosnien Herzegowina wurden mineralogisch untersucht und durch Attrition und Flotation aufbereitet. Die Charakterisierung der Aufbereitungsprodukte erfolgte mittels Säurelöslichkeit, Glühverlust, Weißemessung und Röntgendiffraktometrie. Als Begleitminerale traten Quarz und Karbonate auf. Akzessorische Schwerminerale waren Apatit und Zirkon. Die geringste Säurelöslichkeit (1.29 m%) und der geringste Glühverlust (3.95 m%) wurde mit Konzentraten aus der Flotation erzielt. Die Weiße des Rohgutes (81 – 72 %) konnte nicht erhöht werden. Die Eignung als Füllstoffe in Kunststoff konnte anhand der Resultate dieser Tests und aufgrund der großen Menge (ca. 50 %) an Begleitmineralen nicht bestätigt werden.

Table of Content

1. Assignment of Tasks

New applications for plastics increase the demand for certain raw materials suitable as fillers. Innovative solutions in exploration, mining and processing contribute to provide supply of high quality materials within strict material regulations for best performance products.

In regards of these aspects, this master thesis in hand deals with the raw material characterization and processability of three different industrial minerals with an outlook on their suitability as fillers in plastics.
Multiple samples of **bentonite**, **barite** and **pyrophyllite** were examined. Each sample was separately characterized concerning its mineralogical aspects and also tested regarding mineral processing possibilities. Comparing these results to commonly used raw material requirements provided information about the suitability of the samples as fillers in plastics. All samples were provided by partners of the FFG COIN project "Mineralien für die Kunststoffindustrie – Min4k" (engl.: innovative functional minerals for the plastics industry). "Min4k" was a cooperation of national and international partners from industry and universities for investigations on raw materials from potential European deposits as fillers for the plastic industry.
Project members were:

- Montanuniversität Leoben
- maGeo e.U. – Martin Huber, Ingenieurbüro für Montangeologie + Geothermie
- Advanced Polymer Compounds
- Grafitbergbau Kaisersberg
- Paltentaler Minerals GmbH & Co KG
- Polyconcent
- Uralian Branch of Russian Academy of Sciences, Yekaterinburg
- University of Belgrade
- Geological Institute, Bulgarien Academy of Science
- Gravelita nLtd.
- Celsian Ltd.
- Milicevic d.o.o**.**

2. Bentonite

2.1 Overview

Bentonites are rocks consisting mainly smectite minerals like montmorillonite, beidellite, and nontronite (60–90 %). Accessory minerals vary from deposit to deposit and may be quartz and its modifications (tridymite, cristobalite), feldspar, mica, volcanic glass and colloidal silica (Opal-CT) [POHL 2005A]. Calcite, gypsum and pyrite are the main accessory minerals in Milos bentonites, illite and kaolinite in significant amounts are found in Bavarian bentonites. [OHRDORF 2010A].

Bentonite, as an unconsolidated sedimentary rock, has been considered to consist of characteristic particles below 2 µm [LAGALY AND KÖSTER 1993]. But recent ESEM and TEM pictures of Milos, Bavarian and Sardinian bentonites – the most important European mining regions for bentonites – have provided a different aspect. The montmorillonite lamellas, especially such suitable for the application in plastics, are exceeding the length of 1 - 2 µm [OHRDORF 2010B]

Only montmorillonite is of industrial importance [OHRDORF 2010C]. There is no international agreement on which content of montmorillonite qualifies a mineral as a bentonite. In industry even bentonites of only 40 m% of montmorillonite are processed and sold.

2.1.1 Genesis of Deposits

Nearly all unconsolidated clays are formations dating from the Neogene and Quaternary. [LAGALY AND KÖSTER 1993].

Smectites can be formed: [POHL 2005A]

- as an alteration product of volcanic tuff in alkaline milieu
- in volcanic areas by hydrothermal, alkaline alteration of rocks
- by autochthone weathering of basic tuffs, basalts and ultramafic rocks resulting in smectite soils
- as marine or playa lake clay sediment

Bulgarian bentonites are found in Lower Tertiary sequences of calcareous sediments, tuffs and volcanic tuffs and rhyolitic to andesitic lavas. They have formed by devitrification of volcanic glass accompanied by hydrothermal action. Montmorillonite of these bentonites has developed from acidic tuffs. [GRIM AND GÜVEN 1978].

2.1.2 Mineralogy

Smectites are swellable 2:1 clay minerals. Smectite-minerals comprise montmorillonite, beidellite and nontronite as dioctahedral and saponite as well as hectorite as trioctahedral representatives. Most of the smectite minerals are monoclinic. [KÖSTER 1993]. The classification of montmorillonite, as according to STRUNZ [RAMDOHR AND STRUNZ 1987] is: 9.EC.40.

9: Silicates

E: Phyllosilicates

C: Phyllosilicates with mica sheets, composed of tetrahedral and octahedral nets

40: Montmorillonite (dioctahedral)

2.1.3 Structure

Siliceous clay minerals are built of $[SiO_4]$-tetrahedrons and $[M(O,OH)_6]$-octahedrons (M… metal ion). The tetrahedrons are connected by shared oxygen ions to tetrahedral sheets, in such a way, that the free apexes of the tetrahedrons point in the same direction. In the plain, the tetrahedrons form a network of hexagonal rings. This tetrahedral sheet is condensed to an octahedral sheet, which shares oxygen ions with the tetrahedral apexes. All oxygen ions of the octahedrons, which are not shared with the tetrahedrons, bind a proton, so they form hydroxyl ions (OH^-) in the structure. The layers, consisting of a tetrahedral sheet and an octahedral sheet, form the double layer clay minerals (1:1 layer silicates) of the kaolin- and serpentine minerals. Three layer minerals (2:1 layer silicates) result in the condensation of a second tetrahedral sheet on the octahedral sheet, with the apexes opposite to the apexes of the first tetrahedral sheet. [LAGALY AND KÖSTER 1993].

2.1.4. Morphology

Three main forms of smectite can be distinguished: [MURRAY 1986]

1. Smectite lamellas with rhombic outline and elongated hexagonal films.
2. Thin crystals with irregular contour and a thickness of < 200 nm.

3. Strip-like or ribbon-like crystals of beidellites and nontronites.

Montmorillonites form thin crystals, which appear like slides with irregularly bordered, bent, folded and with rolled up rims. The rims of the “crystals” are not exactly defined; they rather seem frayed by sheets of different length. [LAGALY AND KÖSTER 1993]. Montmorillonite consists of packages of up to 100 primary lamellas with a thickness of 1 nm [KERNER ET AL. 2005].

2.1.5 Swelling Behavior

The reason for the widespread industrial application and the most obvious feature of bentonite is the intercrystalline swelling behavior [OHRDORF 2010D].

In the octahedron of montmorillonite the Al^{3+} is partly substituted by Mg^{2+}. The substitution results in a negative load of the layers, compensated by counter ions, mostly Ca^{2+}, Mg^{2+} and Na^{+} to make the crystal electrostatically neutral [POHL 2005A]. The intercalation of water molecules hydrates the counter-ions causing an expansion of the sheet distances from originally around 10 nm. This process can double the volume of montmorillonite. [MÜLLER-VONMOOS AND KÖHLER 1993].

Bentonites in deposits with Na^{+} as counter ions are called “natural sodium bentonites” or “swelling type” and such with Ca^{2+}, Mg^{2+} as counter ions “calcium bentonites” or “non-swelling type”.

The more Na^{+} available as counter ions the better the hydration and the better the exfoliation of the platelets, measured by the Swelling Index. The better the exfoliation the higher the aspect ratio due to the thinner packages of platelets, in the ideal case single platelets only. For this reason the Swelling Index is determined as a qualitative hint in regards of the aspect ratio.

For this purpose, the Bulgarian calcium bentonites had to be alkali-activated to sodium bentonites with Na_2CO_3.

2.2 Analysis of Raw Material

Two Bulgarian bentonites of the Ralitsa (Fig. 1) and Zelenika (Fig. 1) deposit were analyzed by the following methods.

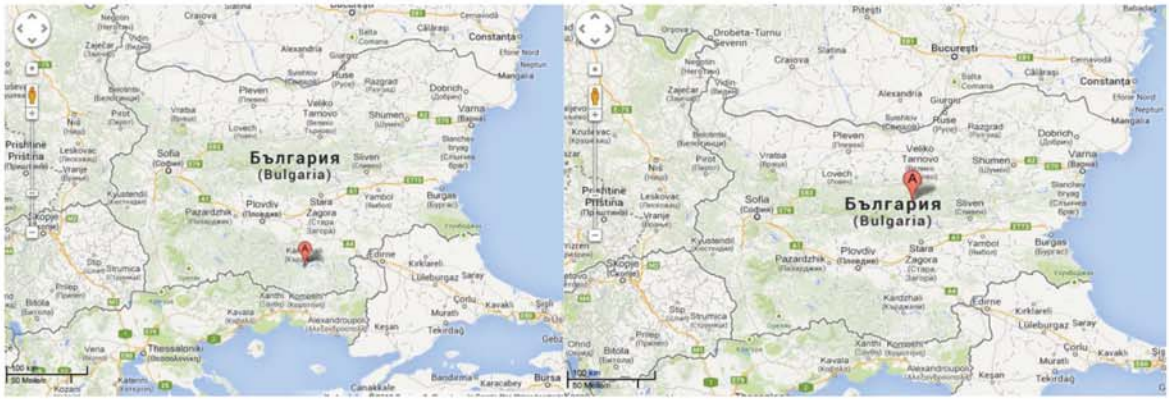

Fig. 1: Locations Ralitsa (left) and Zelenika (right), source: google maps

There was no further information about the samples (Fig. 2).

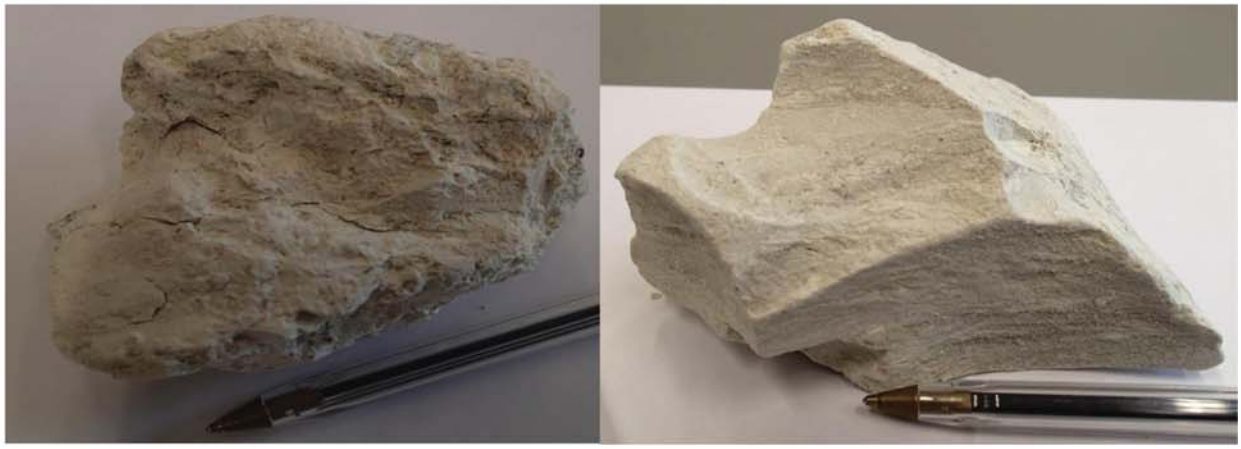

Fig. 2: Bentonites from Zelenika (left) and Ralitsa (right)

2.2.1 X-Ray Diffractometry

The samples were investigated by the Institute for Mineralogy and Crystallography, Bulgarian Academy of Sciences. For the semi-quantitative analysis, the Rietveld-method was used.

2.2.2 Moisture Content of Received Samples

The analysis in principle followed the test procedure I.B.O. 01 / 2003: Determination of the Moisture Content by oven drying.

Process of analysis:
Weight in 20 g ± 0,0001 g of grinded Bentonite using a glass scale pan, drying at 150^{o} C until constant weight, cooling down at room temperature in an desiccator and weigh out the dried sample together with the scale pan.

Calculation:

$$\text{Moisture Content [m\%]} = \frac{\text{(Weigh-in) - (Weigh-out)}}{\text{(Weigh-in)}} \times 100$$

2.2.3 Methylene-blue Adsorption with a Derived Montmorillonite Content as Commonly Applied in Industry

The absorption was determined according to the *VDG - Merkblatt P69, Oktober 1999*. The corresponding montmorillonite content to the absorbed Methylene-blue solution (0,5 m% Methylene-blue) can be read out of the diagram below (Fig.3). The table was kindly provided *by "I.B.O. Ingenieurbüro für Bentonit-Technologie Dipl.-Ing. Ohrdorf"* and is a common conversion tool in industry, although it may vary from producer to producer of alkali-activated bentonites.

Process of analysis:
Preparation of a 0,5 % Methylene-blue solution, a saturated Tetra-Sodiumphosphate solution and a 0,5 mol/l 1 N sulfuric acid. Using a bentonite sample with a moisture content ≥ 6 m% (determine moisture content according to I.B.O. 01 / 2003). Grinding the bentonite sample three times passing through a 0,25 mm sieve. Mixing of 500 mg ±1 mg standard-bentonite, 500 mg ±1 mg of the bentonite sample and the Tetra-Sodiumphosphate solution with sulfidic acid. Adding of about 80 m% of the expected consumption of the Methylene-blue solution. Placing single drops of the suspension on filter paper. Adding Methylene-blue solution, until the blue ring on the filter paper forms a light blue halo. Determining the Methylene-blue absorption capacity of a given bentonite sample.

Calculation of the Methylene-blue absorption capacity:

A = Consumption of the calibrated Methylene-blue solution for the bentonite sample (ml)

B = Quantity of the bentonite sample (g)

C = Moisture content of the bentonite sample (m%)

F = Titre of the Methylene-blue solution (mg/ml)

G = Methylene-blue absorption capacity of the bentonite sample (mg/g)

$$G = \frac{A * F}{B - \frac{B * C}{100}} \quad (mg/g)$$

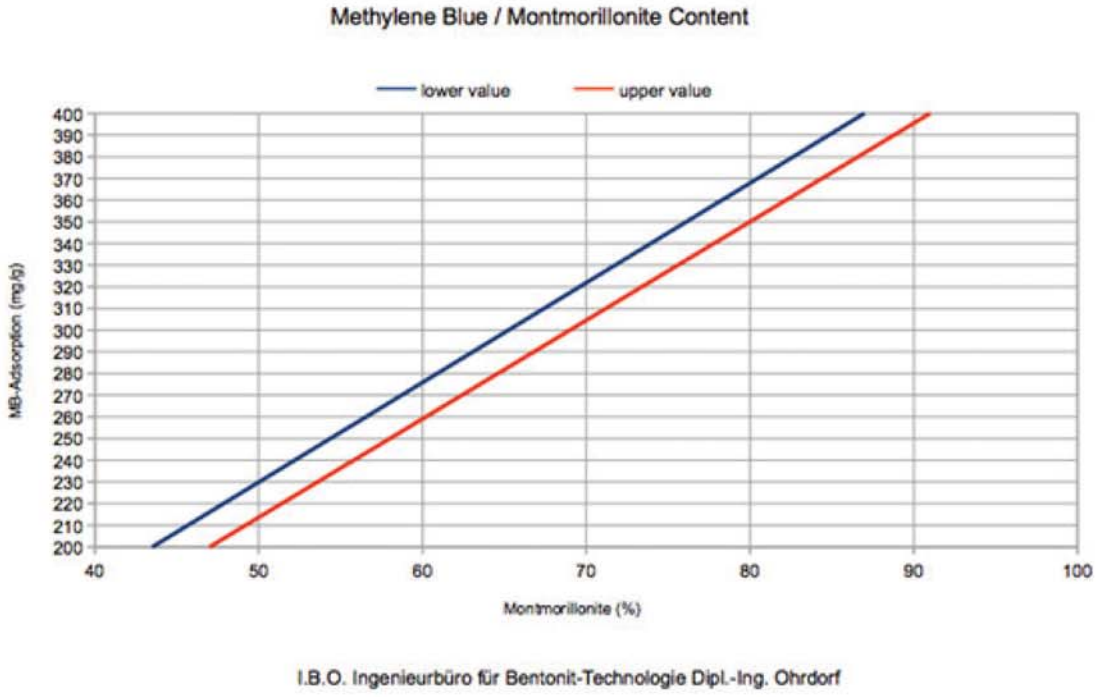

Fig. 3: Methylene-blue Absorption vs. Montmorillonite Content

2.3 Processing and Product Testing

2.3.1 Alkali activation

The two samples were alkali-activated by “I.B.O Ingenieurbüro für Bentonit-Technologie Dipl.-Ing. Ohrdorf, Wiesbaden, Deutschland”.

According to the determined Methylene-blue absorption and based on dry substance the necessary amount of sodium carbonate (Na_2CO_3) was added and mixed with the raw bentonites. The activation technology followed a common, but not standardized laboratory method in industry, the “extrusion method”. The samples were non air-proof packaged, so the air-dried bentonite had to be re-hydrated to an assumed natural moisture content of

29 m% as most of the bentonite deposits are mined at a natural moisture content of 30 ±3 m%. The lower than average moisture value had been chosen, because of the lower montmorillonite content and, even more importantantly, to adjust the bentonite to a sufficient plasticity for the extrusion.

2.3.2 Drying, Grinding, Sieving

The activated bentonite was dried at 150 °C resulting in an adequate-to-industry product temperature of 85 °C and a moisture content of 8 ±1 m%. After drying the samples were grinded, using a “Retsch SR 300” impact rotor mill (Fig. 4 left). The moisture content of the powder was measured (according to I.B.O. 01 / 2003). The dry sieve residue was determined using an “Alpine Augsburg” jet sieve (Fig. 4 right).

Process of analysis:

20 g of the grinded material were sieved for 5 min through a 0.063mm sieve.

Calculation:

$$\text{Sieve residue [m\%]} = \frac{\text{(Weight in)}}{\text{(Weight out)}} * 100\%$$

Fig. 4: Retsch Impact Rotor Mill (left); Alpine Jet Sieve (right)

2.3.3 Swelling Index

The Swelling Index is an industrial standard and the analysis method is following the I.B.O. FP-03/2003:

Process of analysis:

Determination of the moisture content according to I.B.O. 01 / 2003, weighting in 2,000 g ±1mg of the grinded bentonite calculated on a moisture content of 10 m%. Filling a 100 ml graduated measuring cylinder with 100 ml distilled water and dropping small portions of the bentonite into the measuring cylinder by using a small spatula. Waiting until the bentonite portion has sunk down before dropping the next portion.

Calculation:

The bentonite volume = “Swelling Index” (ml/2g) was reached immediately after the termination of the procedure.

The graduated cylinder was 27 mm in diameter and 170 mm in height. The temperature of the distillated water was 23,5 °C.

2.3.4 Viscosity

The rheological properties were investigated in an additional analysis. The task was to check the suitability of the bentonites as optimal viscosity drilling fluids for the drilling industry, since that is a huge market. The activated samples were tested following the *“API Specification 13 A, seventeenth edition, Nov.-2006, chapter 11: OCMA grade bentonite“.*

Process of analysis:
22,5 g ± 0,01g of bentonite calculated on a moisture content of 10 m% were added to 350 ml of distilled water, stirred 20 minutes at a speed of 11.000± 300 rpm using a Hamilton Beach mixer cup M 110D and a single sine-wave impeller of 25 mm diameter. The suspension was aged for 16 hours and stirred again for 5 minutes. The viscosity was measured with a motor-driven direct-indicating FANN 35 SA viscometer (Fig.5) at 600 rpm and 300 rpm.

Calculation:

$\eta_P = R_{600} - R_{300}$ [mPa*s]

$\eta_Y = R_{300} - \eta_P$ [lb*ft^{-2}]

$b = \eta_P / \eta_Y$

It indicates:

R600	dial reading at 600 rpm
R300	dial reading at 300 rpm
η_P	plastic viscosity
η_Y	yield ponit

Fig. 5: Fann Viscometer

2.4 Results of Analysis

2.4.1 Overview of Analysis

The overview of the analysis is listed in Tab.1:

Tab. 1: Overview of Analysis

2.2.1	X-Ray Diffractometry
2.2.2	Moisture Content of the Received Sample
2.2.3	Methylene-blue Absorption with a derived montmorillonite content as commonly applied in industry
2.3.1	Alkali Activation
2.3.2	Drying, Grinding, Sieving
2.3.3	Swelling Index After Activation
2.3.4	Viscosity

2.4.2 Results

The results are listed in the following table (Tab. 2). Additional comments are below Tab. 2 (Chapter 2.4.3).

Tab. 2: Results of Analysis

Analysis \ Sample		Zelenika	Ralitsa
2.2.1	XRD	[1]	[1]
2.2.2	Moisture Content [m%] of Raw Bentonite, as Received	8.95	10.65
2.2.3	Methylene-blue Absorption [mg/g]	260 [2]	230 [2]
	Corresponding Montmorillonite Content [m%], approx.	58	55
	Montmorillonite content by XRD analysis [m%],approx.	58.6	53.4
2.3.1	Moisture Content at Activation [m%]	29	29
	Soda Calculated on Dry Bentonite [m%]	3.6	3.4
2.3.2	Moisture Content, Powder [m%]	7.6	6.9
	Dry Sieve Residue, Powder [m%]	2.15	2.15
2.3.3	Swelling Index [ml]	21[3]	[4]
2.3.4	Corrected Mass of Bentonite [g]	21.92	21.75
	Viscometer Dial Reading at 600 rpm R_{600}	11	[5]
	Viscometer Dial Reading at 300 rpm R_{300}	8.5	[5]
	Plastic Viscosity η_P	2.5	[5]
	Yield Point η_Y	6	[5]
	Yield Point/Plastic Viscosity Ratio b	2.4	[5]

2.4.3 Comments

The spectra are listed in the appendix (Fig. 66 and 67).

[1] X-Ray Results:

The sample Ralitsa consists of (Tab. 3, Fig. 6):

Tab. 3: XRD Ralitsa

53,4 %	Montmorillonite
25,1 %	Albite
11,6 %	Cristobalite
6,8 %	Quartz
3%	Mordenite

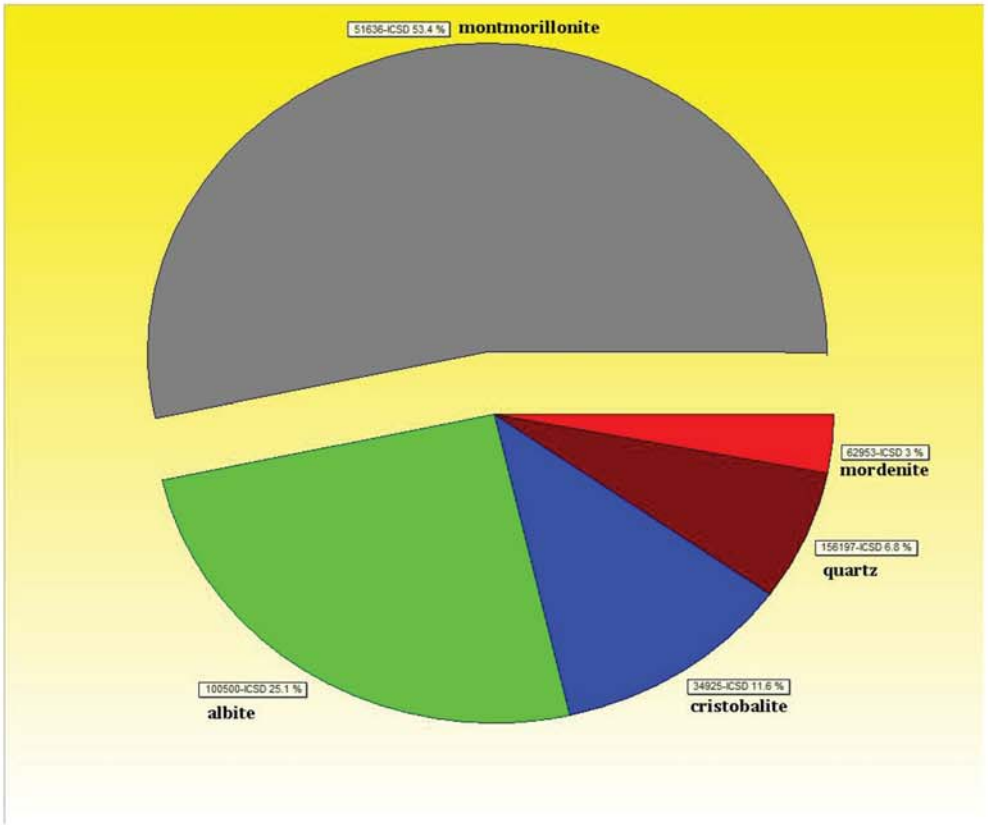

Fig. 6: Semiquantitative X-Ray Analysis of Sample Ralitsa

The sample Zelenika consists of (Tab. 4, Fig. 7):

Tab. 4: XRD Zelenika

58,6 %	Montmorillonite
25,5 %	Cristobalite
15,9 %	Heulandite

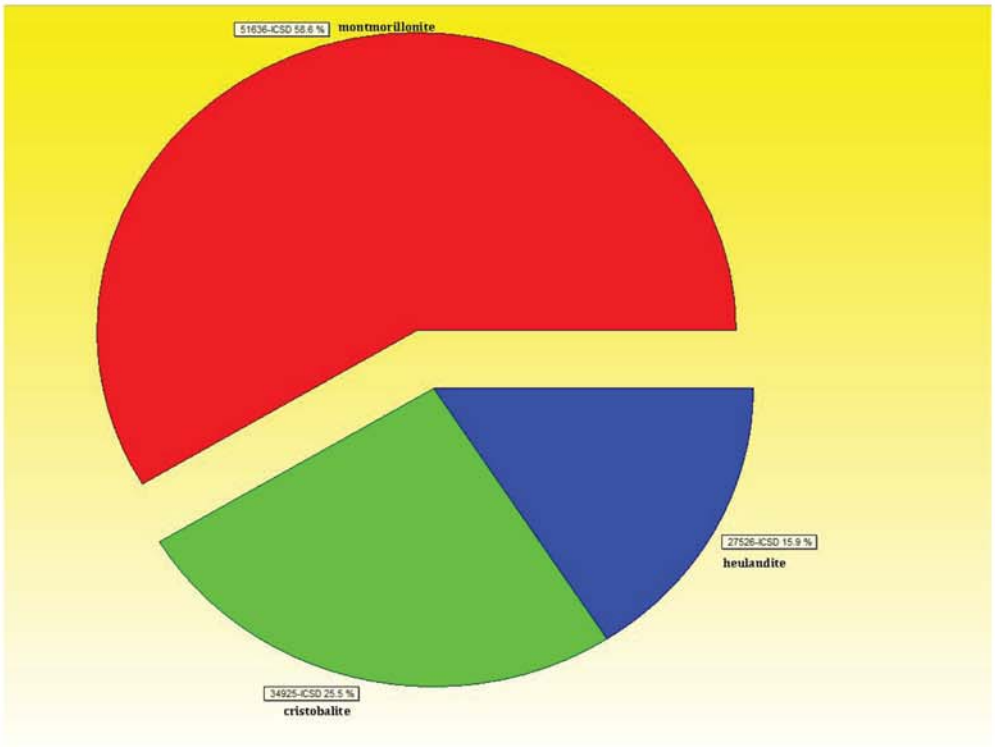

Fig. 7: Semiquantitative X-Ray Analysis of Sample Zelenika

The montmorillonite contents correlate with the ones of the Methylene-blue determination. The diffractograms are listed in the appendix.

[2] The filter paper of the Methylene-blue absorption for the samples "Zelenika" and "Ralitsa" (Fig. 8 and 9):

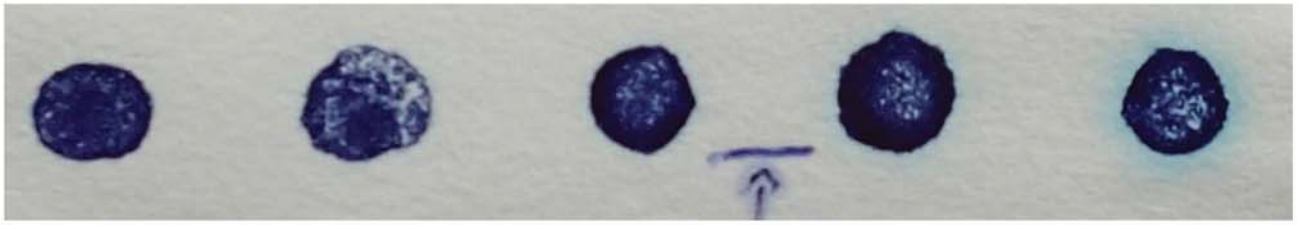

Fig. 8: Methylene-blue Absorption Filter Paper, Sample Zelenika (m = 0,4999 g, H20 = 8,95%, Arrow at 22,5 ml)

Fig. 9: MB Adsorption Filter Paper, Sample Ralitsa (m = 0,5002 g, H_20 = 10,65%, Arrow at 19,5 ml)

[3] The Swelling Index of the sample Zelenika of 21 ml (Fig. 10):

Fig. 10: Swelling Index, Sample Zelenika

[4] The swelling index of the sample "Ralitsa":

The Swelling Index of the sample "Ralitsa" could not be determined. The activated bentonite did not sink to the bottom.

[5] The bentonite-water suspension sedimented into a clarified water layer, a turbid water layer and a mineral solid layer. Consequently no rheological properties were determined.

2.5 Suitability Criteria for the Use as Active Filler in Plastics and Conclusions

2.5.1 Montmorillonite Content for the Use in Plastics

Compared with other industrial bentonites processed in plastics, e.g., “Nanofill” (an organophile modified natural sodium bentonite), a minimum of 90 m% montmorillonite content is required.

The main target of the application of montmorillonite in plastics is to benefit from the tensile strength of the lamellas and the possibility of an organophile modification. Any accessory mineral reduces the efficiency of the montmorillonite reinforcement in such compounds.

Conclusion:

With a montmorillonite content of significantly below 90 m%, both samples do not fulfill the above criteria.

2.5.2 Aspect-ratio

A high aspect-ratio is necessary because the platelets should behave like steel bars in reinforced concrete. Measured maximum values are 2300 nm in length and 1390 nm in width [OHRDORF 2010B] (Fig 11 left). One measured thickness of a platelet is 5,2 nm (Fig 11 right) [OHRDORF 2010B]. But it has to be mentioned that measurements with an Environmental Scanning Electron Microscope (ESEM) bear considerable difficulties. In accordance with the literature the true thickness of a single platelet is near 1-2 nm. The measured bentonite is from Milos, Greece, “Agheria” mine [OHRDORF 2010B]. The true aspect-ratio as a bench mark criteria for the application in plastics is yet unknown. Taking into consideration that the length of montmorillonite lamellas in a suitable deposit varies between approx. 800 and 2300 nm and the true diameter of a single platelet is approx. 1-2 nm, the desired aspect ratio should be > 500. The pictures were taken by the *“A.F. Finger Institut der Bauhausuniversität Weimar”* with an ESEM with a field emission gun (cathode), (FEG, Schottky Emitter) [OHRDORF 2010B].

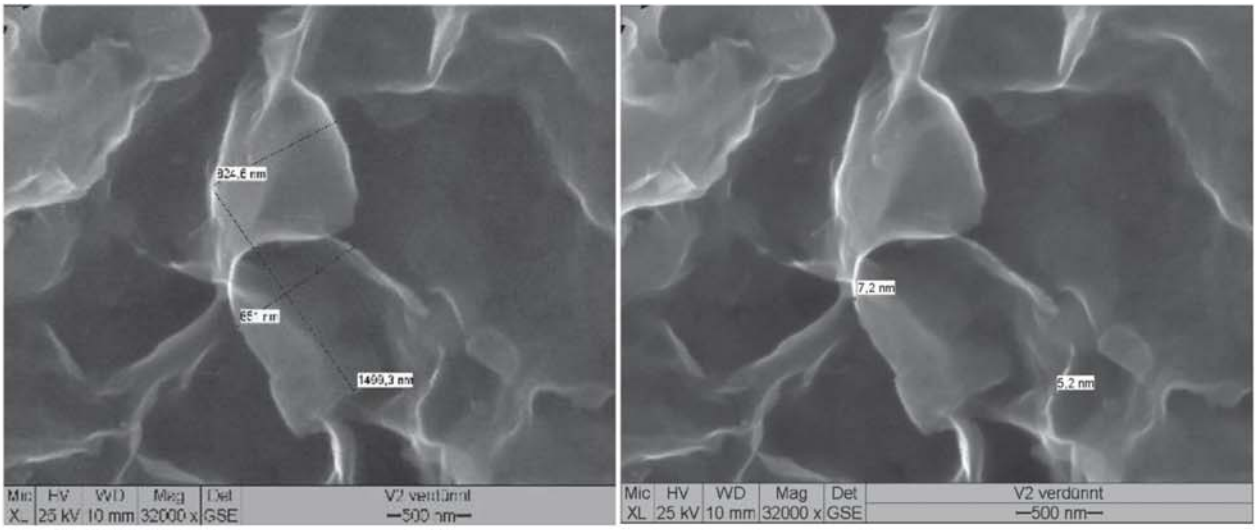

Fig. 11: ESEM Picture of an extreme big single platelet of 2300nm (left) and the thickness (5,2 nm) of the layer (right) [OHRDORF 2010C]

Conclusion:

Due to the low montmorillonite content no electron microscopy was carried out. Technically it is not possible to separate the accessory minerals like cristobalite or heulandite because of physical reasons. In the Bulgarian bentonite samples, e.g. heulandite occurs in quantities around 15 m%. The density of heulandite is 2,18 – 2,22 g/cm^3 and it forms tabular and often radial crystals. [SCHUMANN 2007A]. As the density of bentonite is 2 – 3 g/cm^3 [POHL 2005A] a separation is not feasible for technical and economic reasons.

2.5.3 Delamination of montmorillonite layer packages

The Transmission Electron Microscope (TEM) pictures (with kind permission from Hannelore MATTAUSCH, *Chair of Polymer Processing at Montanuniversität Leoben*), show lamella packages of 2-4 layers and more (Fig. 12) as well as single layers. The experiment was performed with a ZEISS LEO 912 Omega transmission electron microscope (Carl Zeiss Inc. Jena, Germany). The acceleration voltage was 120 kV and the samples were prepared with a Leica Ultracur UCT ultramicrotome (Leica Microsystems Ltd. Wetzlar, Germany) equipped with a cryo chamber. The thin section of about 20 nm was cut using a Diatome diamond knife at -90 °C. [MATTAUSCH].

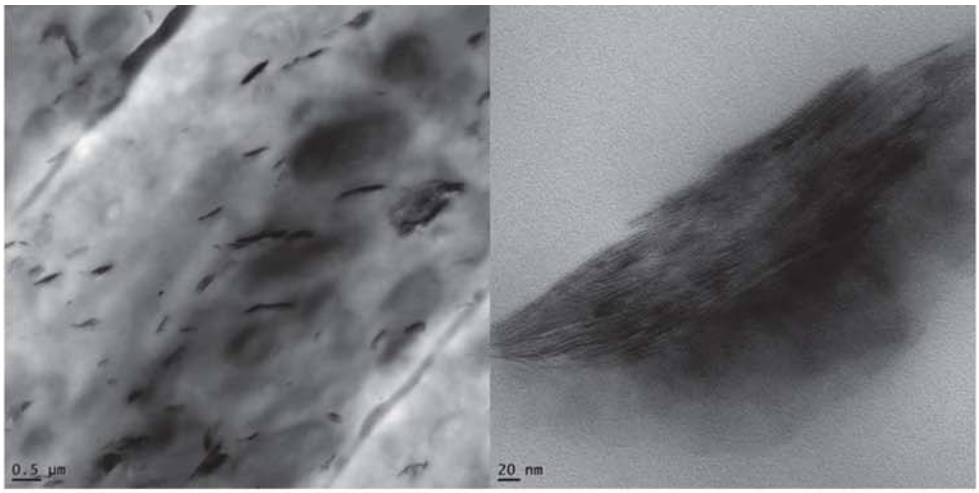

Fig. 12: ESEM Picture of Montmorillonite Platelets in Polymers [MATTAUSCH]

Conclusion:

As the suitability criteria for the montmorillonite content was not fulfilled, no ESEM or TEM pictures were taken.

2.6 Suitability for other Applications

2.6.1 Swelling Index

According to OHRDORF (I.B.O. Ingenieurbüro für Bentonit-Technologie Dipl.-Ing. Ohrdorf, Wiesbaden, Deutschland), common industrial benchmarks are (Tab. 5):

Tab. 5: Industrial Benchmarks of Swelling Index

20 - 28 ml / 2g	European industrial standard
>30 ml / 2g	very good
>40 ml / 2g	excellent

For comparison: The swelling index of an optimally activated Bentonite of Milos, Greek, reaches 56 ml / 2g [OHRDORF 2010E].

Conclusion:

The swelling index of the sample "Zelenika" is 21 ml / 2g. This value is at the lower end of European industrial standards (20 – 28 ml / 2g). The sample "Ralitsa" did not show any swelling.

2.6.2 Viscosity

The sample “Zelenika” was further investigated for an application as drilling bentonite.

The rheological requirements are:

Tab. 6: OCMA Physical Specifications

Viscometer Dial Reading at 600 rpm R_{600}	minimum 30
Yield Point/Plastic Viscosity Ratio b	maximum 6

To compare, optimal-activated bentonites from Milos, Greece reach 82 scale values for 600 rpm and 76 scale values for 300 rpm [OHRDORF 2010F]. A scale value for 300 rpm is not defined in the OCMA Specification.

Conclusion:

The sample “Zelenika” did not fulfill the OCMA (Oil Companies Material Association) Specification requirements with R_{600} = 11 and b = 2,4.

The viscosity of the sample “Ralitsa” could not be measured, because the suspension sedimented, resulting in a clarified water layer, a turbid water layer and a solid mineral layer at the bottom.

3. Barite

3.1 Raw Material Characterization

3.1.1 General

3.1.1.1 Mineralogy, Petrology, Chemistry

Barite, $BaSO_4$, crystallizes rhombohedral-dipyrimidal. The density of pure barite is 4.48 g/cm^3 and the MOHS-Hardness is 2.5 – 3.5. The color is translucent, in most cases cloudy-white. Barite is widely inert. [LORENZ AND GWOSDZ, 1998A]. Sr can replace Ba in the crystal lattice up to 5 m%. Also Pb and Ca can substitute Ba. [POHL, 2005B].

Witherite, $BaCO_3$, crystallizes dipyrimidal-orthorhombic. The density of witherite is 4.2 g/cm^3 and the MOHS-Hardness is 3.5. The color is translucent to yellowish. Witherite is easily soluble in acids.
The economically most important barium mineral is barite. The ideal chemical compositions of barite and witherite are (Tab. 7):

Tab. 7: Ideal Composition of Barite and Witherite

	BaO	**SO_3**	**CO_2**
Barite, $BaSO_4$	65.7 m%	34.3 m%	
Witherite, $BaCO_3$	77.7 m%		22.3 m%

Sanbornit ($BaSi_2O_5$), with BaO grades at around and above 50 m% in the future may become important as raw material for barium chemicals. [LORENZ AND GWOSDZ, 1998A].

Barium is a lithophile alkaline earth element, geochemically similar to Ca. It is an incompatible LIL-element which replaces K^+ in many rock forming minerals, with Ba^{2+} grades up to several percent. Due to this, MOR-Basalts have Ba^{2+} grades of ca. 92 ppm, whereas magmatic rocks with higher SiO_2 grades and clastic sediments have Ba^{2+} grades up to 800 ppm. Consequently the continental crust has a huge potential

for Ba^{2+} mobilization in hydrothermal replacement deposits. In vein deposits of hydrothermal systems, barite is transported as $BaCl_{(aq)}$ in acidic, reducing fluids. Witherite precipitates in alkaline milieus. [POHL 2005B].

3.1.1.2 Genesis of Deposits

Barite origins predominately from hydrothermal systems, where reduced Ba is oxidized by SO_4^{2-}. The types of deposits are listed in order of economic importance [CLARK ET AL, 1990]:

- **Submarine, hydrothermal-exhalative:** The barite reserves are large. Barite occurs as gangue or wall rock of sulfide layers of the Kuroko- or Sedex-type. If chemically differentiated, barite accompanies galenite or is formed immediately thereafter.
- **Epigenetic, hydrothermal barite veins, karst fillings and metasomatic bodies in carbonates:** Correspond largely with Mississippi Valley Type Pb-Zn deposits.
- **Hydrothermal barite veins in non-carbonates**
- **Terrestric, hydrothermal-sedimentary:** This kind of barite deposit can be described as “sinter” deposits.
- **Karst-barite**
- **Stratiform barite layers in evaporation sediments:** This formation occurred during Liassic transgressions. Barite origins from ascending fluids of marine clays or terrestrial water.
- **Residual deposits,** which are formed by eluvial weathering of primary layers.

3.1.1.3 The Barite Deposit of Kreševo

Barite deposits in the region of Kreševo in Bosnia and Herzegovina (Fig. 13 left) are part of the Mid-Bosnian Schist Mountains (MBSM) containing the largest barite ore deposits of the Dinarides. The MBSM are one of four Paleozoic complexes of Bosnia and Herzegovina (Fig. 13 right), mainly consisting of Lower Paleozoic (Ordovician-Silurian-Devonian) rocks and lesser of Lower-Middle Carboniferous to Late Permian rocks [Jurkovic et al. 2010], which is overlain by fossiliferous Devonian carbonate rocks [ZIVANOVIC 1972]. The main rocks of the MBSM are pre-Devonian metamorphic rocks [SOFILJ ET AL. 1980], whose K-Ar dated crystallization age is 343 ± 13 Ma

[PALINKAS ET AL. 1996]. Uplifting in this area was caused by the Hercynian orogeny and rhyolite extrusions. In Kreševo, veins and irregular bodies are widely hosted in Devonian dolomite and limestone [JURKOVIC 1996].

The $^{87}Sr/^{86}Sr$ ratios of the Bosnian barites are 0.710972 – 0.714170 [JURKOVIC ET AL. 2010]. These high values, in association with the high Ba content indicate a hydrothermal leaching of Rb rich altered felsic rocks. High ratios are typical for S-Type magmatism and/or crustal contamination by fluid circulation through Rb rich clastites and extrusive magmatic rocks [FRIMMEL AND PAPESCH 1990]. Barite deposits were formed by hydrothermal fluids linked to magmatism and metamorphism and under the influence of Permian sea water. The Late Variscan phase is responsible for the formation of the barite ore, containing Fe, Cu, Zn, Pb, Sb- (As) sulphides. In the whole Dinarides, barite is located in Upper Silurian, Devonian, Carboniferous and Permian rocks. Ore bodies in clastic rocks usually form veins and imprignations, those in carbonates form irregular- and replacement bodies. The MBSM ore bodies were remobilized in Post Variscan phases. [Jurkovic et al. 2010].

Fig. 13: Location Kresevo Deposit [source: google maps] (left); Location of Paleozoic Complexes: SEB South Eastern Bosnia, EB Eastern Bosnia, Una-Sana Area, MSBC Mid-Bosnian Schist Mountains [Jurkovic et al. 2010] (right)

3.1.2 Methods of Raw Material Characterization

The raw material characterization is based on two aggregate samples. One aggregate sample consists of five barite hand samples, received from Kreševo,

Bosnia and Herzegovina, without further information. It is used mainly for the raw material characterization.

The numbers of the barite hand samples (cut for thin sections) are:

AT-1A (Fig.6)

AT-1B (Fig. 7)

AT-1C (Fig. 8)

AT-1D (Fig. 9)

AT-1E (Fig. 10)

The second aggregate sample is a collection of barite and host rock samples (AT-1K), around 13 kg, which were collected during a field trip to the exploration gallery number 21 and were used mainly for mineral processing analysis (Fig. 19 and 20).

3.1.2.1 Macroscopic Description

The samples were described by visual aspects with focus on grain size, color and impurities.

3.1.2.2 Microscopy

3.1.2.2.1 Transmitted Light Microscopy

For transmitted light microscopy, thin-sections were produced manually. The thickness of the sections was about 25 µm. Due to the different hardness of quartz and barite, the barite in the thin sections appears very contaminated with grinding powder. The thin-sections were analyzed using a "Zeiss Axio Scope.A1" equipped with an "AxioCam ERc 5s" camera (Fig. 14).

Fig. 14: "Zeiss Axio Scope.A1" equipped with an "AxioCam ERc 5s" Camera

3.1.2.2.2 Reflected Light Microscopy

For reflected light microscopy, a polished section of the sample AT-7D (Fig. 18d) was produced (Fig. 15). The polished section was analyzed using a "Zeiss Axio Scope.A1" equipped with a" AxioCam ERc 5s" camera (Fig. 14).

Fig. 15: Polished Section of Barite with Sulfides

3.1.2.3 Raman Spectroscopy

Raman Spectroscopy was used to identify minerals, which could not be specified in reflected light microscopy, and to quickly identify minerals in the mineral processing products, especially of magnetic separation. The Raman Model (Fig. 16) is a Jobin Yvon LABRAM confocal-Raman spectrometer equipped with a frequency-doubled Nd-YAG laser (100 mW, 532.2 nm) and a He-Ne laser (633 nm), and diffraction gratings of 1200 and 1800 grooves/mm. For detection, a Peltier-cooled, slow-scan, CCD matrix-detector is used. Laser focussing and sample viewing are performed through an Olympus BX 40 microscope fitted with 10X, 50X and 100X long-working distance objective lenses (allowing views in reflected- and transmitted-light) [http://www.unileoben.ac.at/content/view/579/1226/lang,de/].

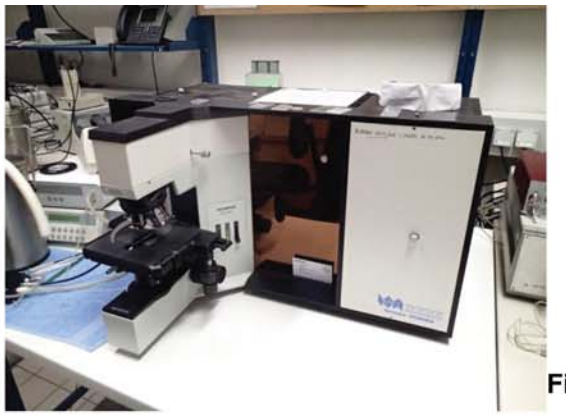

Fig. 16: Raman: Jobin Yvon LABRAM

3.1.2.4 X-Ray Diffractometry

To investigate barite and host rock samples concerning their mineral composition, X-Ray Diffractometry (XRD) was applied. Selected minerals of the mineral processing products were investigated by XRD and evaluated by semiquantitative analysis after the Rietveld Method. The XRD analysis was carried out by the Institute for Mineralogy and Crystallography, Bulgarian Academy of Sciences.

3.1.2.5 Brightness Measurements

To get information concerning the quality of the raw barite, the brightness of the barite hand samples was measured. The barite samples AT-7A, AT-7B, AT-7C, AT-7D, AT-7E were grinded for 15 min in a “Retsch RM100” agate mill (Fig. 17 left). The powder was pressed forming a pellet and analyzed by a “Datacolor Elrepho 3000 Series” spectrophotometer (Fig. 17 right).

Fig. 17: Retsch RM100 Agate Mill (left); Datacolor Elrepho 3000 Spectrophotometer (right)

3.1.2.6 Chemical Analysis

For analysis of the chemical composition of the barite hand samples AT-7A, AT-7B, AT-7C, AT-7D and AT-7E, they were grinded for 15 min in a “Retsch RM 100” agate mill (Fig. 17). The chemical analysis was carried out by the Department of General, Analytical and Physical Chemistry, Montanuniversität Leoben. The analysis measured the quantities of the detected molecules and elements (Tab. 8). The loss of ignition was analyzed at 1000 °C.

Tab. 8: Chemical Analysis of Molecules and Elements

g/100g	mg/kg	mg/kg
Na2O	Sc	Ce
MgO	V	Pr
Al2O3	Cr	Nd
SiO2	Co	Sm
P2O5	Ni	Eu
SO3	Cu	Tb
K2O	Zn	Gd
CaO	Ga	Dy
TiO2	Rb	Ho
Cr2O3	Sr	Er
MnO	Y	Tm
Fe2O3	Zr	Yb
BaO	Nb	Lu
SrO	Ba	Pb
	La	Th
LOI		

Aim of the chemical analysis was to calculate the $BaSO_4$ contents and to check the correlation of the depositional environment. The contents of $BaSO_4$ were calculated according to the formulas in Tab. 9 [LORENZ AND GWOSDZ 1998A]:

Tab. 9: Calculation Formulas [LORENZ AND GWOSDZ 1998A]

$BaSO_4$	x	0.5884	=	**Ba**
Ba	x	1.6995	=	**$BaSO_4$**
$BaSO_4$	x	0.657	=	**BaO**
BaO	x	1.5221	=	**$BaSO_4$**

3.1.3 Results of Raw Material Characterization

3.1.3.1 Macroscopic Description

All barite hand samples (Fig. 18a-e) were white with a sparry ground mass and medium grained (ca. 0,5 – 1 mm). Quartz was visible in sample AT-7A and AT-7B (Fig. 18a and 18b) and disseminated sulfides of mm size in sample AT-7C and AT-7D (Fig 18c and 18d). Sample AT-7E was plain white and monomineralic, however a slight greenish impurity was visible, which seemed to be chlorite, but was too little to be detected by the listed methods (Fig. 18e). The aggregate sample for mineral processing (AT-1K) comprised: barite intergrown with gray dolomite (Fig. 19), white barite, rusty-weathered hematite and very little turquoise malachite (Fig. 20).

Fig. 18: a : AT-7A, Barite with Quartz; b: AT-7B, Barite with Quartz; c: AT-7C, Barite with Sulfides; d: AT-7D, Barite with Sulfides; e: AT-7E, Barite, with greenish Impurities

Fig. 20: AT-1K, Barite intergrown with Dolomite

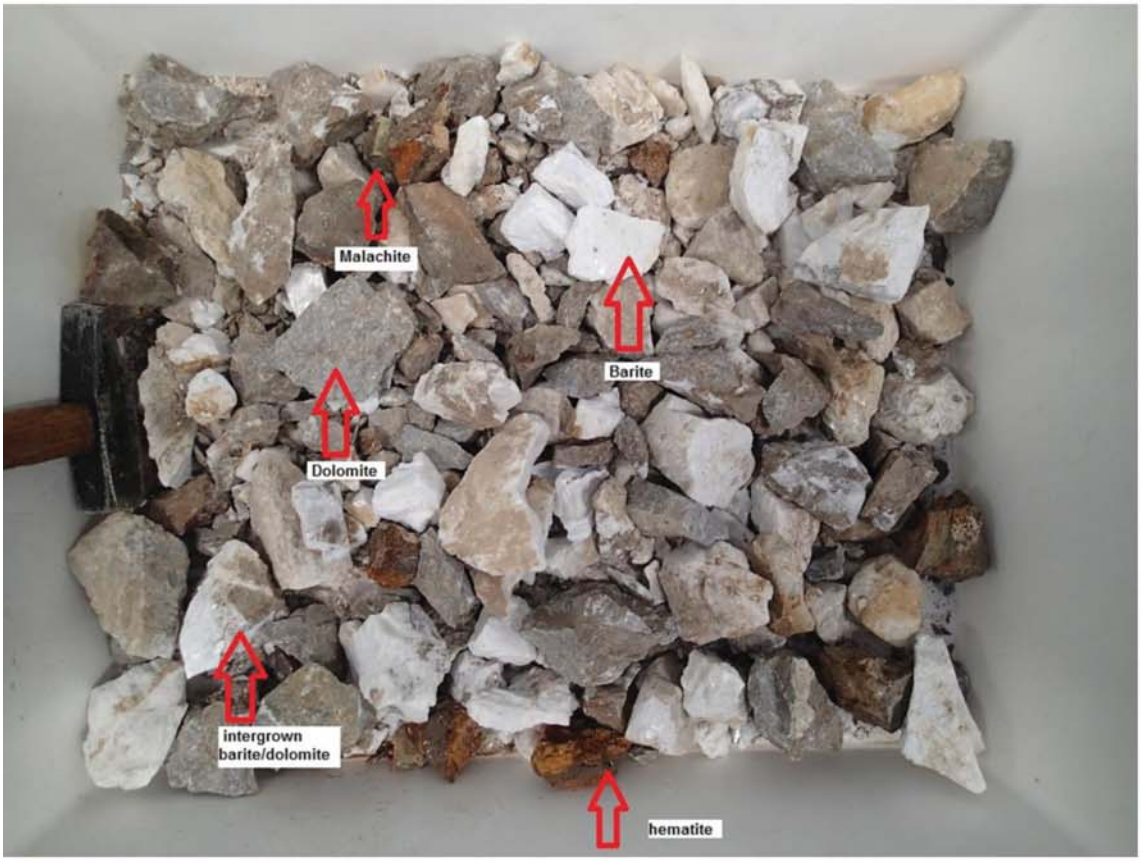

Fig. 20: AT-1K, Barite, Dolomite, Hematite, Malachite

3.1.3.2 Microscopy

3.1.3.2.1 Transmitted Light Microscopy

The main component of all samples was barite. The barite seemed impure and the cleavage was frequently visible (Fig. 21). The barite was hypidiomorph. Quartz occurred in different amounts, depending on the sample: In sample AT-7B, quartz grains of mm size occurred (Fig 22). The quartz was xenomorphic and it extincted wavely. Absolute quantities could not be determined, because quartz and barite could not always be distinguished. When the cleavage of the barite was not visible (cut perpendicular to C-axis), it looked like quartz (Fig. 23). Accessorily epidote and tourmaline occurred and some areas showed traces of phyllosilicates (Fig. 23). The fabric was massy and crystalline. The grain size was around 0.2 – 0.3 mm. Some areas were finer (20 µm) and irregularly distributed. Occasionally rock fragments were visible with a maximum size of 2.5 mm. They seemed sericitized and the boundaries were intergrown with barite and quartz grains (Fig. 24). Dark bubbles resulted from a failure during thin-section production. The scale on the figures is 1:10.

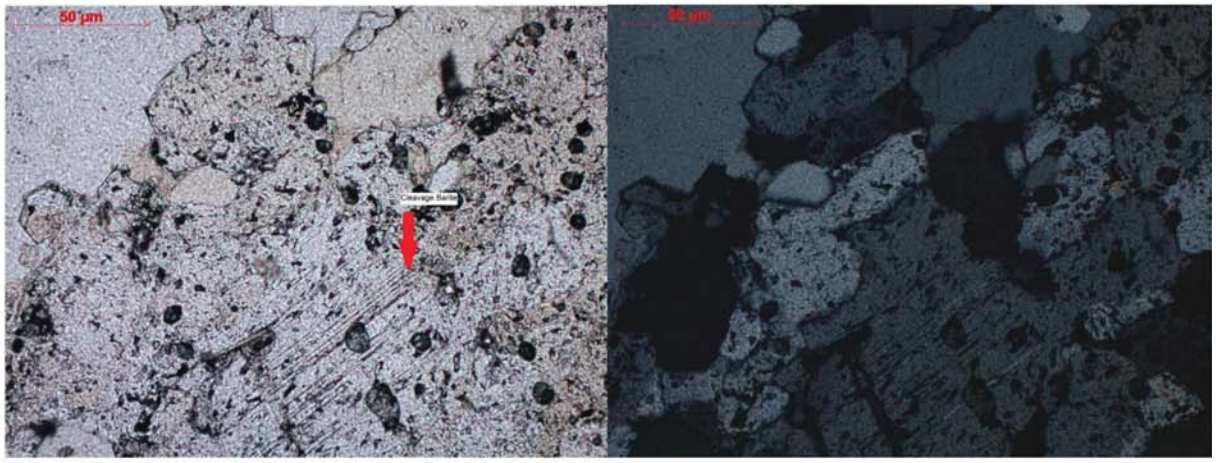

Fig. 21: Cleavage of Barite with Analyzer in parallel (left), Analyzer in cross (right)

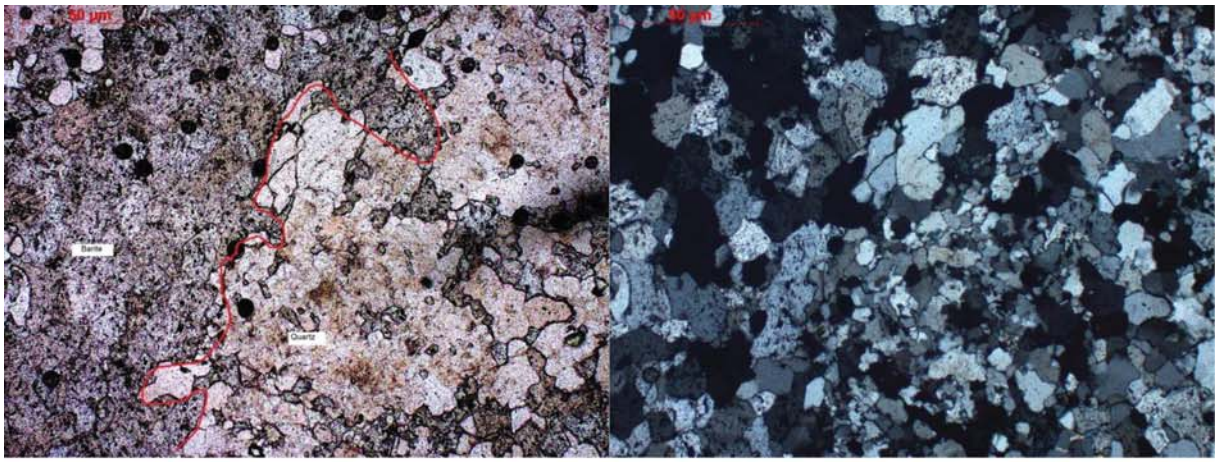

Fig. 22: Barite and Quartz with Analyzer in parallel (left), Analyzer in cross (right)

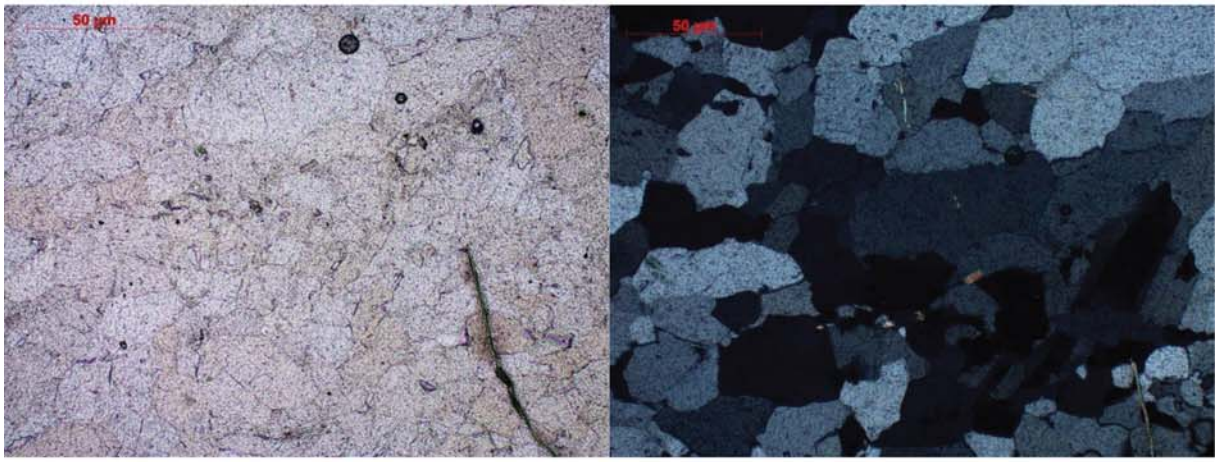

Fig. 23: Barite, no visible Cleavage with Analyzer in parallel (left), Analyzer in cross with visible Phyllosilicates (right)

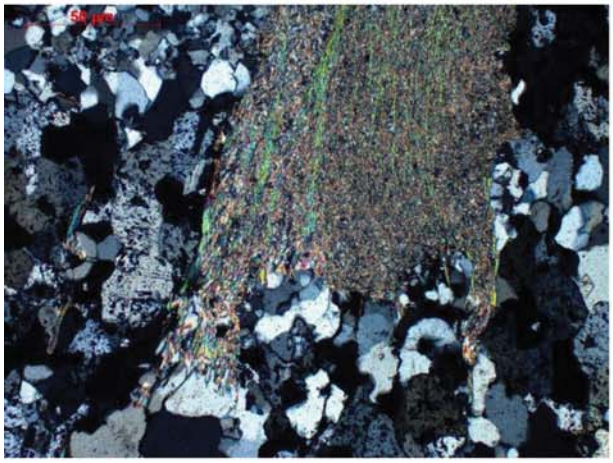

Fig. 24: Rock Fragment, Intergrown with Quartz, Analyzer in cross

3.1.3.2.2 Reflected Light Microscopy

The opaque phases were investigated by reflected light microscopy on a polished section. The major part of the opaque minerals was tetrahedrite (Fig. 25) and traces of pyrite. Tetrahedrite in barite occurred disseminated within areas of 1-2 mm (Fig. 15). The microscopic determination of tetrahedrite was difficult, so Raman spectroscopy was used for support. The scale on the figure is 1:10.

Fig. 25: Tetrahedrite

3.1.3.3 Raman Spectroscopy

The coarse sulfide in sample AT-7D (Fig. 25) was tetrahedrite. The spectrum is shown in the appendix (Fig. 68).

During the mineral processing tests, the minerals of the host rock (sample AT-1K) were investigated, mainly after magnetic separation: The host rock contained mainly dolomite. Impurities in the host rock were calcite, hematite, pyrite and malachite.

3.1.3.4 X-Ray Diffractometry

The host rock consisted mainly of dolomite, with traces of calcite and albite (Fig. 26; Tab. 10). The white barite sample was pure barite. The spectra are listed in the appendix (Fig. 69 and 70).

Tab. 10: Composition of the Host Rock

Mineral	**%**
Dolomite	96.7
Calcite	2.2
Albite	1.1

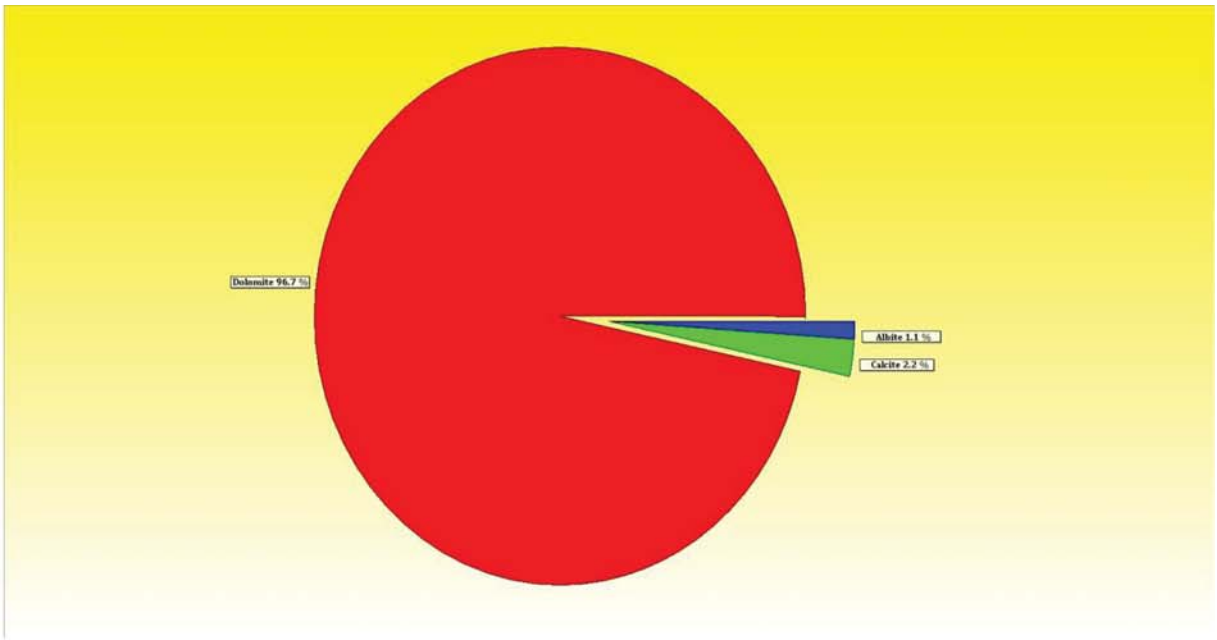

Fig. 26: Semiquantitative Analysis of the Host Rock

3.1.3.5 Brightness Measurements

There were no impurities from the host rock (e.g. dolomite, hematite, malachite) in the barite hand samples. The brightness depended on the intergrown impurities like tetrahedrite (Fig. 15). The results are listed in Tab. 11.

Tab. 11: Brightness Measurements

Sample	Brightness -Y Axis [%]
AT-7A	90.38
AT-7B	88.46
AT-7C	86.35
AT-7D	72.70
AT-7E	95.56

3.1.3.5 Chemical Analysis

The chemical compositions of the samples AT-7A, AT-7B, AT-7C, AT-7D and AT-7E are shown in the appendix (Tab. 39 and 40). The $BaSO_4$ content was calculated (Tab. 12).

Tab. 12: Calculation of $BaSO_4$ Content [m%]

Element	Samples				
	AT-7A	AT-7B	AT-7C	AT-7D	AT-7E
g / 100 g					
BaO	69.27	50.15	56.90	59.47	61.14
BaSO4	105.43	76.34	86.60	90.51	93.06
SrO	0.96	0.39	8.77	9.61	9.19
SrSO4	1.70	0.69	15.56	17.05	16.29

The $BaSO_4$ grade of sample AT-7A (> 100 %) may be a result of analysis-imprecisions and cannot be included in any interpretation. A further corrective analysis could not be performed in the limited frame of this project. The $SrSO_4$ grades of the samples AT-7A and AT-7B (≈ 1 %) were significantly lower than the grades of the remaining samples (> 15 %). This may indicate that the samples were taken from different parts of the deposit.

$SrSO_4$ grades are an indicator for the formation conditions: sedimentary barite and younger reworked barite veins show grades below and around 1 m% $SrSO_4$; primary vein barite shows grades above 3 m% $SrSO_4$ and can reach > 10 m% $SrSO_4$. The $SrSO_4$ grade increases with depth and proximity to the center of the mineralization, which is the origin of the Ba/Sr fluid ascension point. An increase of Sr with the temperature is also reported. [LORENZ AND GWOSDZ, 1998C]. The samples AT-7A and AT-7B may come from distal parts of the ascension point. Hardly any Rare Earth Elements were detected.

3.2 Field Trip to Kreševo

From 29th – 30th of April 2013, a trip to Kreševo, Bosnia and Herzegovina was undertaken. Purpose of the field trip was an on-site inspection of the underground mine and collecting further samples for mineral processing tests. The production of the underground mine ended in 1991 and there are no geological maps available anymore. An old exploration gallery (gallery N° 21), was visited under the guidance of a former miner. It was only re-opened recently for the visit (Fig 27a). The entrance of the main underground mine (gallery N° 20) was filled up at that time (Fig. 27b). Barite there occurs in lenses of about 0,5 – 1,5 m (Fig. 27c) and small veins of cm size (Fig. 27d) within the dolomite-host rock. Dolomite is approximately 5 – 10 cm thick stratified and dips to WNW (285/48) (Fig. 27f). Occasionally areas of malachite and weathered hematite occur in the host rock. These areas are faulty, and they are accompanied by water inlets (Fig. 27e). According to the former miner, the quality of the barite in the gallery N° 21 is better (98-99 m% $BaSO_4$) than it is in the actual mine (95 m% $BaSO_4$), but the amount of barite ore is less. The exploration gallery was built to reach a 50 x 60 m barite lens, but missed its target.

About 13 kg of barite, dolomite and malachite/hematite were collected for mineral processing tests (sample AT-1K).

Fig. 27: a: Re-opened Entrance of Gallery 21; b: Collapsed Entrance of Gallery 20; c: Barite Lens in Dolomite, Width ca. 7 m; d: Barite Veins in Dolomite; e: Rusty Hematite, Malachite on Fault with Water Inlet; f: Dipping of Dolomite (285/48)

3.3 Mineral Processing

Intended was the best possible separation of the barite form the host rock, as well as from impurity minerals. Therefore the processability was tested by the physical properties of the raw material.
The crushed material of the sample was divided into several grain-size fractions. The coarse fraction was optically sorted into pure barite, intergrown barite and waste material. The medium grained fraction was separated by a manual jig (after Büttgenbach) into light and heavy components. The fine and finest fraction was processed by a “Frantz” magnetic separator, heavy media separation (sink/swim analysis), a permanent magnetic separator, electrostatic separation and shaking table separation. The permanent magnetic separator was used before electrostatic and shaking table tests, because oxide minerals might have influenced the results due to their high density.

The degree of liberation and the mass balance study are the major quality indicators for the success of the crushing and separation processes.
For the calculation of the degree of liberation and the mass balance, the density of the products was chosen. Pure barite ore had a measured density of 4.38 – 4.43 g/cm^3, dolomite 2.8 – 2.9 g/cm^3. The calculation scheme is described in chapter 3.3.2.

3.3.1 Methods of Mineral Processing

The aggregate sample of the exploration gallery N° 21 (sample AT-1K) was investigated by the following methods:

3.3.1.1 Primary Crushing

The whole aggregate sample was crushed manually in the cycle to a fraction ca. 0 - 70 mm, using a hammer (Fig. 28).

Fig. 28: Manual Crushing in the Cycle

3.3.1.2 Sieving

The primarily crushed aggregate sample and the secondarily crushed material (intergrown product; Chapter 3.3.1.4) were mixed and sieved manually by hand-sieves. The mesh sizes were [mm]: 10; 5; 1; 0.71; 0.5; 0.315; 0.125; 0.04. The result of the crushing is analyzed in the sieve-analysis.

3.3.1.3 Optical Sorting

One quarter of the crushed aggregate sample (2.4.1.1) (Fig. 29 left) was taken for optical sorting. Therefore only the grain size > 10 mm was analyzed. The subsample was optically sorted into three products: Barite, Barite intergrown with host rock and host rock (Fig. 29 right). To calculate the degree of liberation as well as the mass balance, the densities of the products were determined using a hydrostatic scale (Fig. 30 left). First the sample's weight was measured, followed by measuring the sample's weight under hydrostatic uplift (Fig. 30 right). The weight under hydrostatic uplift equates the weight of the replaced water, which equates its volume at a density of 1 g / cm^3.

Calculation:

$$\text{Density of the Product} = \frac{\text{Mass of Product [g]}}{\text{Volume of Replaced Water [cm}^3\text{]}} \quad [\text{g / cm}^3]$$

To calculate the degree of liberation, a density for pure barite was measured (4.38 g/cm^3) and a dolomite density of 2.8 g/cm^3 was assumed.

Fig. 30: Subsample of One Quarter of the Aggregate Sample (left); Optical Sorting into 3 Products (right)

Fig. 30: Hydrostatic Scale, Product Weight Without (left) and Under Hydrostatic Uplift (right)

3.3.1.4 Secondary Crushing

The intergrown barite (with host rock) was sorted optically form the sieve fraction > 10 mm. The Product was crushed in a “Retsch” jaw crusher (Fig. 31) and put back to sieving (Chapter 3.3.1.2).

Fig. 31: “Retsch” Jaw Crusher

3.3.1.5 Manual Jig after “Büttgenbach”

Manual jigging (Fig. 32 left) works with pulsating water upflow that loosens the grain package. Specific lighter grains are arranged above specific heavier grains. Thus bedding depending on density is achieved. [SCHUBERT 1986A] The separation is based on the principle of the initial fall acceleration of the grains. The height and frequency of the pulse are essential for the efficiency of the separation process. After a visible separation had occurred, the light grains were removed at an assumptive boarder by pushing a stamp through the glass.

Two grain size fractions of the crushed material were investigated: 1 – 5 mm and 5 – 10 mm. The densities of the products were determined by a “Micromeritics AccuPys 1330” helium pycnometer (Fig. 32 right). The degree of liberation and the mass balance were calculated.

Fig. 32: Jig after “Büttgenbach” (left); Helium Pycnometer (right)

The process data for the “Büttgenbach” test for grain sizes (k) are listed in Tab. 13:

Tab. 13: Process Data “Büttgenbach”

k = 1 - 5 mm	Measured Value	Scale Value
Lifting Height	ca. 3.5cm	40 - 75
Duration	1 min 16 sec	
Frequence [s-1]	1	
Stamp	1.8 cm	67 - 48
k = 5 - 10 mm		
Lifting Height	ca. 3.5 cm	45 - 80
Duration	1 min 30 sec	
Frequence [s-1]	1	
Stamp	2 cm	65 - 45

3.3.1.6 Magnetic Separation by “Frantz”-Separator

The fine grain fractions k = 0.315 – 0.5 mm and 0.125 – 0.315 mm were investigated with a “Frantz Isodynamic Magnet Separator, Model L-1” (Fig 33). The magnetic separation assumes that the grains differ enough in their magnetic susceptibility to be separated [SCHUBERT 1986B]. The “Frantz” magnetic separator is an isodynamic separator for laboratory use to fractionate the susceptibility classes. The material is transported through a vibrating channel (inclination ca. 15°) with a transverse inclination (ca. 10°). An electromagnet is situated in an air gap and is controlled by the induction current intensity. As a result of magnetic and gravitational forces, the material is separated into two classes of susceptibility. The longitudinal inclination controls the speed of the transport. [SCHUBERT 1986C].

The feeding was dry. Prior to the “Frantz” separator, all ferromagnetic particles were removed by hand using a permanent magnet. Then the material was processed with the “Frantz” separator beginning at 0.2 A. The magnetic material was removed and the waste material was processed again, at 0.6 A, 1.0 A and 1.4 A (Fig. 34). The products were weighted and the mass percentages plotted in bar diagrams showing susceptibility classes.

Fig. 33: "Frantz" Magnetic Separator

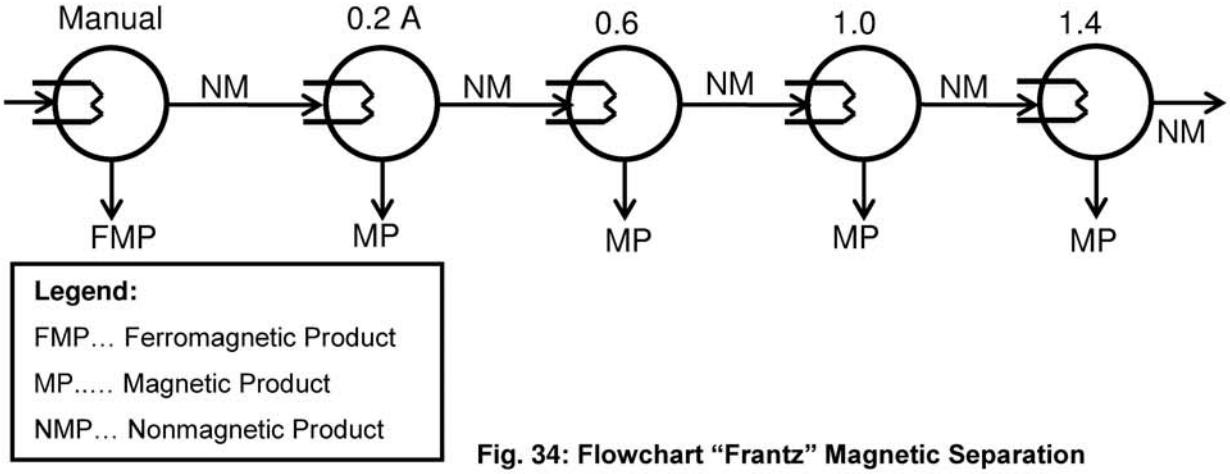

Fig. 34: Flowchart "Frantz" Magnetic Separation

3.3.1.7 Heavy Media Separation - Swim / Sink Analysis

The grain fractions k = 0.71 – 1 mm, 0.5 – 0.71 mm and 0.315 – 0.5 mm were examined by heavy media separation. For a swim/sink separation, material is put in to a separation-medium (heavy media) and is divided into the specific heaviest and the specific lightest components [SCHUBERT 1986D]. The principle of a swim/sink separation is the difference in sinking velocities of grains, which is a function of its density and grain size. Specific heavy grains and big grains have higher sinking velocities than specific light grains or small grains [SCHUBERT 1986E]. In this case using a static fluid and a long time period of sinking, only the density of the grain is crucial.

A heavy media was mixed, using Sodium-Polytungstate (Na_6 [$H_2W_{12}O_{40}$]) with a molar mass of M 2986.12 g/mol and demineralized water. The densities of the media were: ρ = 3.10 g/cm^3, 2.90 g/cm^3, 2.75 g/cm^3 and 2.65 g/cm^3. The heavy media was stirred with the dry material and allowed to rest for about 10 min until a clear

separation between light and heavy components was visible. A small hand sieve was used for the removal of the light product. The separation started with the heaviest media and the light concentrate was removed each time (Fig. 35). The products were washed and the densities were determined using a helium pycnometer. The grain size distribution of the whole test was calculated and the results of the swim sink analysis were balanced and plotted in a Henry-Reinhard diagram.

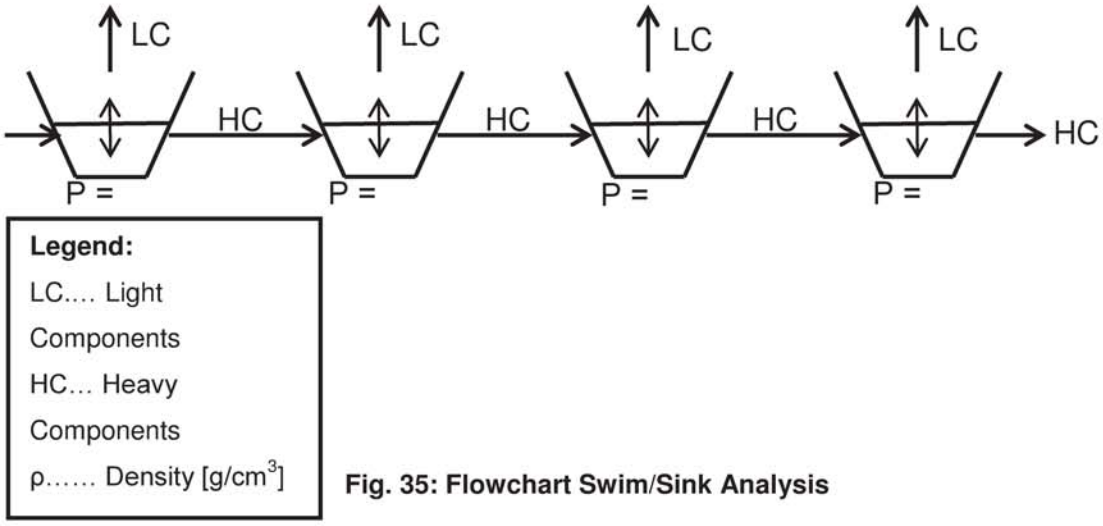

Fig. 35: Flowchart Swim/Sink Analysis

3.3.1.8 Magnetic Separation with an IFE Permanent Magnetic, Strong Field Drum Separator

For more accurate results of the electrostatic and shaking table separation, the ferro- and paramagnetic compounds were removed with a permanent strong field magnetic drum separator “IFE, Type S THP 1-22” (Fig. 36). The grain sizes k = 0.71 – 1 mm; k = 0.5 - 0.71 mm; k = 0.315 – 0.5 mm were separated into two products: a nonmagnetic and a magnetic one. The feeding was dry. The magnetic products were not used in further processing tests, because they might influence the results due to their density. The settings of the machine were as follows: The vibrator for feeding was on stage 2, the drum rotated with 200 rpm for all grain sizes. The mass percentage of removed magnetic components was calculated and plotted in pie charts. Pictures of the products were taken by a binocular microscope.

Fig. 36: Strong Field Magnetic Drum Separator

3.3.1.9 Electrostatic Separation

The grain sizes k = 0.71 – 1 mm; k = 0.5 - 0.71 mm; k = 0.315 – 0.5 mm were processed using a “Carpco” electrostatic separator (Fig. 37 left). Magnetic minerals were removed before (Chapter 3.3.1.8).

The settings of the machine were:

- Partition plate on stage 62 (equals about 75°, 9 cm distance from the drum)
- Drum rotation velocity: stage 12 (equals 0.33 rps)
- Vibration: stage 0.5
- Voltage: 20.2 kV
- Duration of feeding: + k = 0.71 -1 mm: 3 min
  + k = 0.5 – 0.71 mm: 3 min
  + k = 0.315 – 0.5 mm: 4 min
- Distance Electrode/Drum: + k = 0.71 -1 mm: 2.5 cm
  + k = 0.5 – 0.71 mm: 3 cm
  + k = 0.315 – 0.5 mm: 3.5 cm

The experiment was carried out at room temperature, without heating up the minerals. The feeding was dry. The material was divided into nonconductive barite and semi conductive dolomite products (Fig. 37 right) with a cleaner stage for each (Fig. 38). The densities of the products were measured with a helium pycnometer and the degree of liberation as well as the mass balance were calculated. Pictures of the products were taken by a binocular microscope.

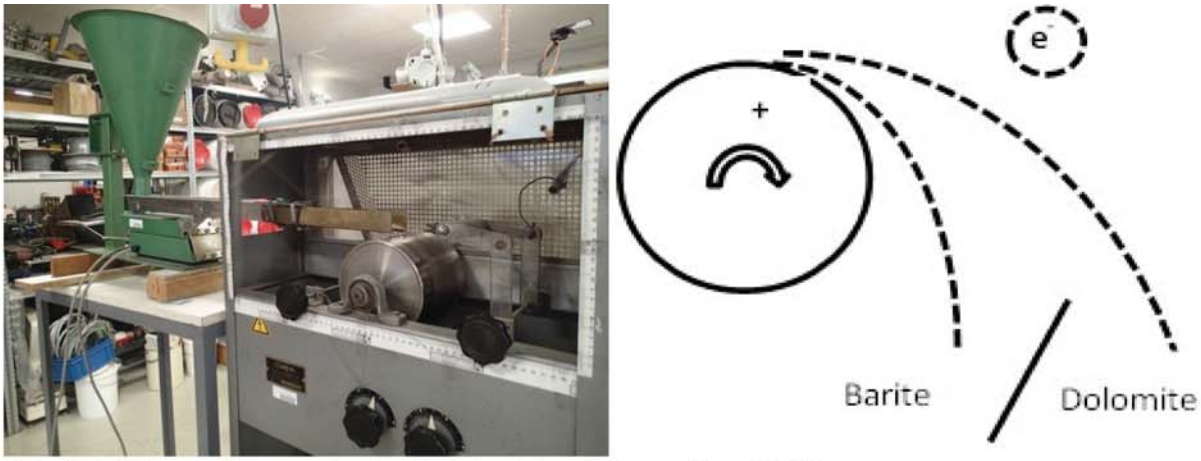

Fig. 37: "Carpco" Separator (left); Principle of Separation (right)

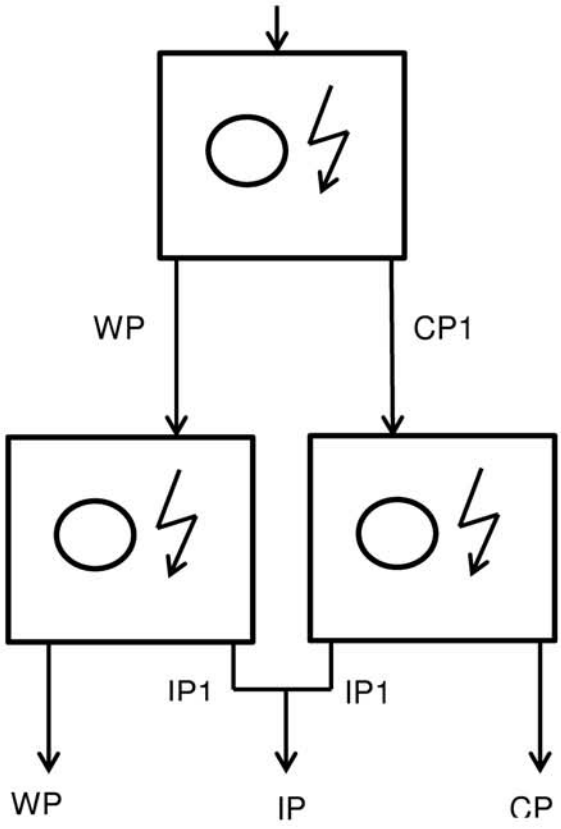

Legend:

WP1… Waste Product 1

CP1…. Concentrate Product1

IP1….. Intermediate Product 1

WP2… Final Waste Product

IP2…… Final Intermediate

Fig. 38: Flowchart Electrostatic Separation

3.3.1.10 Shaking Table

The grain sizes k = 0.71 – 1 mm; k = 0.5 - 0.71 mm; k = 0.315 – 0.5 mm were processed using a shaking table "Multifix Type M80" (Fig. 39 left). Magnetic minerals were removed before (Chapter 3.3.1.8). For feeding, the material was slowly flushed into the feeding mouth with a water spray bottle.

The parameters for the test were as follows: The feeding water (H_2O_F), the transverse water flow (H_2O_T), the frequency (f) and the inclination (i). For each grain size, different parameters were necessary:

k = 0.71 – 1 mm:	+ H_2O_F =105 scale values
	+ H_2O_T = 120 scale values
	+ f = 390 min^{-1}
	+ i = ≈ 5° (6^{th} step form right)
k = 0.5 – 0.71 mm:	+ H_2O_F =110 scale values
	+ H_2O_T = 120 scale values
	+ f = 390 min^{-1}
	+ i = ≈ 6° (7^{th} step form right)
k = 0.315 – 0.5 mm:	+ H_2O_F =120 scale values
	+ H_2O_T = 120 scale values
	+ f = 410 min^{-1}
	+ i = ≈ 6° (7^{th} step form right)

The material was separated into a high-density and a low-density class (Fig. 39 right). Due to the small amount of samples, reaching a separation equilibrium on the table was difficult. The density of the processed material was measured with a helium pycnometer and the degree of liberation as well as the mass balance were calculated. Pictures of the products were taken by a binocular microscope.

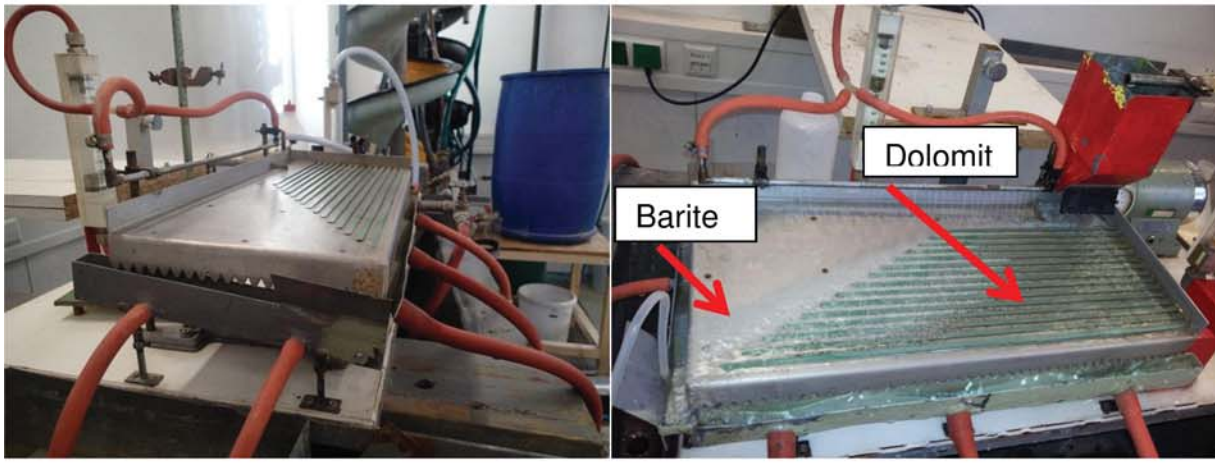

Fig. 39: Shaking Table: Buildup (left); Separation (right)

3.3.2 Calculation

The success of the mineral processing was expressed by the degree of liberation and the mass balance, which include mass, grade, contents and contents recovery. The crucial attribute for the products was the density.

The calculation of the degree of liberation and the balance follows certain formulas:

Mass M [g]

Density ρ [g/cm^3]

Volume V [cm^3]

Grade g [%]

Content I [g]

Mass Recovery r_m [%]

Recovery r [%]

Degree of Liberation DL [%]

Material Index i: 1…n

Product Index j; 1…n

Grade Calculation:

$$V_i = \frac{\rho_i}{M_i} \qquad M_0 = \rho_1 * V_1 + \rho_2 * V_2 \qquad V_0 = V_1 + V_2$$

$$V_1 = \frac{(M_0 - (\rho_2 * V_0))}{(\rho_1 - \rho_2)} \qquad g_i = \frac{M_i}{M_0}$$

Balance Calculation: [amended after SCHUBERT 1989A]:

$$M_0 = M_1 + M_2 \qquad M_0 = \frac{r_{m1} + r_{m2}}{M_0} \qquad r_{m1} + r_{m2} = 100$$

$$I_{i,0} = I_{i,1} + I_{i,2} \qquad I_{i,j} = M_i * g_{i,j} \qquad r_{i,j} = \frac{I_{i,j}}{I_{i,0}} = \frac{r_{m,j} * g_{i,j}}{g_{i,0}}$$

Degree of Liberation Calculation: [amended after SCHUBERT 1989B]:

$$DL = \frac{(M_{1,1} * g_{1,1})}{(M_{1,1} * g_{1,1} + M_{2,2} * g_{1,2})} = \frac{I_{1,1}}{I_{1,1} + I_{2,2}}$$

In words:

The degree of liberation is the percentage of barite contents in the concentrate to barite contents in the concentrate plus barite contents in the waste.

3.3.3 Flow sheet

The flow sheet of the barite processing scheme is given in Fig. 40. Details are described in chapter 3.3.1.

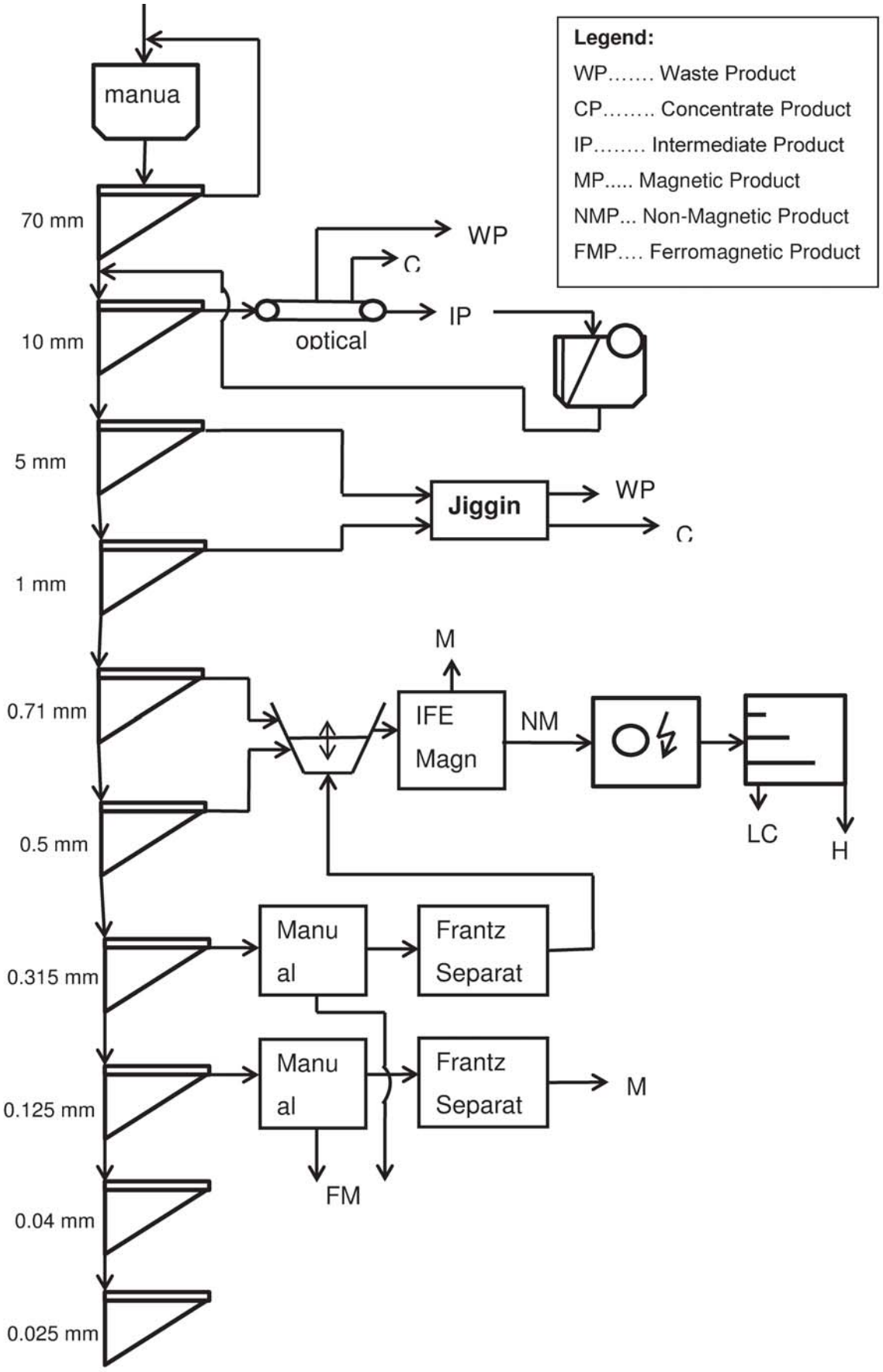

Fig. 40: Flow Sheet Barite Processing

3.3.4 Results of Mineral Processing and Comments

The results of the mineral processing tests of the aggregate sample AT-1K were expressed in a sieve analysis, balance studies, magnetic susceptibility classes and an Henry-Reinhard diagram. The calculation is according to chapter 3.3.2.

3.3.4.1 Sieving

The grain size distribution of the sieve analysis of the crushed aggregate sample is shown in Fig.41:

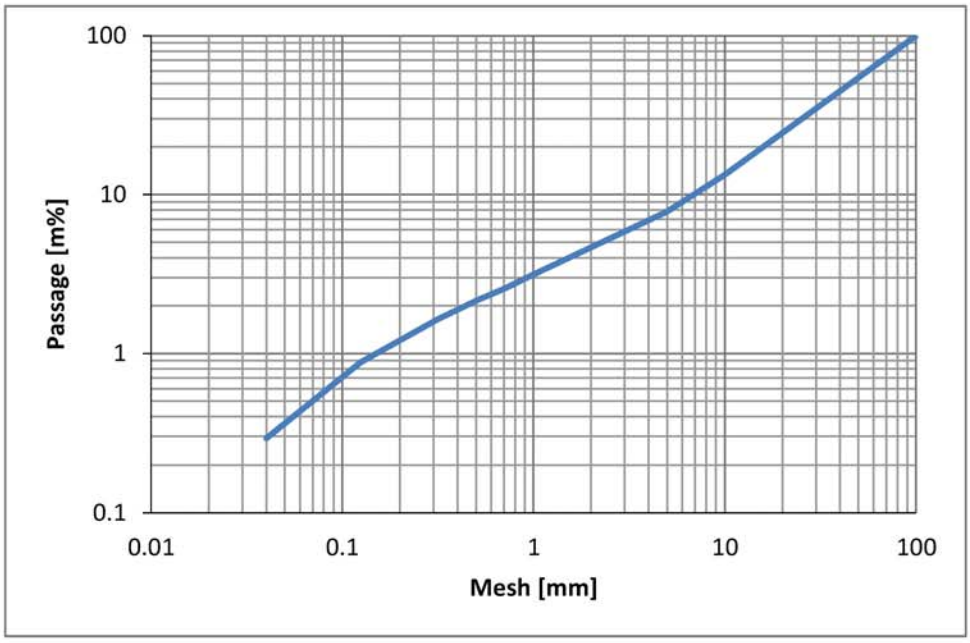

Fig. 41: Grain Size Distribution of Barite

The data of the diagram (Fig. 41) are listed in the appendix (Tab. 41).

Comments:

About 87 m% of the crushed material was larger than 10 mm. Only ca. 4 m% of the material was smaller than 1 mm.

3.3.4.2 Optical Sorting

The optical sorting of the grain size k = 10 – 70 mm was balanced (Tab. 14 and 15) according to the formulas of chapter 3.3.2. The barite grade of the heavy product was assumed 100 %, the barite grade of the waste product was assumed 0 %. A dolomite density 2.8 g/cm^3 was assumed based on common dolomite densities and a barite density of 4.38 g/cm^3 was measured.

Tab. 14: Grade Calculation of Optical Sorting of Barite

Product	Mass	Density	V	V Barite	Mass Barite	Grade
	[g]	g/cm3	cm3	cm3	g	%
CP	8242.00	4.38	1881.74	1881.74	8242.00	100.00
IP	2653.49	3.37	787.39	284.06	1244.17	46.89
WP	5229.00	2.80	1867.50	0.00	0.00	0.00
Feeding	16124.49	3.55	4536.62	2165.79	9486.17	58.83

Tab. 15: Balance of Optical Sorting of Barite

Product	Mass	Yield	Grade	Content	Units	Recovery
	[g]	[%]	[%]	[g]	[%%]	[%]
CP	8242.00	51.11	100.00	8242.00	5111.48	86.88
IP	2653.49	16.46	46.89	1244.17	771.60	13.12
WP	5229.00	32.43	0.00	0.00	0.00	0.00
Feeding	16124.49	100.00	58.83	9486.17	5883.08	100.00

CP = Concentration Product, IP = Intermediate Product, WP = Waste Product, V = Volume.

The degree of liberation was:

DL_{Barite} = 86.88 %

DL_{Waste} = 78.77 %

Comments:

In case of larger amounts of non intergrown barite, pre-sorting between concentration and waste product appears reasonable.

3.3.4.3 Manual Jig after "Büttgenbach"

The jigging products were balanced (Tab. 16 - 19) and the degree of liberation was calculated.

k = 5 – 10 mm:

Tab. 16: Grade Calculation, Büttgenbach, Barite, k = 5 – 10 mm

Product	Mass	Density	V	V Barite	Mass Barite	Grade
	[g]	[g/cm3]	[cm3]	[cm3]	[g]	[%]
CP	177.07	4.32	41.02	38.07	168.55	95.19
WP	122.11	3.24	37.64	8.83	39.11	32.03
Feeding	299.18	3.80	78.67	46.90	207.66	69.41

Tab. 17: Mass Balance Study, Büttgenbach, Barite, k = 5 – 10 mm

Product	Mass	Yield	Grade	Content	Units	Recovery
	[g]	[%]	[%]	g	%%	%
CP	578	40.65	95.19	550.19	3869.13	67.05
WP	844	59.35	32.03	270.35	1901.18	32.95
Feeding	1422.00	100.00	57.70	820.54	5770.30	100.00

CP = Concentration Product, WP = Waste Product, V = Volume.

The degree of liberation:

DL_{Barite} = 67.05 %

DL_{Waste} = 96.81 %

k = 1 – 5 mm:

Tab. 18: Grade Calculation, Büttgenbach, Barite, k = 1 - 5 mm

Product	Mass	Density	V	V Barite	Mass Barite	Grade
	[g]	g/cm3	cm3	cm3	g	%
CP	177.42	4.37	40.59	39.09	173.10	97.57
WP	130.95	3.56	36.75	16.21	71.79	54.83
Feeding	308.37	3.99	77.34	55.31	244.90	79.42

Tab. 19: Mass Balance Study, Büttgenbach, Barite, k = 1 - 5 mm

Product	Mass	Yield	Grade	Content	Units	Recovery
	[g]	[%]	[%]	g	%%	%
CP	429	43.60	97.57	418.56	4253.67	57.91
WP	555	56.40	54.83	304.28	3092.27	42.09
Feeding	984.00	100.00	73.46	722.84	7345.94	100.00

CP = Concentration Product, WP = Waste Product, V = Volume.

The degree of liberation:

DL_{Barite} = 57.91 %

DL_{Waste} = 98.15 %

Comments:

The degree of liberation was directly proportional to grain size: $DL_{Barite\ k=5\text{-}10mm}$ = 67.05 %; $DL_{Barite,\ k=1\text{-}5mm}$ = 57.91 %. This is very unusual. A potential source of error could have been some very fine barite traces adhering to the dolomite grains and consequently falsifying the density measurements. Furthermore hematite grains may have been enriched in the heavy product and their high density falsifying the grade calculation. This problem may have affected all processing results. Another possible source of error was the relatively large grain size of 5 – 10 mm for the laboratory jig.

The recoveries of the concentration products are moderate (around 60 m%) however the grades are high (> 95 m% barite).

3.3.4.4 Magnetic Separation by "Frantz"-Separator

The products of the "Frantz" separator were plotted as mass percentage vs. current (Fig. 42):

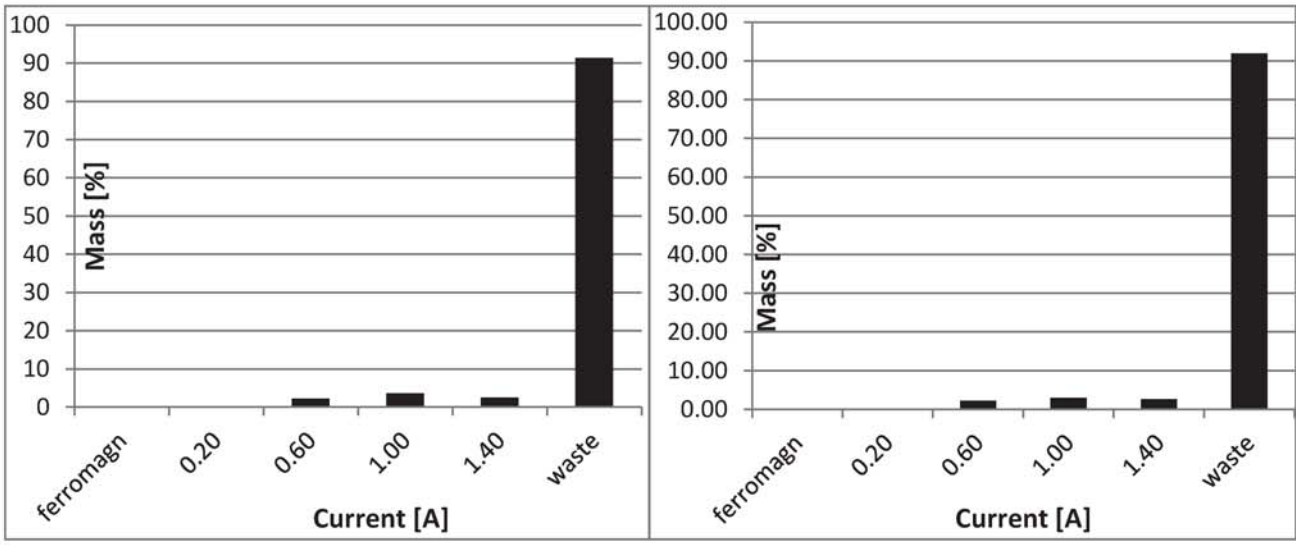

Fig. 42: Susceptibility Classes ob Barite: k = 0.315 – 0.5 mm (left); k = 0.125 – 0.315 mm (right)

The data of the diagrams (Fig. 42 left and right) are listed in the appendix (Fig. 42 and 43).

Comments:

More than 90 m% of the material was nonmagnetic. For removal of the ferro- and paramagnetic components, a current of 1.4 A had to be expended to the Frantz separator.

3.3.4.5 Heavy Media Separation – Sink-Float Analysis

Grain Size Distribution (Fig. 43):

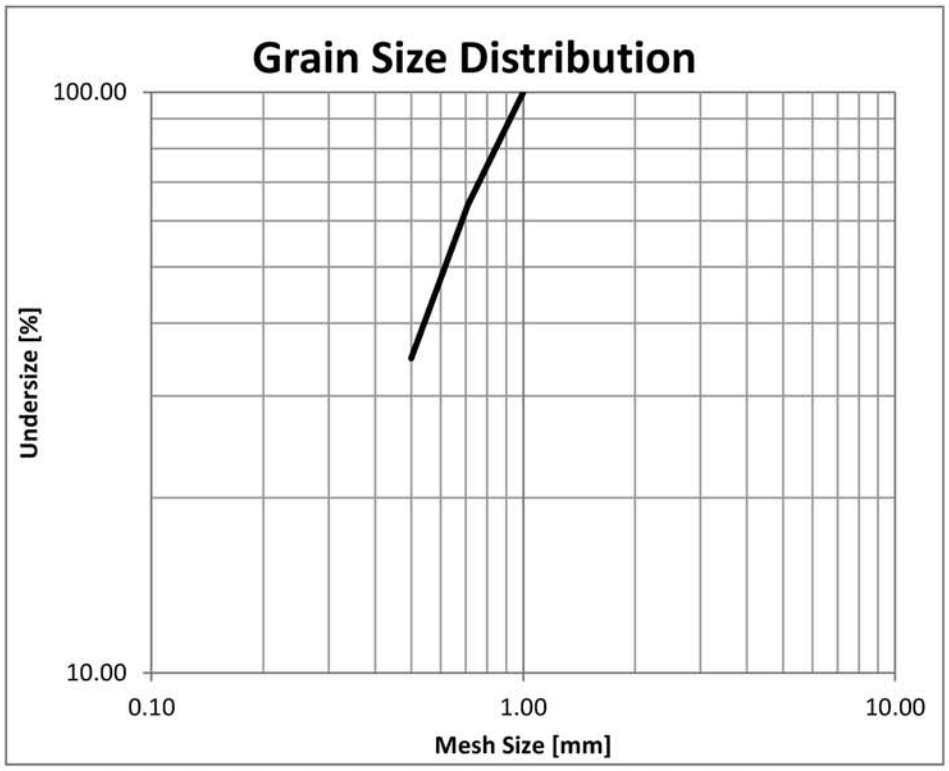

Fig. 43: Grain Size Distribution of Sink Float Analysis of Barite

Mass Recovery Depending on Grain Size (Fig. 44):

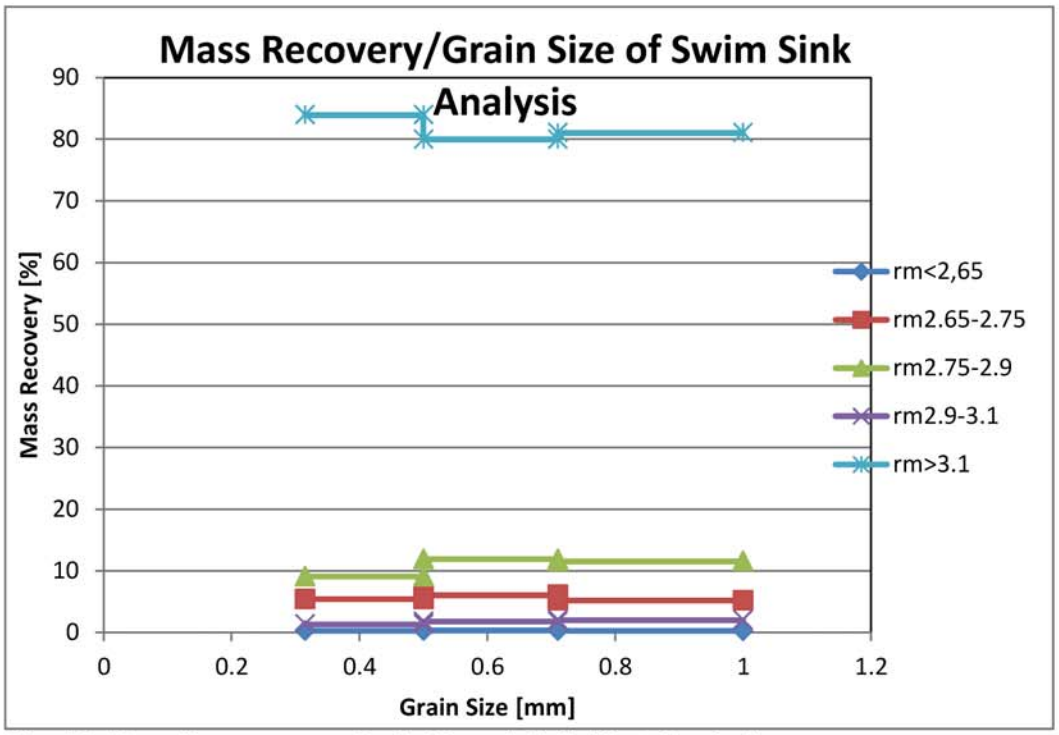

Fig. 44: Mass Recovery vs. Grain Size of Sink-Float Analysis

Henry-Reinhardt Diagram (Fig. 45):

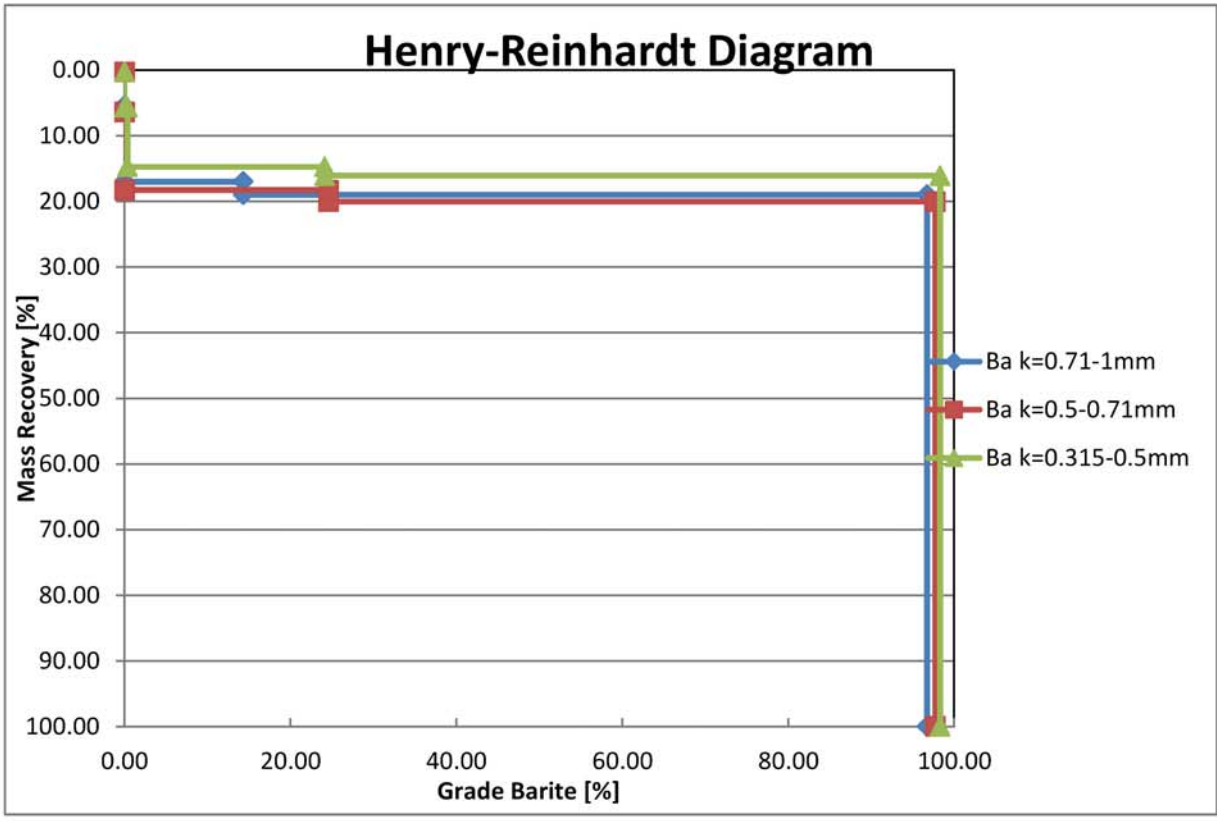

Fig. 45: Henry-Reinhardt Diagram of Sink-Float Analysis of Barite

The data of the diagrams (Fig. 43 - 45) are listed in the appendix (Tab. 44 – 51).

The degree of liberation (DL) was calculated for each grain size class (Tab. 20):

Tab. 20: Degrees of Liberation, Sink-Float Analysis, Barite

	k = 0.71 – 1 mm	k = 0.5 – 0.71 mm	k = 0.315 – 0.5 mm
DL_{Barite} [%]	99.64	99.94	99.57
DL_{Waste} [%]	71.29	58.82	52.86

Comments:

The mass recovery was rather constant for different grain sizes. The highest mass recoveries were those for the density class > 3.1 g/cm^3.

The liberation properties of the barite were rather similar for all three grain sizes. The highest grades (Ø 97.6 m %) were reached in the density class >3.1 g/cm^3 with a mass recovery of 81.6 m%

A potential source of error was washing the material, which can cause losses. Further a magnetic separation of the iron oxides is advisable, since they are not

separated from the barite by sink-float tests, due to a density >3.1 g/cm^3. The degree of liberation is very high (> 99 %) for barite. This indicates a perfect liberation of the barite at these grain size fractions by crushing. The separation by heavy-media separation is very efficient.

3.3.4.6 Magnetic Separation with an IFE Permanent Magnetic, Strong Field Drum Separator

The mass percentage of the magnetic and nonmagnetic products are shown in Fig.46:

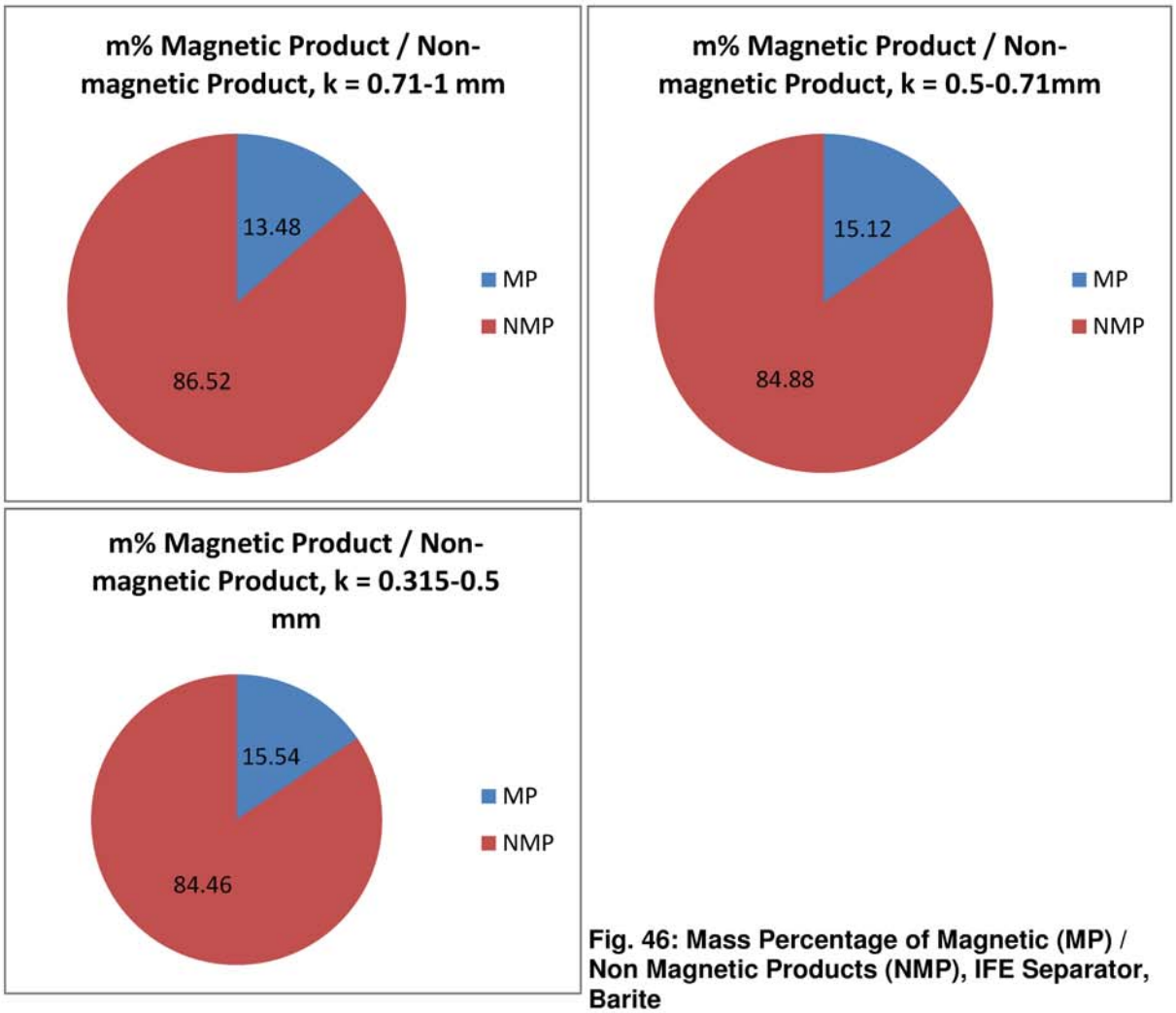

Fig. 46: Mass Percentage of Magnetic (MP) / Non Magnetic Products (NMP), IFE Separator, Barite

The data of the diagrams (Fig. 46) are listed in the appendix (Tab. 52).

The products were analyzed with a binocular microscope (Fig. 47):

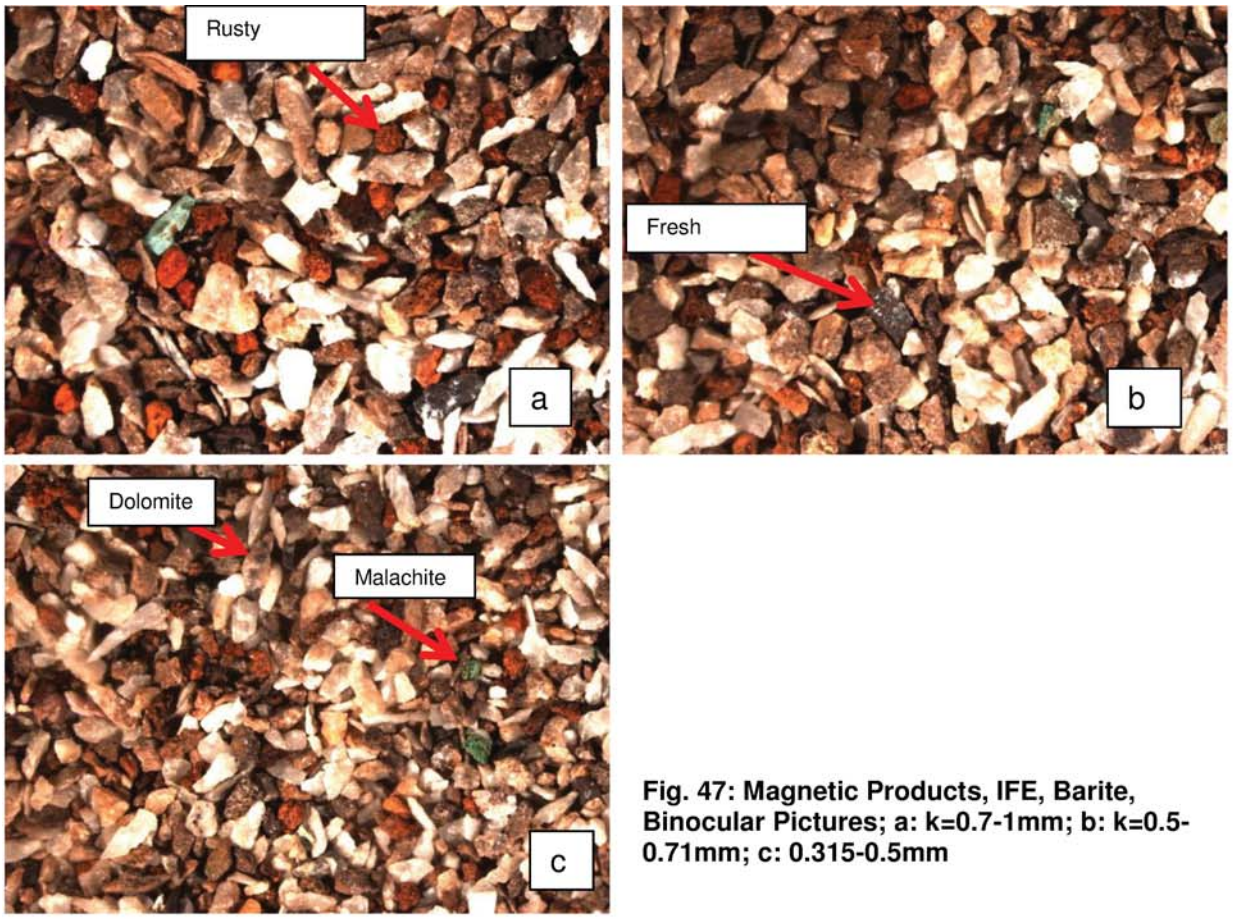

Fig. 47: Magnetic Products, IFE, Barite, Binocular Pictures; a: k=0.7-1mm; b: k=0.5-0.71mm; c: 0.315-0.5mm

Comments:

All grain sizes comprise about the same amount of magnetic compounds (Ø 14.71 m %). In the magnetic product there are: rusty and fresh hematite, malachite and some dolomite. Accessorily barite occurs.

3.3.4.7 Electrostatic Separation

The electrostatic separation products of the grain sizes: k = 0.71 – 1 mm, 0.5 – 0.71 mm and 0.315 – 0.5 mm were balanced (Tab. 21 – 23). The degree of liberation (DL) was calculated for each grain size class.

k = 0.71 – 1 mm:

Tab. 21: Balance Study, Electrostatic Separation, Barite k=0.71-1mm

Balance Study, k = 0.71 - 1 mm						
Product	Mass	Yield	Grade	Content	Units	Recovery
	[g]	[%]	[%]	[g]	[%%}	[%]
CP	61.56	64.84	94.59	58.23	6133.25	72.66
IP	20.90	22.01	76.67	16.02	1687.90	20.00
WP	12.48	13.15	47.16	5.89	619.96	7.34
Feeding	94.94	100.00	84.41	80.14	8441.11	100.00
Grade Calculation						
Product	Mass	Density	V	V Barite	Mass Barite	Grade
	[g]	[g/cm3]	[cm3]	[cm3]	[g]	[%]
CP	17.59	4.30	4.09	3.76	16.64	94.59
IP	13.59	3.94	3.45	2.35	10.42	76.67
WP	11.82	3.45	3.43	1.26	5.57	47.16
Feeding	43.00	3.92	10.97	7.37	32.63	75.89

DL_{Barite} = 72.66 %

DL_{Waste} = 44.55 %

k = 0.5 – 0.71 mm:

Tab. 22: Balance Study, Electrostatic Separation, Barite, k=0.5-0.71mm

Balance Study, k = 0.5 - 0.71						
Product	Mass	Yield	Grade	Content	Units	Recovery
	[g]	[%]	[%]	[g]	[%%}	[%]
CP	63.84	72.41	96.32	61.49	6973.75	79.30
IP	14.34	16.26	80.10	11.49	1302.68	14.81
WP	9.99	11.33	45.68	4.56	517.62	5.89
Feeding	88.17	100.00	87.94	77.54	8794.05	100.00
Grade Calculation						
Product	Mass	Density	V	V Barite	Mass Barite	Grade
	[g]	[g/cm3]	[cm3]	[cm3]	[g]	[%]
CP	15.18	4.34	3.50	3.30	14.62	96.32
IP	13.56	4.00	3.39	2.45	10.86	80.10
WP	10.00	3.43	2.92	1.03	4.57	45.68
Feeding	38.74	3.95	9.80	6.79	30.05	77.57

DL_{Barite} = 79.30 %

DL_{Waste} = 51.03 %

k = 0.315 – 0.5 mm:

Tab. 23: Balance Study, Electrostatic Separation, Barite, k=0.315-0.5mm

Balance Study, k = 0.315 - 0.5 mm						
Product	Mass	Yield	Grade	Content	Units	Recovery
	[g]	[%]	[%]	[g]	[%%}	[%]
CP	72.31	82.04	95.55	69.09	7838.99	87.23
IP	11.40	12.93	74.87	8.54	968.36	10.78
WP	4.43	5.03	35.75	1.58	179.70	2.00
Feeding	88.14	100.00	89.87	79.21	8987.05	100.00
Grade Calculation						
Product	Mass	Density	V	V Barite	Mass Barite	Grade
	[g]	[g/cm3]	[cm3]	[cm3]	[g]	[%]
CP	14.99	4.32	3.47	3.23	14.32	95.55
IP	11.36	3.90	2.91	1.92	8.51	74.87
WP	4.43	3.29	1.35	0.36	1.58	35.75
Feeding	30.78	3.99	7.72	5.51	24.41	79.31

Legend: CP Concentration Product, IP Intermediate Product, WP Waste Product

DL_{Barite} = 87.26 %

DL_{Waste} = 31.88 %

The products were further analyzed with a binocular microscope (Fig. 48 - 50):

k = 0.71 – 1 mm:

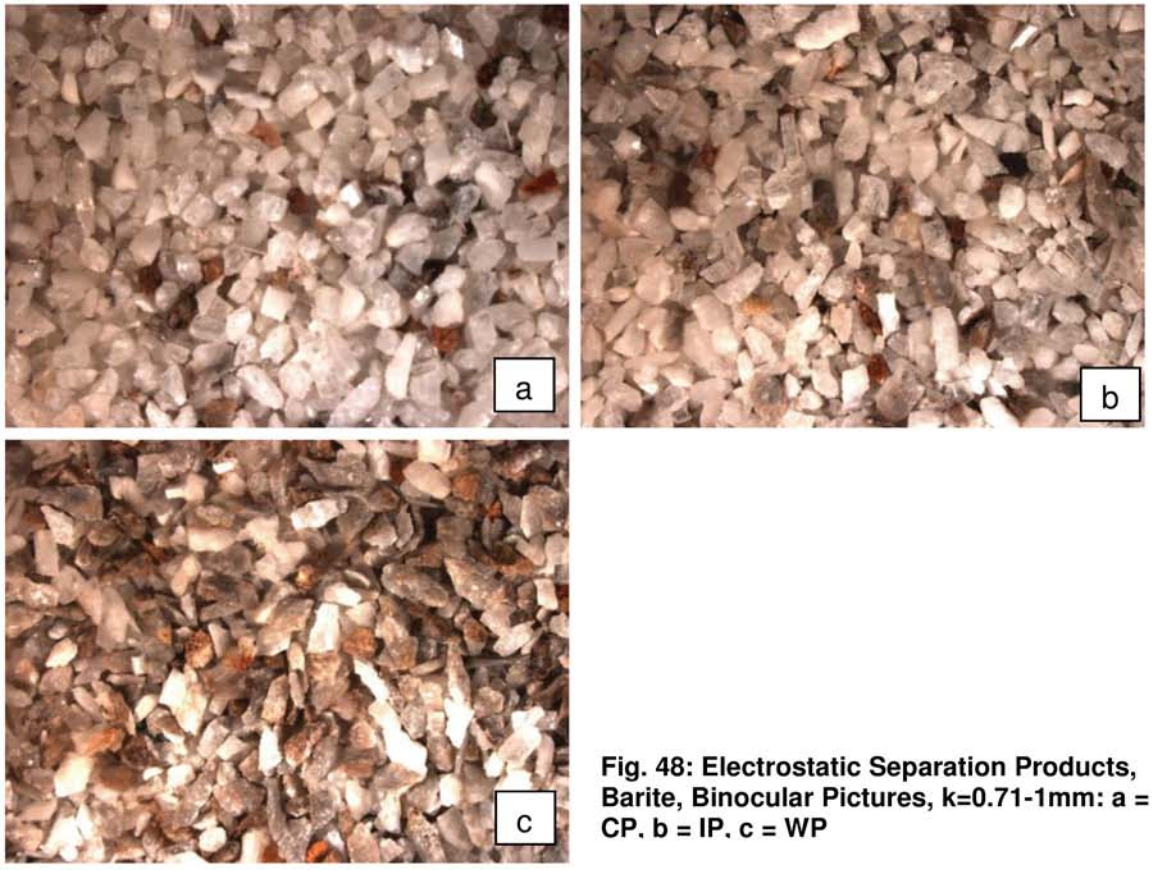

Fig. 48: Electrostatic Separation Products, Barite, Binocular Pictures, k=0.71-1mm: a = CP, b = IP, c = WP

k = 0.5 – 0.71 mm:

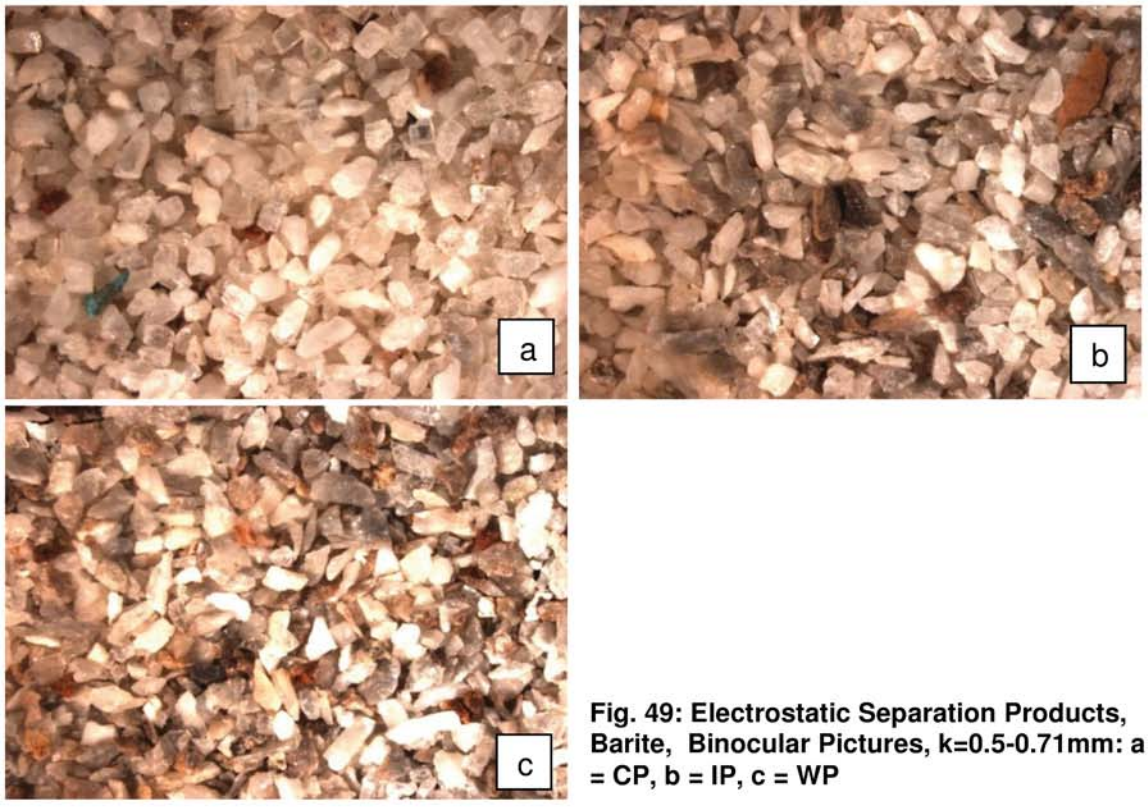

Fig. 49: Electrostatic Separation Products, Barite, Binocular Pictures, k=0.5-0.71mm: a = CP, b = IP, c = WP

k = 0.315 – 0.5 mm:

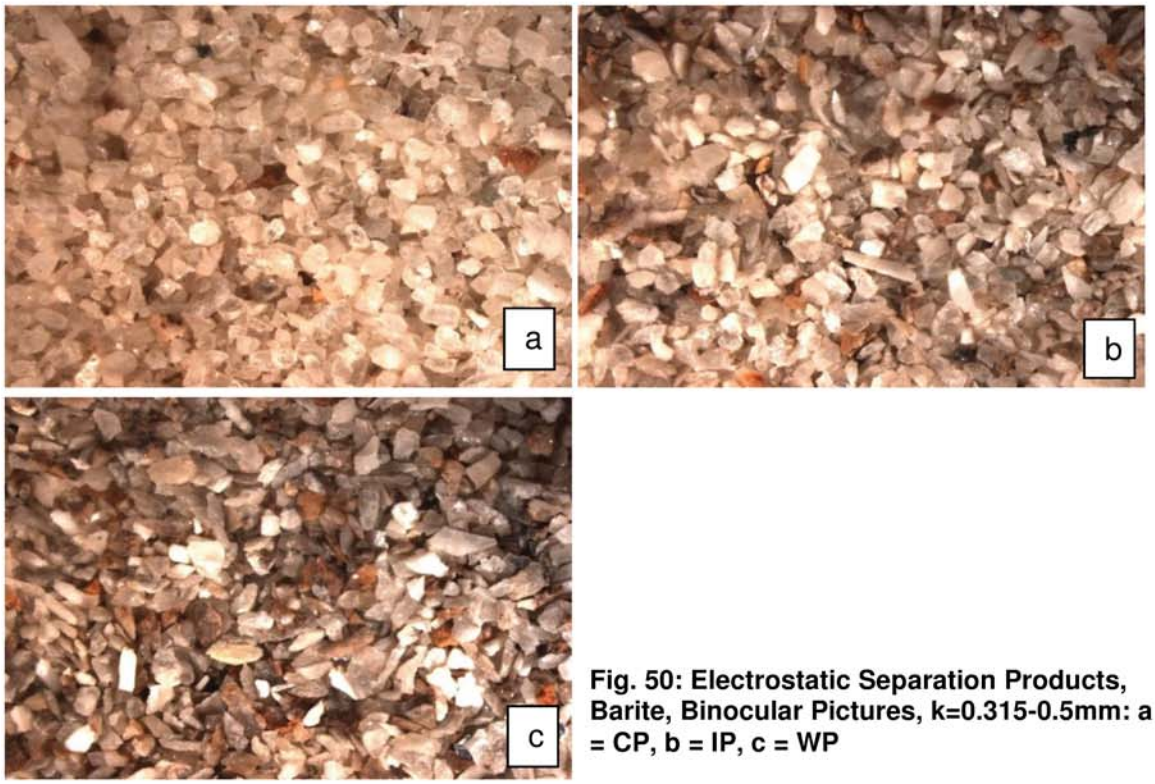

Fig. 50: Electrostatic Separation Products, Barite, Binocular Pictures, k=0.315-0.5mm: a = CP, b = IP, c = WP

Comments:

The products varied visibly in the amount of waste material. Although the magnetic grains were removed with a magnetic separator and a second cleaner stage, some hematite and malachite particles remained in the concentration product. The waste material consisted largely of dolomite and magnetic particles (Fig. 42-44). The recoveries of the concentration products were around 80 m% and differed widely from the intermediate product (around 15 m%). The grades of the concentration products were ca. 95 m% barite. The grades of the intermediate products were around 80 m% barite.

3.3.4.8 Shaking Table

The products for the grain sizes k = 0.71 – 1 mm, 0.5 – 0.71 mm and 0.315 – 0.5 mm were balanced (Tab. 24 – 26). The degree of liberation (DL) was calculated for each grain size class.

k = 0.71 – 1 mm:

Tab. 24: Balance Study, Shaking Table, Barite, k=0.71-1mm

Balance Study, k = 0.71 - 1 mm						
Product	Mass	Yield	Grade	Content	Units	Recovery
	[g]	[%]	[%]	[g]	[%%}	[%]
CP	66.96	70.86	97.92	65.57	6938.64	80.81
WP	27.54	29.14	56.55	15.57	1647.92	19.19
Feeding	94.50	100.00	85.87	81.14	8586.56	100.00
Grade Calculation						
Product	Mass	Density	V	V Barite	Mass Barite	Grade
	[g]	[g/cm3]	[cm3]	[cm3]	[g]	[%]
CP	16.25	4.38	3.71	3.59	15.91	97.92
WP	13.31	3.59	3.71	1.70	7.53	56.55
Feeding	29.56	3.98	7.42	5.29	23.44	79.29

DL_{Barite} = 80.81 %

DL_{Waste} = 19.19 %

k = 0.5 – 0.71 mm:

Tab. 25: Balance Study, Shaking Table, Barite, k=0.5-0.71mm

Balance Study, k = 0.5 - 0.71 mm						
Product	Mass	Yield	Grade	Content	Units	Recovery
	[g]	[%]	[%]	[g]	[%%}	[%]
CP	49.50	56.62	98.00	48.51	5548.29	62.26
WP	37.93	43.38	77.51	29.40	3362.74	37.74
Feeding	87.43	100.00	89.11	77.91	8911.04	100.00
Grade Calculation						
Product	Mass	Density	V	V Barite	Mass Barite	Grade
	[g]	[g/cm3]	[cm3]	[cm3]	[g]	[%]
CP	16.55	4.38	3.78	3.66	16.22	98.00
WP	14.29	3.95	3.62	2.50	11.08	77.51
Feeding	30.84	4.17	7.39	6.16	27.30	88.51

DL_{Barite} = 62.26 %

DL_{Waste} = 37.74 %

k = 0.315 – 0.5 mm:

Tab. 26: Balance Study, Shaking Table, Barite, k=0.315-0.5mm

Balance Study, k = 0.315 - 0.5 mm						
Product	Mass	Yield	Grade	Content	Units	Recovery
	[g]	[%]	[%]	[g]	[%%}	[%]
CP	51.19	59.11	98.13	50.24	5800.84	64.16
WP	35.41	40.89	79.25	28.06	3240.54	35.84
Feeding	86.60	100.00	90.41	78.30	9041.38	100.00
Grade Calculation						
Product	Mass	Density	V	V Barite	Mass Barite	Grade
	[g]	[g/cm3]	[cm3]	[cm3]	[g]	[%]
CP	16.55	4.38	3.78	3.67	16.24	98.13
WP	15.61	3.98	3.92	2.79	12.37	79.25
Feeding	32.16	4.18	7.69	6.46	28.61	88.97

CP = Concentration Product, WP = Waste Product, V = Volume.

DL_{Barite} = 64.16 %

DL_{Waste} = 35.84 %

The products were also analyzed with a binocular microscope (Fig. 51 - 53):

k = 0.71 - 1 mm:

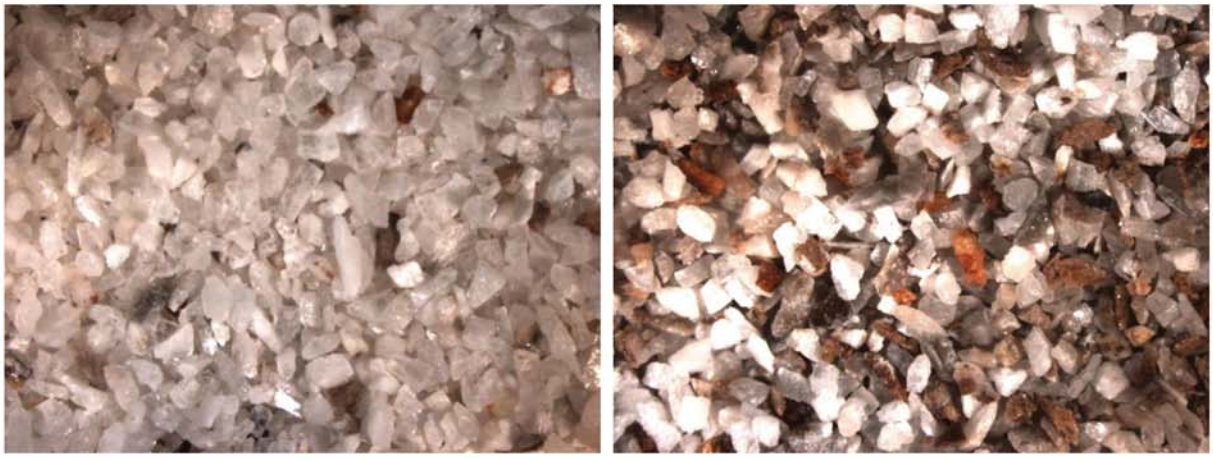

Fig. 51: Shaking Table Products, k=0.7-1mm: High Density (left), low density (right)

k = 0.5 – 0.71 mm:

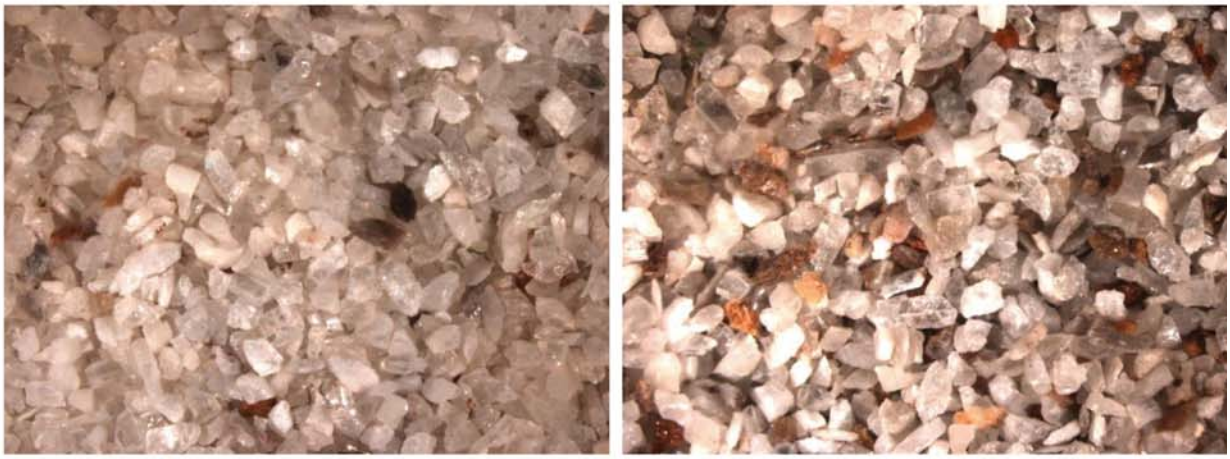

Fig. 52: Shaking Table Products, k=0.5-0.71mm: High Density (left), low density (right)

k = 0.315 – 0.5 mm:

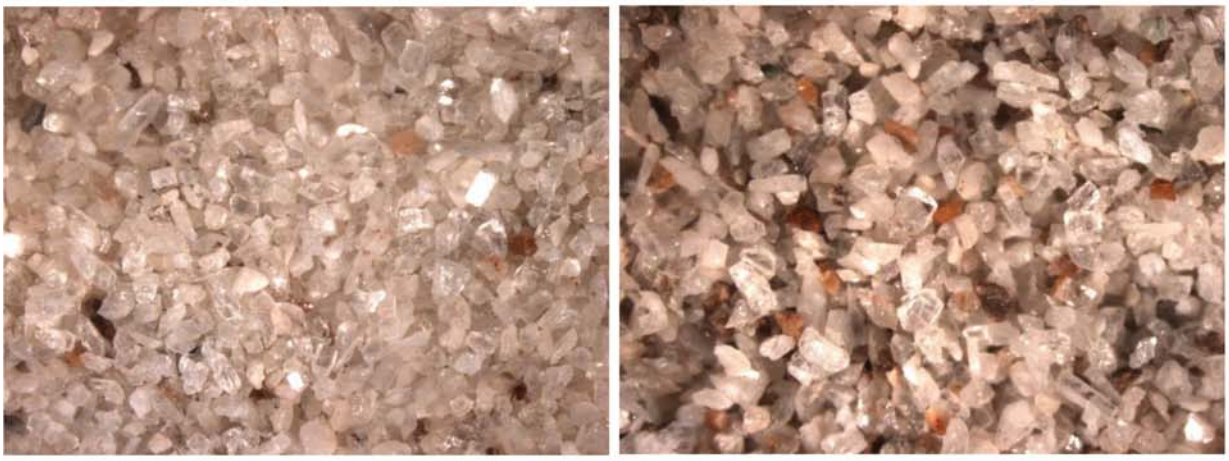

Fig. 53: Shaking Table Products, k=0.315-0.5mm: High Density (left), low density (right)

Comments:

The products varied visibly in the amount of waste material. Although the magnetic grains were removed with a magnetic separator, some hematite particles remained in the heavy density concentration product. The waste material with low densty consisted of dolomite, barite and hematite (Fig. 51 - 53). The grades of the concentration products were high (about 98 m% barite) however the recoveries were low (< 65 m%) for the fractions k = 0.5 – 0.71 mm and 0.315 – 05 mm. The degree of liberation, unusually decreasing directly proportional to smaller grain sizes, maybe was caused by the lamellas of the shaking table, which possibly were too high for small grains. Also the amount of feeding material was very little (around 30 g) making it hard to establish a separation equilibrium of the process.

3.4 Suitability Criteria for the Use as a Filler in Plastics; Discussion

Suitability criteria for the use as a filler in plastics are among others:

- A $BaSO_4$ grade of 88 – 94 m%
- A SiO_2 grade of < 3,0 m%
- No heavy metals
- A density of 4.1 – 4.3 g/cm^3
- A degree of brightness of 86 – 91 % (MgO standard)

[LORENZ AND GWOSDZ, 1988B]

Only properties tested are listed.

The criteria comparison with the hand samples AT-1A - E as a filler in plastics (Tab. 27):

Tab. 27: Criteria and Results for Barite as Filler in Plastics

	Criteria	AT-7A	AT-7B	AT-7C	AT-7D	AT-7E
chemical Composition (m %)						
BaSO4	88 - 94	105.43	76.34	86.60	90.51	93.06
SiO2	< 3.0	2.14	26.60	4.65	0.03	<0.01
Density (g/cm3)	4.1 - 4.3					
Brightness (%)						
MgO Standard	86 - 91					
Elrepho		90.38	88.46	86.35	72.70	95.56

Discussion:

The samples AT-7D and E reach the criteria as a filler in plastics considering the $BaSO_4$ grade. The brightness measurements were performed with a different measurement standard, but indicate which samples are of interest as a filler in plastics.

No chemical compositions of the mineral processing products and the collective sample AT-7K were analyzed as per the limited frame of this project. Instead the barite grades were calculated by a balance study, which cannot be compared to the grades of the chemical composition.

However, the barite of the collective sample AT-7K was assumed to be the same as the one of the samples AT-7C - E. The density of the pure barite from sample AT-7K is 4.43 g/cm^3, which fulfills the above criteria. With the best possible recovery of the barite form the raw material, the criteria as a filler in plastics can be achieved.

4. Pyrophyllite

4.1 Raw Material Characterization

4.1.1 General

4.1.1.1 Mineralogy, Petrology, Chemistry

Pyrophyllite is an anhydrous aluminum phyllosilicate ($Al_2O_3.SiO_2.H_2O$), similar in appearance to talc. In statistics it is often grouped with talc. The appearance in pure form is rare. Pyrophyllite has a micaeous habit, cleavage and feels greasy. [RIEGER 1997]. The crystal lattice is a dioctahedral three-layer structure, widely similar to the structure of talc. A reliable identification of pyrophyllite can only be assured by X-ray diffraction. [MATTHES 1996]. The density is 2.66 – 2.90 g/cm^3, the Mohs hardness is 1 - 1.5 [SCHUMANN 2007B]. A synonym is “Wonderstone”.

The chemical composition in pure form is:

SiO_2 = 66.7 m%

Al_2O_3 = 28.3 m%

H_2O = 5.0 m%

Pyrophyllite is hard to melt and loses its crystal-water when being annealed. It does not form single crystals, but fine scaly, radial aggregates, which are hard to be brought in pure form. [LORENZ AND GWOSDZ 2005A].

4.1.1.2 Genesis of Deposits

Pyrophyllite occurs in deposits, often as irregular or layered massive lenses and veins. Two formations of deposits, hydrothermal and metamorphic, can be distinguished: [LORENZ AND GWOSDZ 2005B]

- **Hydrothermal deposits** are most common and associated with acid to intermediate volcanism. Hydrothermal circulating fluids, originating from fault zones, alter rhyolite, dacite, andesite or feldspar/quartz-rich wall rock to pyrophyllite/quartz. The fluids enrich the rocks in Al content and deplete alkalis. It is common that the original rock structures are preserved. The pyrophyllite is often enriched in irregular lenses.

- **Metamorphic deposits** are rare and originate from metamorphosed volcanic ashes out of which pyrophyllite-schist is formed, which also can change to other metamorphic schists.

Pyrophyllite deposits often show different mineralization zones from the margin to the center:

- Quartz rich pyrophyllite
- Pyrophyllite
- Al rich minerals like alunite, diaspora, corundum, kaolinite.

[LORENZ AND GWOSDZ 2005B]

4.1.2 Methods of Raw Material Characterization

The raw material characterization is based on two samples of a pyrophyllite deposit in Parsovići, Bosnia and Herzegovina (Fig.54). Each sample comprises about 8 kg. The exact origin of the samples in the deposit and further details are unknown. The numbers of the samples are AT-1 (greenish) and AT-2 (purple). For the raw material characterization similar methods were applied as for the barite characterization (chapter 3.1). The samples AT-1 and AT-2 were used for the raw material characterization as well as for the mineral processing tests.

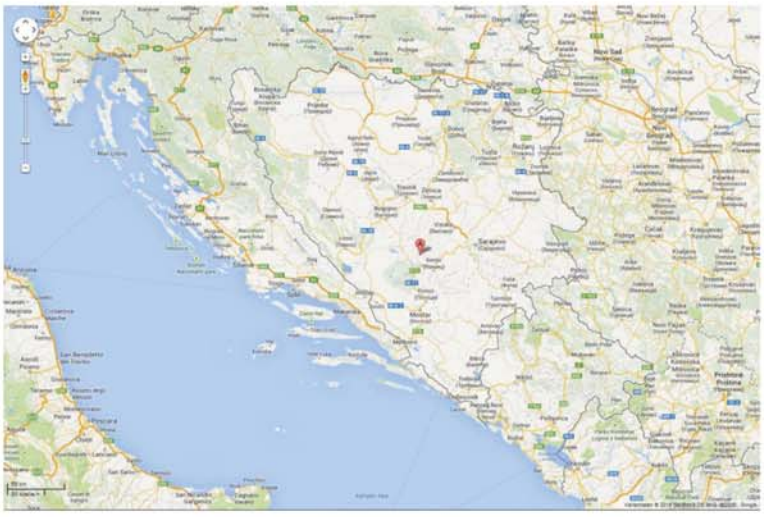

Fig. 54: Location A = Parsovići, Bosnia and Herzegovina. Source: Google Maps

4.1.2.1 Macroscopic Description

The samples were described by visual aspects. The focus was on color, grain size, impurities and fabric.

4.1.2.2 Transmitted Light Microscopy

For transmitted light microscopy thin sections of the samples AT-1 and AT-2 were produced. Further the heavy mineral concentrate (chapter 4.1.2.3) was analyzed by transmitted light microscopy. The procedure is described in chapter 3.1.2.2.

4.1.2.3 Heavy Mineral Analysis

To investigate the heavy minerals in the pyrophyllite, a heavy mineral concentrate was produces from sample AT-1 and AT-2. That for a part of the pyrophyllite sample was crushed manually and sieved into two grain size fractions: k = 0.125 – 0.250 mm and k = 0.250 – 0.500 mm. To separate the heavy minerals from the matrix, a heavy media was mixed using Sodium-Polytungstate ($Na_6[H_2W_{12}O_{40}]$) and demineralized water (Fig. 55a). The density of the solution was set to 2.92 g/cm^3 and filled into a separating funnel (Fig.55b). About 3 g of each grain size fraction was stirred with the heavy media (Fig. 55c) and allowed to rest for half an hour, then stirred again and resting thereafter for half an hour, until a clear separation was visible (Fig. 55d). Afterwards the heavy (density > 2.92 g/cm^3) and light fractions (density < 2.92 g/cm^3) were separated from each other and washed in a filter. Six thin sections of the grain concentrates were produced, using artificial resin.

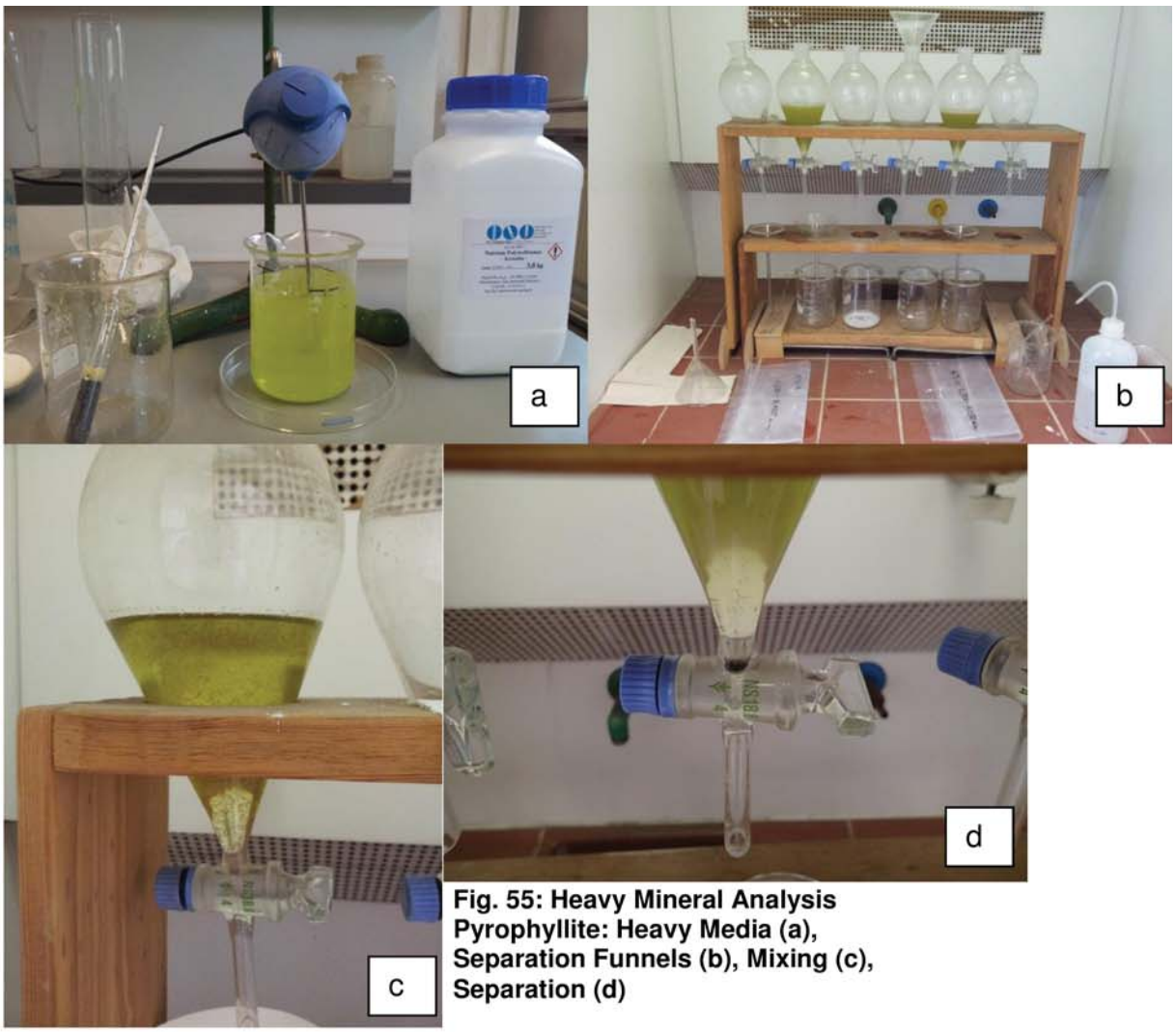

Fig. 55: Heavy Mineral Analysis Pyrophyllite: Heavy Media (a), Separation Funnels (b), Mixing (c), Separation (d)

4.1.2.4 Raman Spectroscopy

The Raman spectroscopy was used to identify small, opaque grains of the heavy mineral concentrate. The method and model are described in chapter 3.1.2.3.

4.1.2.5 X-Ray Diffractometry

To investigate the mineral composition of the pyrophyllite raw material and the mineral processing products, X-Ray Diffractometry (XRD) was applied. The raw material was evaluated by semiquantitative analysis after the Rietveld Method. The mineral processing products were not evaluated after Rietveld, due to large experimental uncertainties. The XRD analysis was carried out by the Institute for Mineralogy and Crystallography, Bulgarian Academy of Sciences.

4.1.2.6 Brightness Measurements

Brightness measurements were applied as qualitative criteria for the suitability as filler in plastics for the raw material samples AT-1 and AT-2 as well as for the mineral processing products. The sample preparation and the machinery are described in chapter 3.1.2.5.

4.1.2.7 Chemical Analysis

The samples AT-1 and AT-2 were chemically analyzed. The procedure is described in chapter 3.1.2.6.

4.1.3 Results of Raw Material Characterization

4.1.3.1 Macroscopic Description

The pyrophyllite sample AT-1 (Fig. 56, left) was of greenish-white color with some reddish layers. The fabric was foliated into ca. 3 mm thick layers. It felt greasy and soft. The grain size was very small (invisible). Some particles of the sample were not foliated, but contained unidentified coarser grains and they seemed crumbly. The sample AT-2 (Fig. 56, right) was of purple color and tightly foliated (<1 mm). It felt greasy, and soft, but more compact than sample AT-1. The grain size of AT-2 was very small (invisible).

Fig. 56: Handsamples: AT-1 (left), AT-2 (right)

4.1.3.2 Transmitted Light Microscopy

Sample AT-1:

The matrix was fine grained (<20 µm) and probably consisting of pyrophyllite. The fabric was densely foliated. Alternating layers of 1 mm thickness were pyrophyllite or quartz rich (Fig. 57a and Fig. 57b). Carbonate grains were rare and had a size up to 400 µm in diameter. Quartz was abundant in some areas (Fig. 57b) and could reach a maximum of 1mm. Some coarse rock fragments formed shear-clasts (Fig. 57c), which might indicate tectonic strain. Accessorily plagioclase and opaque grains appeared. To identify the pyrophyllite was not possible by microscopy but had to be carried out by X-ray diffraction. The identification of the carbonate (e.g. calcite, dolomite, etc.) was not possible in the frame of the project.

Sample AT-2:

The matrix was homogeneously and consisted of pyrophyllite. The fabric was densely foliated (<20 µm). Quartz grains were common and reached 100 – 200 µm, in exceptional cases up to 3 mm. Carbonate was far more abundant than in the sample AT-1 and appeared as calcite. Some coarse rock fragments formed shear-clasts, which might indicate tectonic stain. Accessorily plagioclase and opaque grains appeared. Some of the opaque grains gleamed reddish. They possibly were hematite, which could also contribute to the purple color. The identification of the pyrophyllite and calcite was not possible by microscopy and had to be carried out by X-ray diffraction.

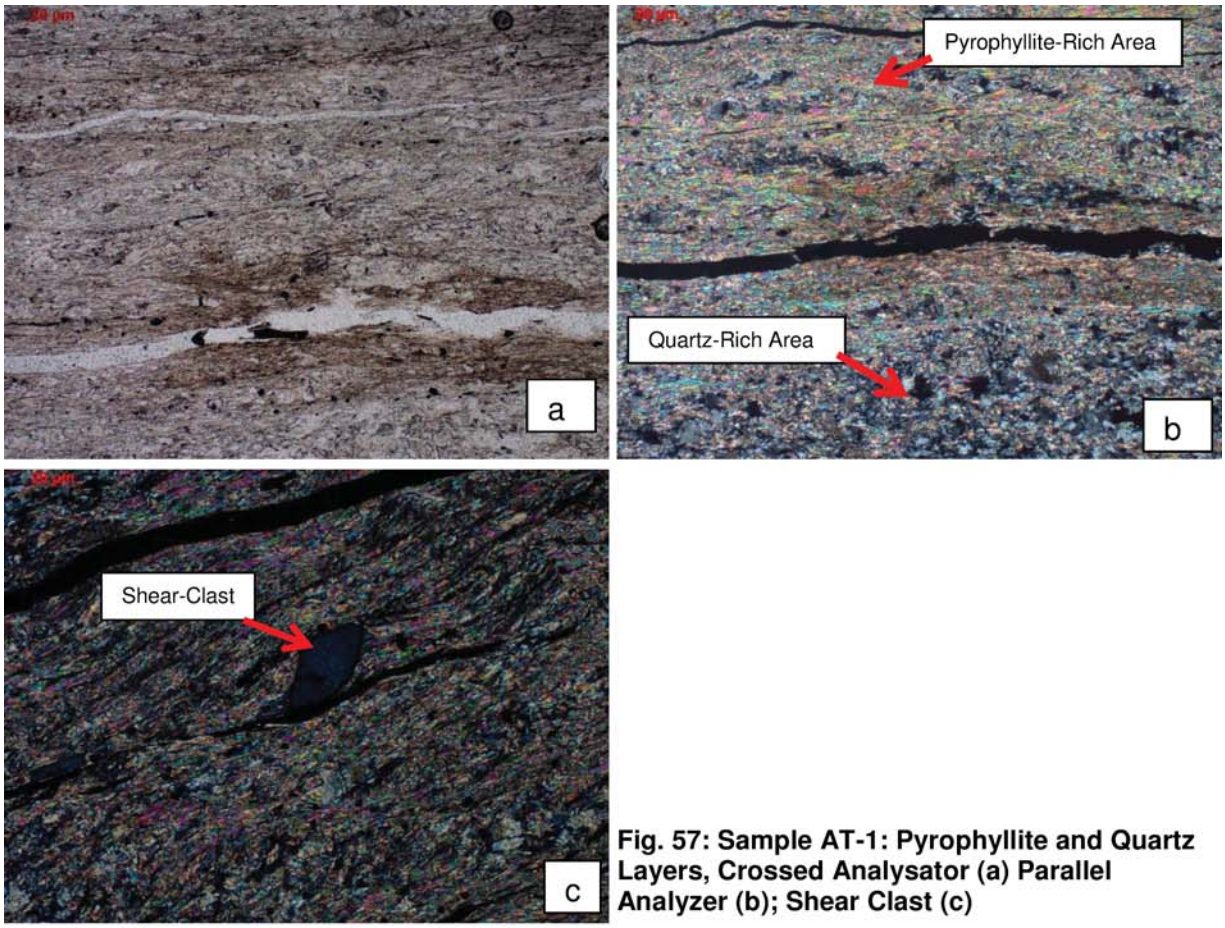

Fig. 57: Sample AT-1: Pyrophyllite and Quartz Layers, Crossed Analysator (a) Parallel Analyzer (b); Shear Clast (c)

4.1.3.3 Heavy Mineral Concentrate

The heavy mineral concentrates of the samples AT-1 and AT-2 were investigated by transmitted light microscopy and Raman spectroscopy.

AT-1:

Both grain sizes (k = 0.125 – 0.250 mm and k = 0.250 – 0.500 mm) showed the same composition in the concentrate. The main mineral phases were apatite and pyrite (Fig. 58a). Some rock fragments, which were no heavy minerals, remained in the concentrate.

AT-2:

Both heavy mineral concentrate tests using the grain sizes (k = 0.125 – 0.250 mm and k = 0.250 – 0.500 mm) failed. The entire feeding sank to the bottom of the separating funnel, although the density of the heavy media was checked as ρ = 2.9 g/cm^3. A possible reason might have been oxide crusts on the surface of the rock fragments, but no reliable evidence or explanation was found. The thin section mainly showed rock fragments (Fig. 58b). One zircon was found.

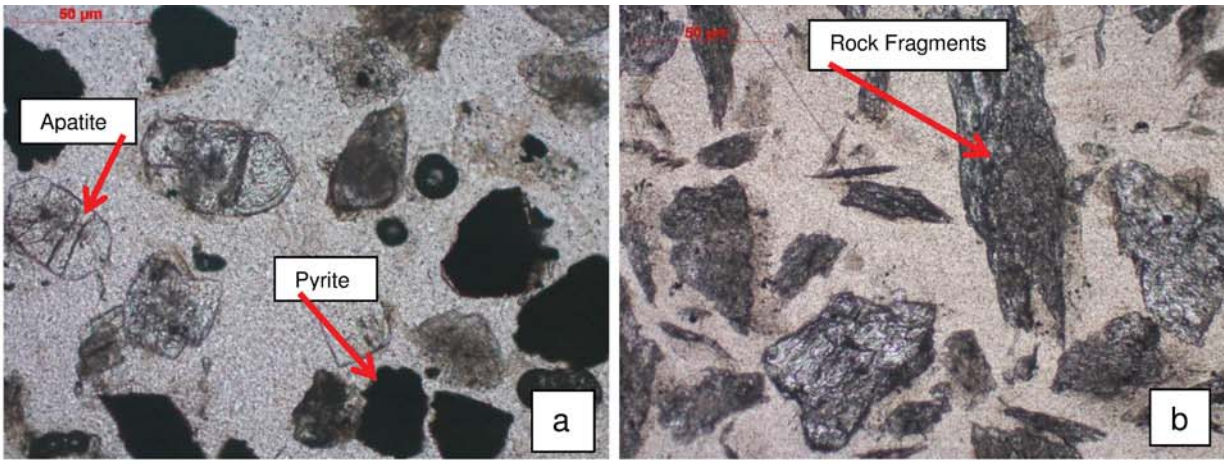

Fig. 58: Heavy Mineral Concentrates, Parallel Analyzer: AT-1 (a), AT-2 (b)

4.1.3.4 X-Ray Diffractometry

Only the results for the raw material are listed. The results of the mineral processing products are listed in chapter 4.2.4.4. The semiquantitative results may reflect experimental uncertainties due to the crystal orientation of the flaky minerals. Unexpectedly the raw material probes analyzed by the Institute for Mineralogy and Crystallography, Bulgarian Academy of Sciences showed chabazite, which could not be verified in the XRD analysis of the mineral processing products. The spectra are listed in the appendix (Fig. 71 and 72).

AT-1: (Tab. 28 and Fig. 59)

Tab. 28: Mineral Composition AT-1

Mineral	%
Pyrophyllite	48.7
Quartz	43
Chabazite	8.3

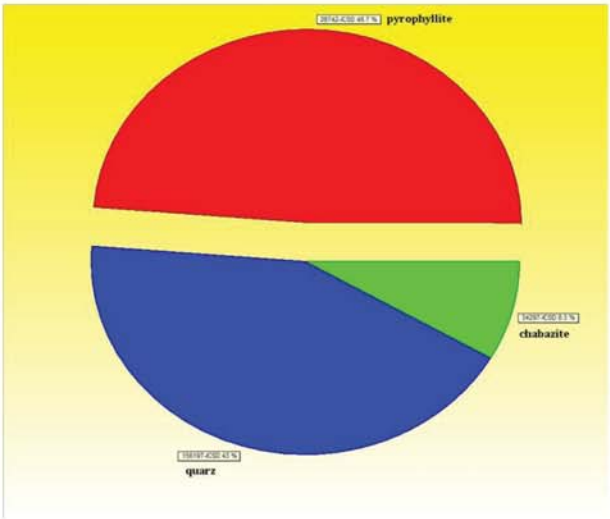

Fig. 59: Mineral Composition AT-1

The quartz and pyrophyllite content correlated with the content found using transmitted light microscopy. Chabazite was absent in all thin sections.

AT-2: (Tab.29 and Fig. 60)

Tab. 29: Mineral Composition AT-2

Mineral	%
Calcite	41.2
Quartz	36.8
Pyrophyllite	21.5
Chabazite	0.5

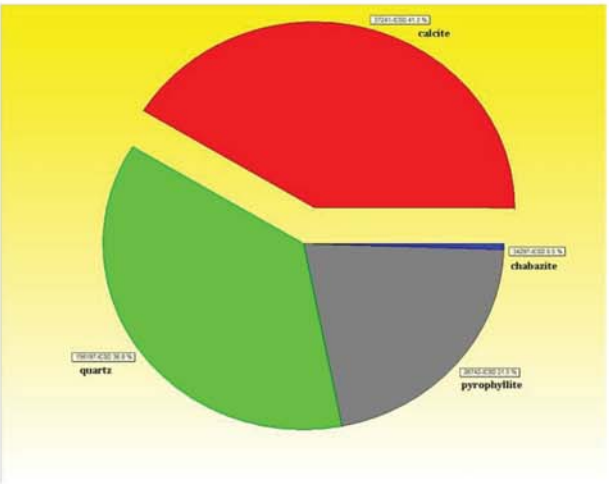

Fig. 60: Mineral Composition AT-2

The calcite, quartz and pyrophyllite content correlated with the transmitted light microscopy. Chabazite was absent in all thin sections.

4.1.3.5 Brightness Measurements

Only the results for the raw material are listed. The results of the mineral processing products are listed in chapter 3.2.4.

Sample **AT-1** had a Y-axis value of **81.18 %** and sample **AT-2** had a Y-axis value of **72.29 %** according to Elrepho standard.

4.1.3.6 Chemical Analysis

The results of the chemical analysis are listed in Tab. 30 – 32:

Tab. 30: Chemical Analysis of Pyrophyllite, g/100g, AT-1 and AT-2

Element	Sample	
	AT-1	AT-2
g/100g		
Na2O	0.12	0.42
MgO	1.61	0.89
Al2O3	15.28	14.64
SiO2	66.16	65.46
P2O5	0.057	0.054
SO3	0.39	0.14
K2O	0.25	1.27
CaO	5.19	4.55
TiO2	0.13	0.12
Cr2O3	<0.01	<0.01
MnO	0.04	0.01
Fe2O3	1.1	0.97
LOI	9.06	7.43
TOTAL	99.39	95.95

Tab. 31: Chemical Analysis of Pyrophyllite, mg/kg, AT-1

Element	Sample	Element	Sample
	AT-1		AT-1
mg/kg		mg/kg	
Sc	7.6	Ce	4.09
V	5.6	Pr	1.47
Cr	3.2	Nd	5.99
Co	4.9	Sm	1.07
Ni	12	Eu	0.32
Cu	8.5	Tb	0.09
Zn	35	Gd	0.79
Ga	15	Dy	0.45
Rb	1.19	Ho	0.08
Sr	162	Er	0.22
Y	2.44	Tm	0.03
Zr	76	Yb	0.22
Nb	<10	Lu	0.03
Ba	66	Pb	8.18
La	5.12	Th	0.74

Tab. 32: Chemical Analysis of Pyrophyllite, mg/kg, AT-2

Element	Sample	Element	Sample
	AT-2		AT-2
mg/kg		mg/kg	
Sc	7.3	**Ce**	3.23
V	4.1	**Pr**	7.06
Cr	2.6	**Nd**	0.55
Co	<1	**Sm**	0.00
Ni	<10	**Eu**	1.18
Cu	<5	**Tb**	4.84
Zn	17	**Gd**	0.93
Ga	15	**Dy**	0.31
Rb	4.93	**Ho**	0.08
Sr	234	**Er**	0.67
Y	2.13	**Tm**	0.41
Zr	68	**Yb**	0.07
Nb	<10	**Lu**	0.18
Ba	147	**Pb**	0.03
La	4.07	**Th**	0.19

4.2 Mineral Processing

The aims were a best possible enrichment of pyrophyllite in the products and a best possible removal of accompanying minerals like quartz and calcite.

The crushed raw material was processed by attrition. The attrition products were divided into two grain size fractions. The coarse grain material was directly analyzed in regard to impurities and the fine grain fraction was continuatively processed by flotation. The flotation resulted in two froth products and a residual product. To qualify and quantify the success of mineral processing procedures, several analytical methods were applied. Among these were: X-ray diffraction, brightness measurements, loss of ignition and acid solubility (chapter 4.2.2.).

4.2.1 Methods of Mineral Processing

4.2.1.1 Crushing

The samples AT-1 and AT-2 were crushed manually in a cycle to a maximum grain size of 6 mm, using a hammer and a sieve with 6 mm mesh size. The resulting

products were analyzed by X-ray diffraction, ignition loss and content of acid-soluble minerals.

4.2.1.2 Attrition

The process of attrition-grinding is an intense agitation of a slurry containing raw material, a granular medium and a suspending fluid. Granular medium is not necessary in all applications and was not used in this particular experiment. [FELD ET AL. 1960]. The attrition machine was a "WEMCO Fagergren Mineral-Master", serial: 8-5035-50CY, size: 600 (Fig. 61). Basically it consisted of a steal cylinder containing the slurry and a motor driven rotator.

As a suspending fluid, demineralized water was used. The solid content of the slurry was 70 m%. The rotation speed was set at 1150 rpm. The feeding consisted of 700 g pyrophyllite (grain size k < 6.0 mm) and 300 g demineralized water. The duration of the attrition process was 3 min for sample AT-1, and 4 min for sample AT-2. The agitated raw material was wet-sieved resulting in two products of grain size fractions k = 0 – 0.1 mm and k = 0.1 – 6 mm. The products were weighted, analyzed by X-ray diffraction, ignition loss, brightness measurements and content of acid-soluble minerals. Furthermore the products < 100 µm were processed by flotation.

Fig. 61: WEMCO Attrition Cell

4.2.1.3 Flotation

A flotation process is characterized by adherence of the grains to be removed to gas- or oil bubbles. The dynamics of the separation process are determined by the properties of the grains, especially their surface properties. For the selective adherence of the mineral grains to the gas bubbles a hydrophobic grain surface is crucial. In a foam flotation process, the slurry is exposed to turbulent flow conditions causing grain-bubble aggregates, which ascend if their density is lower than the density of the slurry and then can be removed as froth product (Fig. 62a). [SCHUBERT 1986F]. As the hydrophobic grains adhere to froth, a frother needs to be added to the slurry. [SCHUBERT 1986G].

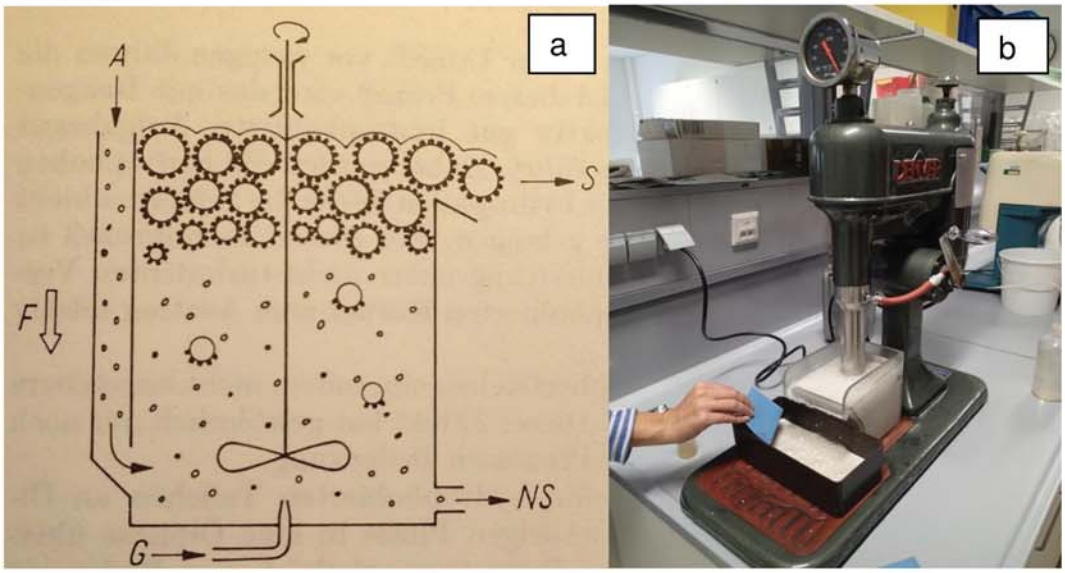

Fig. 62: Principle of a Flotation [Schubert 1986f]: A Feeding, F Gravity, G Air, S Froth Product, NS Residual Product (a), "Denver" Flotation Cell (b)

In this experiment (Fig. 62b), MIBC (methylisobutylcarbinol) was used as foaming agent. The solid content was about 10 m% and the volume of the flotation cell was 1421 ml. The feeding was processed in a rougher cell to a froth product 1 and a residual product 1. The residual product 1 then was separated in a scavenger cell into a froth product 2 and a residual product 2 (waste) (Fig. 63). Both samples were processed according to the flotation protocols (Tab. 33 and 34). The products then were weighted, analyzed by X-ray diffraction, ignition loss, brightness measurements and content of acid-soluble minerals.

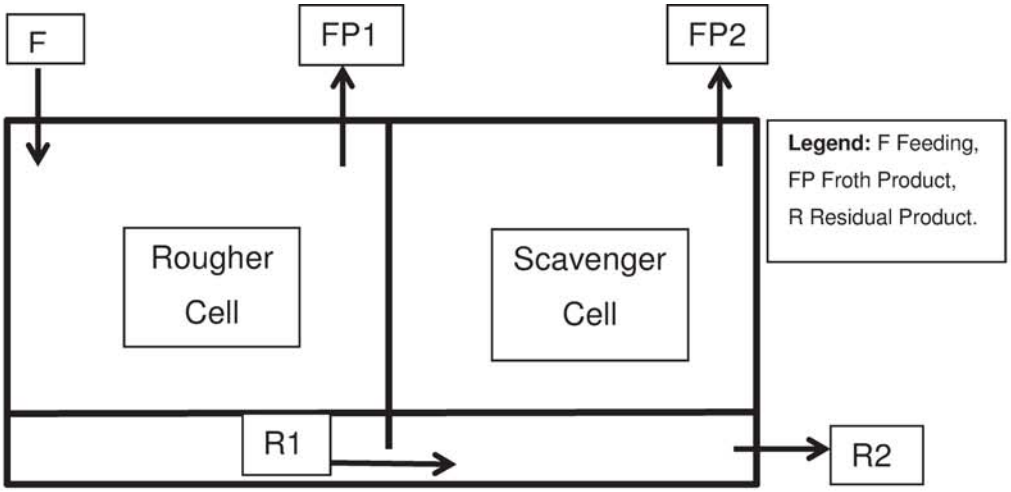

Fig. 63: Flow Sheet Flotation of Pyrophyllite

Tab. 33: Flotation Record: Sample AT-1

Flotation Record: AT-1	
Time [min]	**Action**
0	Filling: 123g Feeding, 1249 g H2O
1	Stirring, Homogenization, 1700 rpm
2	1.5 Drops of Frother (≈ 0.8 g / l H2O)
4	Air (half open)
6	Air (fully open)
7.5	Air off (39 l)
	1 Drop of Frother (≈ 0.6 g / l H2O)
	Remove Froth Product 1 (FP1-AT1)
9.5	Air (fully open)
23.25	Air off (153 l)
	Stirring off
	Remove Froth Product 2 (FP2-AT1)
	Remove Residual Product 2 (RP2-AT1)

Tab. 34: Flotation Record: Sample AT-2

Flotation Record: AT-2	
Time [min]	**Action**
0	Filling: 115 g Feeding, 11229 g H2O
	Stirring, Homogenization, 1700 rpm
1	1 Drop of Frother (≈ 0.6 g / l H2O)
2	Air (half open)
3	Air (fully open)
7	Air off (26 l)
	1 Drop of Frother (≈ 0.6 g / l H2O)
	Remove Froth Product 1 (FP1-AT2)
7.5	Air (fully open)
12	Air off (45 l))
	Stirring off
	Remove Froth Product 2 (FP2-AT2)
	Remove Residual Product 2 (RP2-AT2)

During the flotation of sample AT-2 the stirrer probably was not fully working, therefore the froth product 1 possibly had less, but more refined output.

4.2.2 Methods for the Determination of the Mineral Processing Success

The products of the mineral processing tests were analyzed, concerning their change in mineral composition, especially the enrichment of pyrophyllite. All products of the crushing, the attrition and the flotation tests were analyzed. The analysis methods to quantify/qualify the products were: Acid solubility, loss of ignition, brightness measurements and X-ray diffraction.

4.2.2.1 Acid Solubility

To determine the mass percentage of acid-soluble minerals in the mineral processing products, the material was boiled in diluted hydrochloric acid. Pyrophyllite is inert to diluted acid. The following method is a non-standardized, but industrially common material test.

Procedure:

- Weight in 1 g, accuracy ± 0.0001 g of the sample
- Mix a 1% hydrochloric acid

- Fill 1 g sample and 100 ml diluted acid in a 250 ml beaker glass
- Stir with a glass rod
- Boil the suspension together with the glass rod for 20 min (Fig. 64)
- Filter off the solution
- Wash the filtrate thoroughly with demineralized water
- Dry the filtrate at 105 °C until constant weight
- Weight out the filtrate

For more accurate results the filtrate was weighted together with the filter paper. Each filter paper was previously dried and weighted and this weight was later subtracted from the filtrate weight. To minimize measurement errors, three filter papers were used as blank samples with no suspension in it, but flushed with the acid. The average error of the blank sample weights was considered in the calculation.

The calculation formula of the percentage of acid-soluble components is:

$$\text{Soluble Components [m\%]} = \frac{\text{(Weight Out Filtrate – Weight Out Filter Paper ± Average Error) [g]}}{\text{Weight In Sample [g]}} * 100$$

Fig. 64: Boiling Diluted Acid and Samples of Pyrophyllite Processing Products

4.2.2.2 Loss of Ignition

The loss of ignition (LOI) is used to determine the mass variation of certain volatile mineral phases due to changes in the chemical composition. In the case of sample AT-1 and AT-2 the mass changes resulted from the loss of water from the pyrophyllite and the chabazite and the loss of CO_2 from the calcite. The mass

variation cannot be contributed to a specific mineral phase however the loss of ignition is a common material test in industry.
The procedure is slightly modified after DIN 51081:

- Pestle the samples to an approximate grain size < 100 µm
- Dry the samples at 105 °C until constant weight
- Pre-ignite the crucibles for cleaning
- Weight the empty crucibles
- Weight-In 5 g (accuracy ± 0.0001 g) of the dry sample
- Put the filled crucibles in the oven
- Heat up the oven to 1050 °C
- Anneal the samples until constant weight
- Weight-Out the cool crucibles
- Subtract the weight of the crucibles from the weight-out

Calculation Formula:

$$\text{Volatile Components [m\%]} = \frac{\text{(Weight-Out Crucible/Sample – Weight-Out Crucible) [g]}}{\text{Weight-In Sample [g]}} * 100$$

4.2.2.3 Brightness Measurements

The brightness of the mineral processing products of sample AT-1 and AT-2 was measured to detect brightness variations in different stages of the mineral processing and to gain information about the suitability of the products as filler for plastics. The brightness does not need to increase with increasing pyrophyllite content, if the pyrophyllite itself is not white. The procedure is described in chapter 3.1.2.5.

4.2.2.4 X-Ray Diffractometry

To investigate the mineral composition of the mineral processing products, X-Ray diffraction (XRD) was applied. The XRD analysis was carried out by the Institute for Mineralogy and Crystallography, Bulgarian Academy of Sciences. Due to several issues concerning the crystal orientation of muscovite, chlorite and kaolinite, no quantifications of the samples were possible. Only the spectra with the mineral phases are shown. However they give little information about the content of flaky minerals in the samples.

4.2.3 Flow Sheet

The flow sheet of the pyrophyllite processing is shown in Fig. 65.

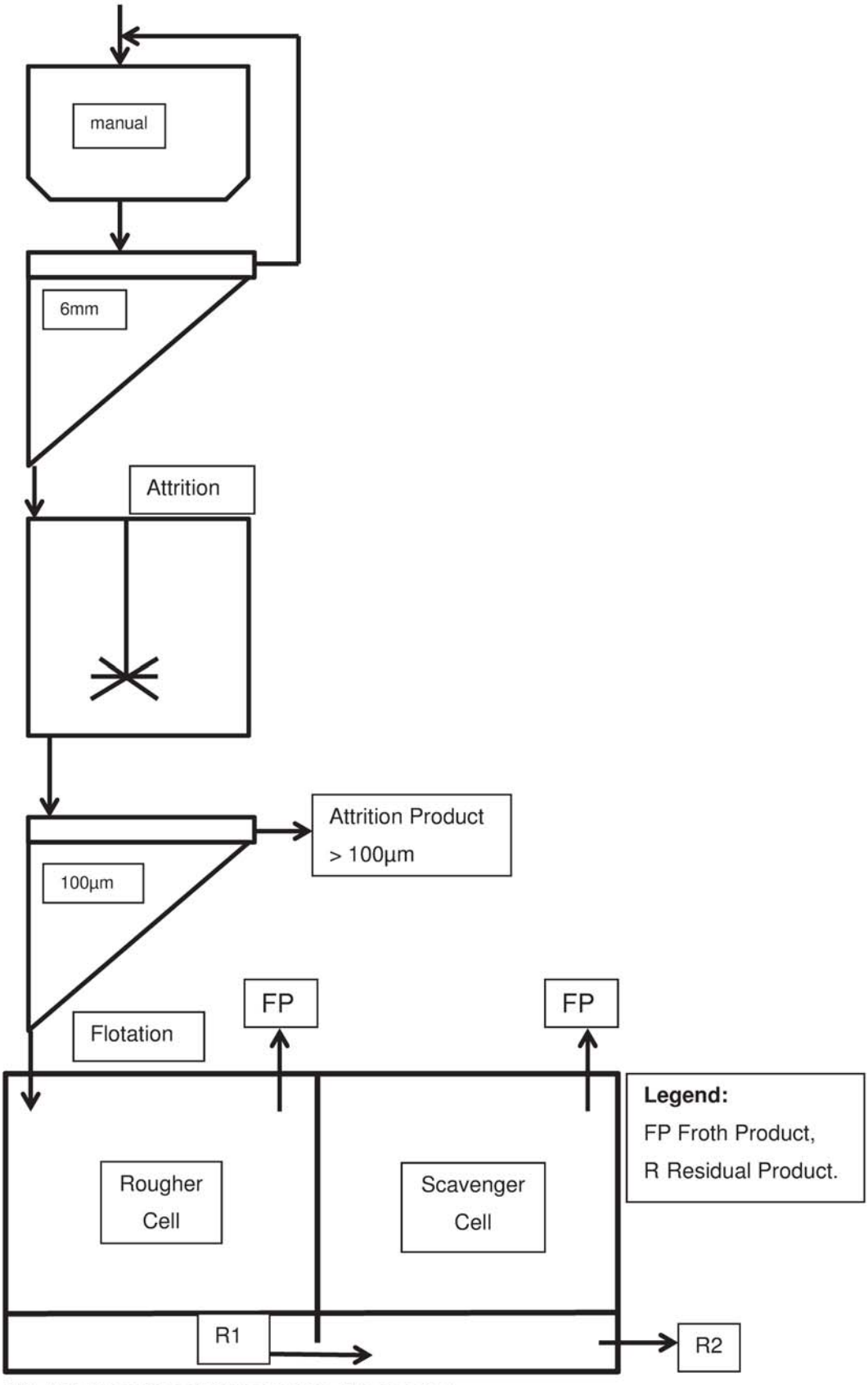

Fig. 65: Flow Sheet Pyrophyllite Processing

4.2.4 Results of Mineral Processing and Comments

The results of the mineral processing tests were obtained using the methods listed in chapter 4.2.2. The calculation tables (Tab. 53 and 54) and the X-ray spectra are listed in the appendix.

4.2.4.1 Crushing

The results of crushed material with mesh size < 6mm are listed in Tab. 35:

Tab. 35: Results Crushing of Pyrophyllite, < 6 mm

Sample	Acid Solubility	LOI	Brightness
	[m%]	[m%]	[%]
AT-1	12.28	1.89	81.18
AT-2	11.15	2.97	72.29

The XRD spectra of the crushed material mesh size < 6mm are listed in the appendix (Fig. 73). Sample AT-1 comprises quartz and pyrophyllite in the major phases and dolomite, calcite and kaolinite in the minor phases. The major phases of sample AT-2 are quartz and pyrophyllite, the minor phases are dolomite, muscovite, calcite, chlorite and kaolinite.

Comments:

The XRD results of the raw material samples did not correlate with the XRD results of the fraction of grain size < 6 mm in all mineral phases.

4.2.4.2 Attrition

The attrition process divided each sample into two products. The products of grain size < 0.1 mm were numbered “AT-1<0.1” and “AT-2<0.1”. The products of grain size 0.1 – 6 mm were numbered “AT-1>0.1” and “AT-2>0.1”. The results are listed in Tab. 36.

Tab. 36: Results of Attrition of Pyrophyllite

Sample	Acid Solubility	LOI	Brightness
	[m%]	[m%]	[%]
AT-1<0.1	7.73	1.58	76.71
AT-1>0.1	17.98	5.32	
AT-2<0.1	7.41	1.87	64.09
AT-2>0.1	12.94	4.6	

The XRD spectra of the attrition process products are listed in the appendix (Fig. 74 and 75). The grain size fraction < 100 µm of sample AT-1 contained pyrophyllite and quartz as major phases and kaolinite, dolomite and muscovite as minor phases. The grain size fraction > 100 µm comprised major phases of quartz and dolomite and minor phases of pyrophyllite, calcite and kaolinite.
The grain size fraction < 100 µm of sample AT-1 contained quartz and pyrophyllite as major phases and muscovite, chlorite and kaolinite as minor phases. The grain size fraction > 100 µm comprised a major phase of quartz and minor phases of pyrophyllite, dolomite, calcite, muscovite and kaolinite.
Quartz and dolomite were enriched in the coarse fractions of both samples. Still, the fine fractions of both samples contained quartz.

Comments:
The acid solubility of the fine (k< 0.1 mm) products was significantly lower than that of the coarse (k> 0.1 mm) products. A concentration of inert pyrophyllite in the fine product can be reached by attrition. The LOI was higher in the coarse products. This can be contributed to a carbonate content. An improvement of the brightness compared with the raw material (AT-1: 81.18 % and AT-2: 72.29 %) could not be achieved. The XRD spectra showed significant variations of the pyrophyllite content between the concentration product (k< 100 µm) and the coarse product (> 100 µm). A pyrophyllite enrichment in the fraction k < 100 µm was obvious. As an additional purifying process, the remaining quartz in the fractions k < 100 µm can be removed by further screening with smaller mesh sizes.
The fine product of sample AT-1 showed a little higher pyrophyllite content and a higher brightness, than the fine product of sample AT-2.

4.2.4.3 Flotation
The flotation process resulted in three products for each sample of k < 0.1 mm mesh size. The samples were named “FP1” for the froth products of the rougher cell, “FP2” for the froth products of the scavenger cell and “R” for the residual products. The results are listed in Tab. 37.

Tab. 37: Results Flotation of Pyrophyllite

Sample	Acid Solubility	LOI	Brightness
	[m%]	[m%]	[%]
FP1-AT1	7.61	2.92	76.68
FP2-AT1	5.29	1.52	77.73
R-AT1	18.52	1.66	73.46
FP1-AT2	5.38	1.29	65.71
FP2-AT2	3.95	2.17	66.44
R-AT2	8.37	2.27	56.40

The XRD spectra of the flotation products are listed in the appendix (Fig. 76 and 77).

The mineral composition of the flotation process (Tab.38):

Tab. 38: Mineral Phases of Flotation Products of Pyrophyllite

AT-1		
FP1	**FP2**	**R**
Pyrophyllite	Pyrophyllite	Pyrophyllite
Quartz	Quartz	Quartz
Muscovite	Muscovite	Muscovite
Kaolinite	Kaolinite	Chlorite
Dolomite	Dolomite	Kaolinite
	Calcite	Dolomite
AT-2		
FP1	**FP2**	**R**
Pyrophyllite	Pyrophyllite	Pyrophyllite
Quartz	Quartz	Quartz
Muscovite	Muscovite	Muscovite
Chlorite	Chlorite	Chlorite
Kaolinite	Kaolinite	Kaolinite
	Calcite	Dolomite
		Calcite

FP1 Froth Product 1, FP2 Froth Product 2, R Residual Product

Sample AT-1 showed only marginal differences in the mineral phases. Major phases in all products were pyrophyllite and quartz.

Sample AT-2 showed clear differences between the froth products and the residual product. In this case, it was possible to enrich the pyrophyllite and decrease the quartz in the froth product.

Comments:

The acid solubility varied significantly between the froth products and the residual products. The froth products of the scavenger cell showed the best results with the lowest concentrations of soluble components. The highest concentrations of soluble components were in the residual products. The results of the loss of ignition did not show a clear trend, however the high LOI of the froth product 1 of AT-1 indicated high pyrophyllite content. The high LOI of the residual product of AT-2 may indicate that there was still plenty of pyrophyllite in the residue. The brightness measurements correlated with the acid solubility. The scavenger cell foam products showed the highest Y-axis values, the residue showed the lowest values. The XRD results for the froth products indicated a higher pyrophyllite content of AT-2 compared to AT-1. Both residual products still showed high pyrophyllite concentrations. The separation by flotation of sample AT-1 was not successful in this particular case. Further investigations, like finer screening and more flotation tests are advisable to reach a higher purification of the pyrophyllite.

4.3 Suitability Criteria for the Use as Filler in Plastics and Discussion

4.3.1 Suitability Criteria as Filler in Plastics

The criteria for the use as filler in plastics are not generally standardized and vary from producer to producer. However, some industrial benchmarks are listed in LORENZ AND GWOSDZ 2005C:

4.3.1.1 Raw Material Requirements

LORENZ AND GWOSDZ 2005C published some benchmarks for the use of Australian raw pyrophyllite as filler in plastics:

	[m%]
Al_2O_3	24 – 28
K_2O	0.2 – 0.5
Fe_2O_3	0.2

Conclusion:

Both raw material samples did not meet the suitability criteria because of too low Al_2O_3 contents.

4.3.1.2 Mineral Composition of Processed Pyrophyllite

As filler in plastics, only flaky minerals can be used. Minerals with cubic or similar habits are not suitable. Pyrophyllite as filler in plastics should not contain quartz [LORENZ AND GWOSDZ 2005C].

Conclusion:

The mineral processing products of both samples did contain certain amounts of quartz. They did not fulfill the suitability criteria.

4.3.1.3 Brightness

For the use as filler in plastics, the brightness (GE brightness) of the processed pyrophyllite should be 80 – 90 % [LORENZ AND GWOSDZ 2005C].

Conclusion:

Only the raw material sample of AT-1 fulfilled this suitability criterion with a brightness of 81.18 % (ELREPHO Standard). All the other samples and mineral processing products did not meet this criterion, possibly because the pyrophyllites' brightness was less than that of the foreign minerals.

4.3.2 Discussion

The results of the particular tests applied, classified both samples (AT-1 and AT-2) from Parsovići, Bosnia and Herzegovina, as unsuitable to be used as filler in plastics. Additional methods to purify pyrophyllite, such as finer milling, finer sieving and gravity separation may have led to different conclusions. However, these additional methods were beyond the scope of this study.

List of Figures

List of Tables

Literature

CLARK S. H. B., GALLAGHER M. J., POOLE F. G., 1990: World barite resources: a review of recent production patterns and a genetic classification. – Trans. Instn. Min. Metall. 99: B125-132.

FELD I.L., MCVAY T.N., GILMORE H.L., CLEMMONS B.H., 1960: Paper-Coating Clay from Coarse Georgia Kaolins by a New Attrition-Grinding Process. BuMines RI 5697. 6f.

FRIMMEL H.E., PAPESCH W., 1990: Sr, O and C isotope study of the Brixlegg barite deposit, Tyrol (Austria).– Economic Geology, 85, 1162–1171

GRIM R. E., GÜVEN N., 1978: Bentonites. Geology, Mineralogy, Properties and Uses. Developments in Sedimentology 24. Elsevier Amsterdam – Oxford – New York. 76.

I.B.O. Ingenieurbüro für Bentonit-Technologie Dipl.-Ing. Ohrdorf, Wiesbaden, Deutschland.I.B.O. 01 / 2003 I.B.O. FP-03/2003

Institute for Mineralogy and Crystallography, Bulgarian Academy of Sciences, 107 Acad. G. Bonchev str., Sofia 1113, Bulgaria.

JURKOVIĆ I., 1996: Barite, hematite and cinnabar ore deposits in the Dusina area, Mid– Bosnian Schist Mountains.– Rudarsko-geološkonaftni zbornik, 8, 51–65.

JURCOVIĆ I., GARAŠIĆ V., HRVATOVIĆ H., 2010: Geochemical characteristic of barite occurences in the Palaeozoic complex of South-eastern Bosnia anf their relationship to the barite deposit of the Mid-Bosnian Schist Mountains. Geologia Croatia. 63/2. Zagreb. 241-258

KERNER D., SCHALL N., SCHMIDT W., SCHMOLL R. 2005: Siliciumverbindungen. In: Dittmeyer R., Keim W., Kreysa G., Oberholz A.(Eds): Winnacker-Küchler: Chemische Technik, Prozesse und Produkte, Band 3, Wiley-VCH Verlag GmbH & Co. KGaA, Weinheim, 811.

KÖSTER H.M. 1993: Beschreibung einzelner Tonminerale. In: K. Jasmund, G. Lagaly (Eds): Tone und Tonminerale: Struktur, Einsatz, Anwendung und Einsatz in Industrie und Umwelt. Steinkopff Verlag, Darmstadt, 46-53.

LAGALY G., KÖSTER H.M. 1993: Tone und Tonminerale. In: K. Jasmund, G. Lagaly (Eds): Tone und Tonminerale: Struktur, Einsatz, Anwendung und Einsatz in Industrie und Umwelt. Steinkopff Verlag, Darmstadt, 1-11.

LORENZ W., GWOSDZ W., 1998A: Bewertungskriterien für Industrieminerale. Steine

und Erden - Teil 2: Karbonat- und Sulfatgesteine. Geol. Jahrb., Reihe H, 4 Hannover. 87.

LORENZ W., GWOSDZ W., 1998B: Bewertungskriterien für Industrieminerale. Steine und Erden - Teil 2: Karbonat- und Sulfatgesteine. Geol. Jahrb., Reihe H, 4 Hannover. Tab. 39.

LORENZ W., GWOSDZ W., 1998C: Bewertungskriterien für Industrieminerale. Steine und Erden - Teil 2: Karbonat- und Sulfatgesteine. Geol. Jahrb., Reihe H, 4 Hannover. 83.

LORENZ W., GWOSDZ W., 2005A: Bewertungskriterien für Industrieminerale. Steine und Erden - Teil 8: Aluminiumoxidreiche Rohstoffe. Geol. Jahrb., Reihe H, 11. Hannover. 78.

LORENZ W., GWOSDZ W., 2005B: Bewertungskriterien für Industrieminerale. Steine und Erden - Teil 8: Aluminiumoxidreiche Rohstoffe. Geol. Jahrb., Reihe H, 11. Hannover. 82.

LORENZ W., GWOSDZ W., 2005C: Bewertungskriterien für Industrieminerale. Steine und Erden - Teil 8: Aluminiumoxidreiche Rohstoffe. Geol. Jahrb., Reihe H, 11. Hannover. 85ff.

MATTAUSCH H. 2013: Ongoing Dissertation on the *Chair of Polymer Processing at Montanuniversität Leoben.* Provided with kind Permission by Hannelore Mattausch.

MATTHES S., 1996: Mineralogie - Eine Einführung in die spezielle Mineralogie, Petrologie und Lagerstättenkunde. Springer-Verlag Berlin Heidelberg New York. 84.

MÜLLER-VONMOOS M., KÖHLER E. E. 1993: Geotechnik und Entsorgung. In: K. Jasmund, G. Lagaly (Eds): Tone und Tonminerale: Struktur, Einsatz, Anwendung und Einsatz in Industrie und Umwelt. Steinkopff Verlag, Darmstadt, 326f.

MURRAY H.H. 1986: Clays. In: Arpe H.J. et al (eds) Ullmanns Encyclopedia of Industrial Chemistry vol A 7. VCH, Weinheim, 109-136.

OHRDORF K. H. 2010A: Zu Fragen der alkalischen Aktivierung von Bentoniten, univ. Diss., Montanuniversität Leoben, 151.

OHRDORF K. H. 2010B: Zu Fragen der alkalischen Aktivierung von Bentoniten, univ. Diss., Montanuniversität Leoben, 165-184.

OHRDORF K. H. 2010C: Zu Fragen der alkalischen Aktivierung von Bentoniten, univ. Diss., Montanuniversität Leoben, 2.

OHRDORF K. H. 2010D: Zu Fragen der alkalischen Aktivierung von Bentoniten, univ. Diss., Montanuniversität Leoben, 8.

OHRDORF K. H. 2010E: Zu Fragen der alkalischen Aktivierung von Bentoniten, univ. Diss., Montanuniversität Leoben, 126f.

OHRDORF K. H. 2010F: Zu Fragen der alkalischen Aktivierung von Bentoniten, univ. Diss., Montanuniversität Leoben, 135ff.

PALINKAŠ L.A., MAJER V., BALOGH K.A.D., BERMANEC V., JURKOVIC I., 1996: Geochronometry and termochronometry of the metamorphism in the Inner Dinarides, MBSM.– Annual Meeting of UNESCO IGCP Project, No 356, Sofi a, 1.

POHL W. L. 2005A**:** Mineralische und Energie-Rohstoffe, Eine Einführung zur Entstehung und nachhaltigen Nutzung von Lagerstätten. E. Schweizerbart'sche Verlagsbuchhandlung (Nägele u. Obermiller) Stuttgart . 241-243.

POHL W. L. 2005B: Mineralische und Energie-Rohstoffe, Eine Einführung zur Entstehung und nachhaltigen Nutzung von Lagerstätten. E. Schweizerbart'sche Verlagsbuchhandlung (Nägele u. Obermiller) Stuttgart. 237-241.

RAMDOHR P., STRUNZ H. 1987: Klockmanns Lehrbuch der Mineralogie. F. Enke Verlag, Stuttgart, 384, 741.

RIEGER K.C., 1997: Pyrophyllite. American Ceramic Society Bulletin 76, Issue 6, 124f.

SCHUBERT H., 1986A: Aufbereitung fester mineralischer Rohstoffe. Band 2. VEB Deutscher Verlag für Grundstoffindustrie, Leipzig. 60.

SCHUBERT H., 1986B: Aufbereitung fester mineralischer Rohstoffe. Band 2. VEB Deutscher Verlag für Grundstoffindustrie, Leipzig. 125.

SCHUBERT H., 1986C: Aufbereitung fester mineralischer Rohstoffe. Band 2. VEB Deutscher Verlag für Grundstoffindustrie, Leipzig. 187f.

SCHUBERT H., 1986D: Aufbereitung fester mineralischer Rohstoffe. Band 2. VEB Deutscher Verlag für Grundstoffindustrie, Leipzig. 16.

SCHUBERT H., 1986E: Aufbereitung fester mineralischer Rohstoffe. Band 2. VEB Deutscher Verlag für Grundstoffindustrie, Leipzig. 25.

SCHUBERT H., 1986F: Aufbereitung fester mineralischer Rohstoffe. Band 2. VEB

Deutscher Verlag für Grundstoffindustrie, Leipzig. 237f.

SCHUBERT H., 1986G: Aufbereitung fester mineralischer Rohstoffe. Band 2. VEB Deutscher Verlag für Grundstoffindustrie, Leipzig. 346.

SCHUBERT H., 1989A: Aufbereitung fester mineralischer Rohstoffe. Band 1. VEB Deutscher Verlag für Grundstoffindustrie, Leipzig. 60ff.

SCHUBERT H., 1989B: Aufbereitung fester mineralischer Rohstoffe. Band 1. VEB Deutscher Verlag für Grundstoffindustrie, Leipzig. 51.

SCHUMANN W. 2007A: Der große BLV Steine- und Mineralienführer. BLV Buchverlag GmbH & Co. KG, München, 60.

SCHUMANN W., 2007B: Der große BLV Steine- und Mineralienführer. BLV Buchverlag GmbH & Co. KG, München, 84.

SOFILJ J., ŽIVANOVIĆ M., PAMIĆ J., 1980: Osnovna geološka karta SFRJ 1:100000, Tumač za list Prozor [Basic Geological Map of SFRY 1:100000, Geology of the Prozor sheet – in Serbian].– Savezni geološki zavod, Beograd, 49 p.

Specification for Drilling Fluid Materials, Spec. 13A, Capt. 11 “OCMA- grade bentonite”, Nov. 2006, American Petroleum Institute.

VDG - Merkblatt P69, Oktober 1999: Prüfung von tongebundenen Formstoffen. Bestimmung des Anteils an bindefähigem Ton.

ŽIVANOVIĆ M., 1972: Geological structure and tectonic framework of the Vranica Mountain in Central Bosnia (in Serbian).– Unpubl. PhD Thesis, University of Beograd.

Appendix

2.4.3 X-Ray Diffractometry of Bentonites

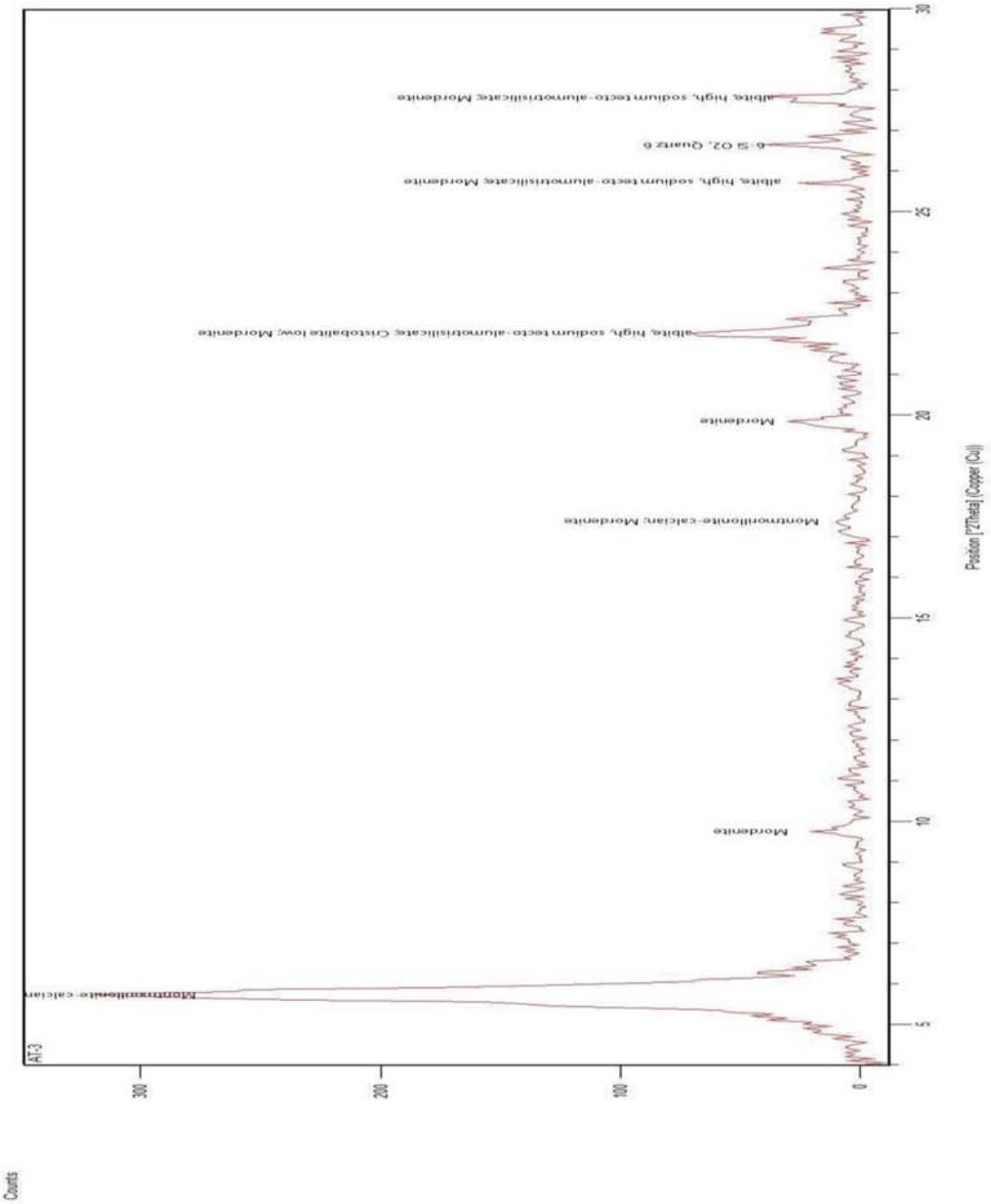

Fig. 66: X-Ray Diffractogram Bentonite, Sample Ralitsa

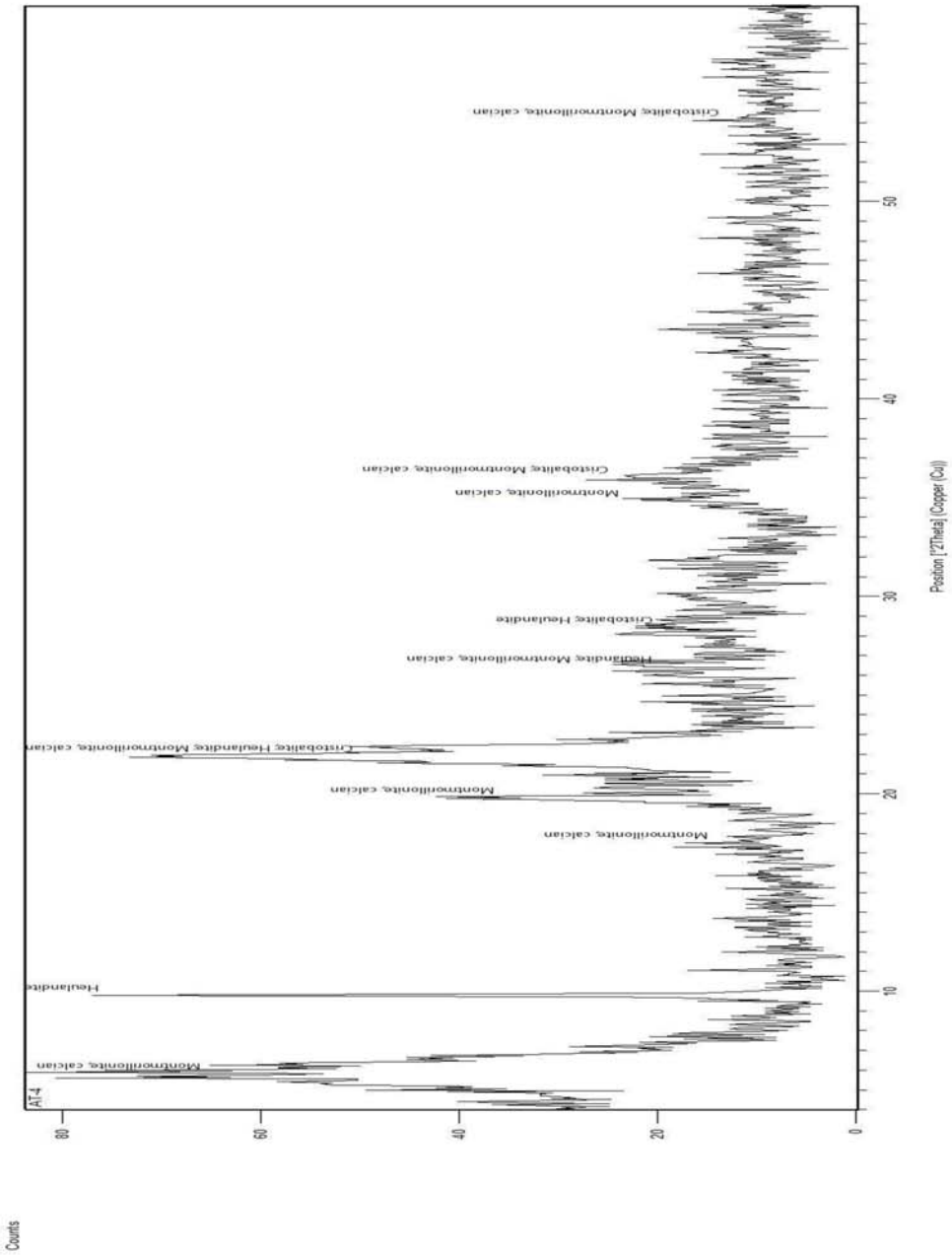

Fig. 67: X-Ray Diffractogram Bentonite, Sample Zelenika

3.1.3.3 Raman Spectroscopy

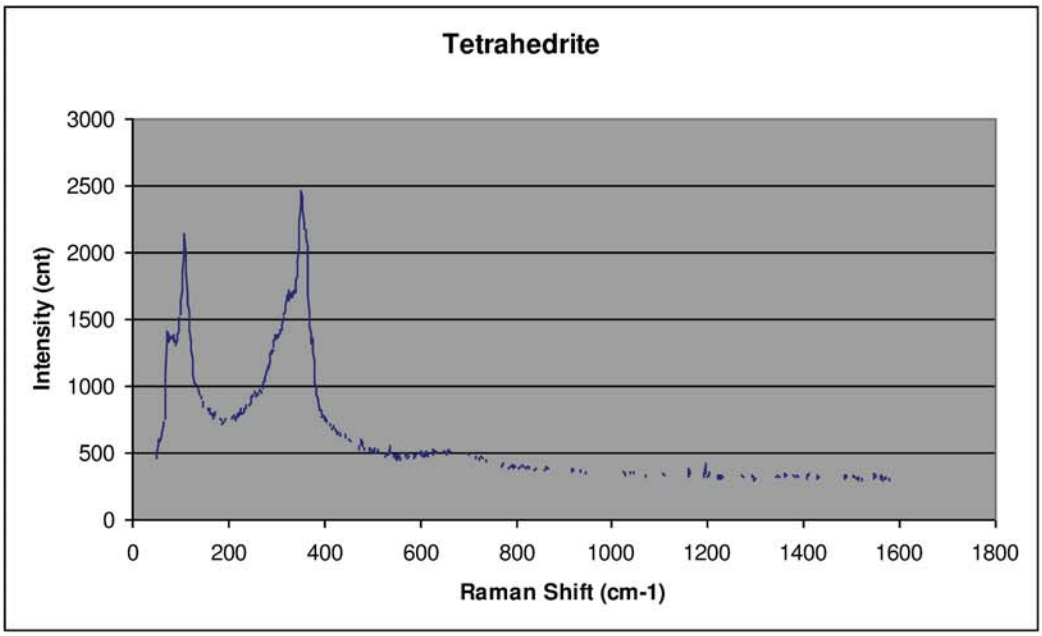

Fig. 68: Raman Spectrum of Tetrahedrite

3.1.3.4 X-Ray Diffractometry of Barite

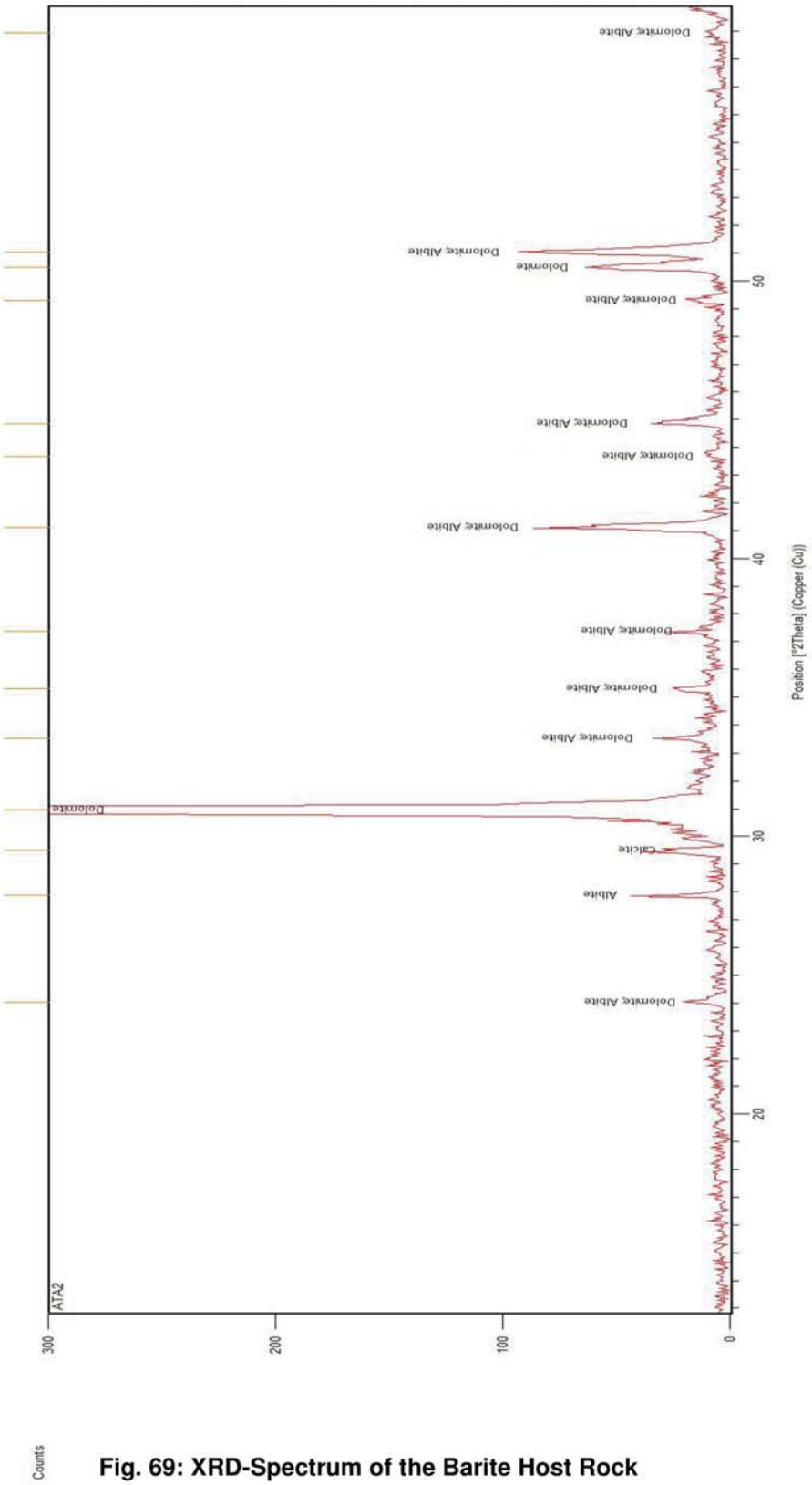

Fig. 69: XRD-Spectrum of the Barite Host Rock

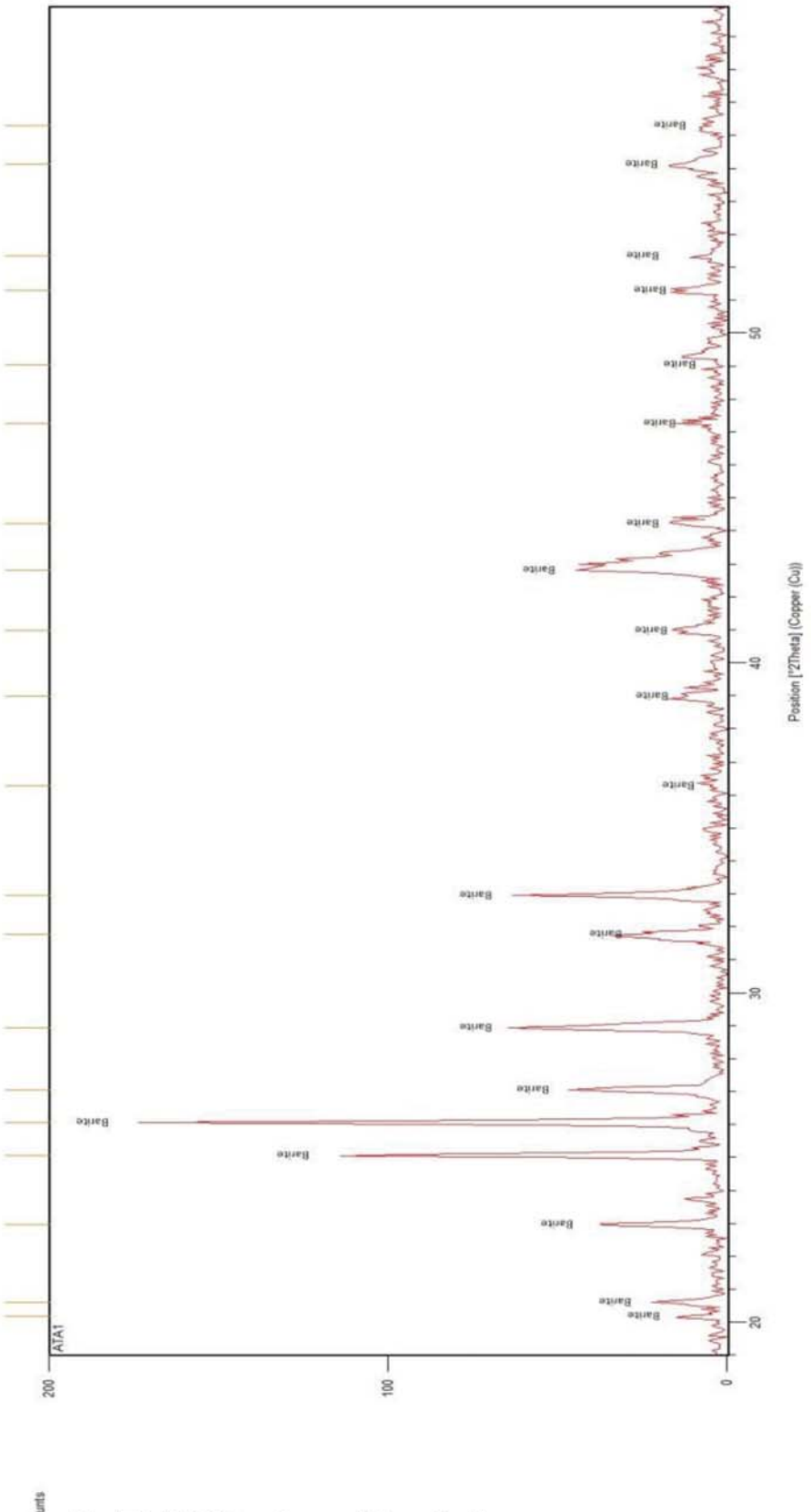

Fig. 70: XRD-Spectrum of Pure Barite

3.1.3.5 Chemical Analysis of Barite

Tab. 39: Chemical Analysis of Barite in g/100g

Element	Samples				
	AT-7A	AT-7B	AT-7C	AT-7D	AT-7E
g / 100 g					
Na2O	<0.01	<0.01	<0.01	<0.01	<0.01
MgO	<0.01	<0.01	<0.01	<0.01	<0.01
Al2O3	0.11	0.37	0.55	0.07	0.07
SiO2	2.14	26.6	4.65	0.0279	<0.01
P2O5	0.014	0.013	0.017	<0.01	<0.01
SO3	27.4	22.1	28.19	29.92	29.55
K2O	<0.01	0.1	0.09	<0.01	<0.01
CaO	<0.01	<0.01	0.05	0.02	0.02
TiO2	<0.01	<0.01	<0.01	<0.01	<0.01
Cr2O3	<0.01	<0.01	<0.01	<0.01	<0.01
MnO	<0.01	<0.01	<0.01	<0.01	<0.01
Fe2O3	<0.01	0.02	<0.01	<0.01	<0.01
BaO	69.27	50.15	56.90	59.47	61.14
SrO	0.96	0.39	8.77	9.61	9.19
LOI	0.23	0.32	0.45	0.36	0.09
TOTAL	100.12	100.06	99.67	99.48	100.06

Tab. 40: Chemical Analysisof Barite in mg / kg

Element	Samples				
	AT-7A	AT-7B	AT-7C	AT-7D	AT-7E
mg / kg					
Sc	0.7	3.1	0.5	0.0	0.1
V	1.4	1.7	3.2	3.2	3.1
Cr	1.0	1.1	1.6	1.9	1.6
Co	<1	<1	<1	<1	<1
Ni	<10	<10	<10	<10	<10
Cu	75.9	10.4	647.1	12865.4	36.3
Zn	13	20	109	498	15
Ga	<10	<10	91	91	97
Rb	0.08	0.57	0.57	0.03	0.06
Sr	8130	3270	74200	81300	77700
Y	0.81	1.26	0.77	0.29	0.80
Zr	<10	<10	<10	<10	<10
Nb	<10	<10	<10	<10	<10
Ba	620400	449200	509600	532600	547600
La	0.42	1.01	1.43	0.13	0.51
Ce	0.16	0.45	1.10	0.07	0.96
Pr	0.52	0.00	2.25	1.38	2.59
Nd	<0.05	0.07	0.25	<0.05	0.17
Sm	0.00	0.00	0.00	0.00	0.00
Eu	0.04	0.19	0.32	0.01	0.03
Tb	0.24	0.80	1.27	0.07	0.18
Gd	0.32	0.31	0.32	0.08	0.31
Dy	5.56	2.42	1.73	0.86	6.44
Ho	0.01	0.05	0.03	0.00	0.01
Er	0.25	0.34	0.23	0.05	0.32
Tm	0.05	0.22	0.10	0.01	0.02
Yb	0.01	0.04	0.02	0.00	0.00
Lu	0.03	0.09	0.05	0.01	0.02
Pb	0.01	0.01	0.01	0.00	0.01
Th	0.54	0.29	0.23	0.10	0.85

3.3.4.1 Sieving

Tab. 41: Data of Grain Size Distribution of Barite

Sample Mass = 12790.42 g				
Mesh Size	**Mass**		**Residue**	**Undersize**
[mm]	[g]	[m%]	[m%]	[m%]
10.00	11087.00	86.68	86.68	13.32
5.00	702.00	5.49	92.17	7.83
1.00	600.00	4.69	96.86	3.14
0.71	71.96	0.56	97.42	2.58
0.50	54.94	0.43	97.85	2.15
0.315	64.72	0.51	98.36	1.64
0.125	96.98	0.76	99.12	0.88
0.04	75.45	0.59	99.71	0.29
0.00	37.37	0.29	100.00	0.00
Sum	12790.42	100.00		

3.3.4.4 Magnetic Separation by “Frantz”-Separator

Tab. 42: Data for susceptibility classes of Barite, k = 0.315 – 0.5 mm, Fig. 44

	Mass [g]	**Mass [%]**
Feeding	13.5731	100.00
ferromagn	0.0068	0.05
0.20	0.0025	0.02
0.60	0.3149	2.32
1.00	0.4933	3.63
1.40	0.3457	2.55
Waste	12.4099	91.43

Tab. 43: Data for susceptibility classes of Barite, k = 0.125 - 0.315 mm, Fig. 45

	Mass [g]	Mass [%]
Feeding	20.2132	100.00
ferromagn	0.0043	0.02
0.20	0.0030	0.01
0.60	0.4654	2.30
1.00	0.6015	2.98
1.40	0.5480	2.71
Waste	18.5910	91.97

3.3.4.5 Heavy Media Separation – Sink-Float Analysis

Tab. 44: Data for Grain Size Distribution of Sink-Float Analysis, Barite, Fig. 46

Sample Mass = 12790.42 g				
Mesh Size	**Mass**		**Residue**	**Passage**
[mm]	[g]	[m%]	[m%]	[m%]
100	0	0	0	100
10.00	11087.00	86.68	86.68	13.32
5.00	702.00	5.49	92.17	7.83
1.00	600.00	4.69	96.86	3.14
0.71	71.96	0.56	97.42	2.58
0.50	54.94	0.43	97.85	2.15
0.315	64.72	0.51	98.36	1.64
0.125	96.98	0.76	99.12	0.88
0.04	75.45	0.59	99.71	0.29
0.00	37.37	0.29	100.00	0.00
Sum	12790.42	100.00		

Tab. 45: Data for Masses of the Density Classes of Barite

Mass of Density Classes					
ρ<0.65	2.65<ρ<2.75	2.75<ρ<2.9	2.9<ρ<3.1	ρ>3.1	Sum
[g]	[g]	[g]	[g]	[g]	[g]
0.15	3.02	6.71	1.16	47.1	58.14
0.15	2.75	5.4	0.8	36.29	45.39
0.14	2.87	4.84	0.71	44.63	53.19

Tab. 46: Data for Mass Recovery and Grade of Barite

Mass Recovery from Density Classes										
$r_{m<2,65}$	g $Ba_{<2,65}$	$r_{m2.65-2.75}$	g $Ba_{2.65-2.75}$	$r_{m2.75-2.9}$	g $Ba_{2.75-2.9}$	$r_{m2.9-3.1}$	g $Ba_{2.9-3.1}$	$r_{m>3.1}$	g $Ba_{>3.1}$	Sum r_m
%	%	%	%	%	%	%	%	%	%	%
0.26	0.00	5.19	0.00	11.54	0.00	2.00	14.32	81.01	96.73	100.00
0.33	0.00	6.06	0.00	11.90	0.00	1.76	24.61	79.95	97.74	100.00
0.26	0.00	5.40	0.00	9.10	0.37	1.33	24.14	83.91	98.31	100.00

Tab. 47: Data for Mass Recovery/Grain Size Diagram, Barite, Fig 47

Mass Recovery of Swim Sink Analysis					
Grain Size	$r_{m<2,65}$	$r_{m2.65-2.75}$	$r_{m2.75-2.9}$	$r_{m2.9-3.1}$	$r_{m>3.1}$
[mm]	[%]	[%]	[%]	[%]	[%]
1	0.26	5.19	11.54	2	81.01
0.71	0.26	5.19	11.54	2	81.01
0.71	0.33	6.06	11.9	1.76	79.95
0.5	0.33	6.06	11.9	1.76	79.95
0.5	0.26	5.4	9.1	1.33	83.91
0.315	0.26	5.4	9.1	1.33	83.91

Tab. 48: Data for Henry-Reinhardt Diagram, Barite, Fig. 48

Henry-Reinhard Diagram			*Cum = Cumulative, Ba = Barite		
$r_{m0.71\text{-}1mm\ Cum}$	$g\ Ba_{0.71\text{-}1mm}$	$r_{m0.5\text{-}0.71mm\ Cum}$	$g\ Ba_{0.5\text{-}0.71mm}$	$r_{m0.315\text{-}0.5mm\ Cum}$	$g\ Ba_{0.315\text{-}0.5mm}$
[%]	[%]	[%]	[%]	[%]	[%]
100.00	96.73	100.00	97.74	100.00	98.31
18.99	96.73	20.05	97.74	16.09	98.31
18.99	14.32	20.05	24.61	16.09	24.14
16.99	14.32	18.29	24.61	14.76	24.14
16.99	0.00	18.29	0.00	14.76	0.37
5.45	0.00	6.39	0.00	5.66	0.37
5.45	0.00	6.39	0.00	5.66	0.00
0.26	0.00	0.33	0.00	0.26	0.00
0.26	0.00	0.33	0.00	0.26	0.00

Tab. 49: Balance and Grade Calculation, Sink-Float Analysis, Barite, k = 0.71 – 1 mm

k = 0.71 - 1 mm: Balance Study							
Product	ρL	Mass	Yield	Grade	Content	Units	Recovery
	[g/cm3]	[g]	[%]	[%]	g	%%	%
HC1	3.1	47.10	85.42	96.73	45.56	8262.93	99.64
HC2	2.9	1.16	2.10	14.32	0.17	30.12	0.36
HC3	2.75	6.71	12.17	0.00	0.00	0.00	0.00
HC4	2.65	0.02	0.04	0.00	0.00	0.00	0.00
LC	2.65	0.15	0.27	0	0.00	0.00	0.00
Feeding		55.14	100.00	45.73	45.73		100.00
Grade Calculation							
Product	ρL	Mass	Density	V	V Barite	Mass Barite	Grade
	[g/cm3]	[g]	g/cm3	cm3	cm3	g	%
HC1	3.1	13.53	4.35	3.11	2.96	13.09	96.73
HC2	2.9	1.16	3.03	0.38	0.04	0.17	14.32
HC3	2.75	6.70	2.87	2.34	0.00	0.00	0.00
HC4	2.65	3.02	2.77	1.09	0.00	0.00	0.00
LC	2.65	too little			0.00	0.00	0.00
Feeding		24.41	3.53	6.92	2.99	13.25	54.30

Tab. 50: Balance and Grade Calculation, Sink-Float Analysis, Barite, k = 0.5 – 0.71 mm

k = 0.5 - 0.71 mm: Balance Study							
Product	ρL	Mass	Yield	Grade	Content	Units	Recovery
	[g/cm3]	[g]	[%]	[%]	[g]	[%%]	[%]
HC1	3.1	36.29	81.24	97.74	35.47	7940.36	99.94
HC2	2.9	0.08	0.18	24.61	0.02	4.41	0.06
HC3	2.75	5.40	12.09	0.00	0.00	0.00	0.00
HC4	2.65	2.75	6.16	0.00	0.00	0.00	0.00
LC	2.65	0.15	0.34	0	0.00	0.00	0.00
Feeding		44.67	100.00	35.49	35.49		100.00
Grade Calculation							
Product	ρL	Mass	Density	V	V Barite	Mass Barite	Grade
	[g/cm3]	[g]	[g/cm3]	[cm3]	[cm3]	[g]	[%]
HC1	3.1	14.78	4.37	3.38	3.26	14.45	97.74
HC2	2.9	0.80	3.15	0.25	0.04	0.20	24.61
HC3	2.75	5.40	2.87	1.88	0.00	0.00	0.00
HC4	2.65	2.75	2.74	1.00	0.00	0.00	0.00
LC	2.65	too little			0.00	0.00	0.00
Feeding		23.73	3.64	6.52	3.31	14.64	61.71

Tab. 51: Balance and Grade Calculation, Sink-Float Analysis, Barite, k = 0.315 – 0.5 mm

k = 0.315 - 0.5 mm: Balance Study							
Product	ρL	Mass	Yield	Grade	Content	Units	Recovery
	[g/cm3]	[g]	[%]	[%]	[g]	[%%]	[%]
HC1	3.1	44.63	83.91	98.31	43.88	8248.93	99.57
HC2	2.9	0.71	1.33	24.41	0.17	32.59	0.39
HC3	2.75	4.84	9.10	0.37	0.02	3.34	0.04
HC4	2.65	2.87	5.40	0.00	0.00	0.00	0.00
LC	2.65	0.14	0.26	0	0.00	0.00	0.00
Feeding		53.19	100.00	44.07	44.07		100.00
Grade Calculation							
Product	ρL	Mass	Density	V	V Barite	Mass Barite	Grade
	[g/cm3]	[g]	[g/cm3]	[cm3]	[cm3]	[g]	[%]
HC1	3.1	14.77	4.39	3.37	3.28	14.52	98.31
HC2	2.9	0.72	3.15	0.23	0.04	0.18	24.41
HC3	2.75	4.84	2.88	1.68	0.00	0.02	0.37
HC4	2.65	2.86	2.76	1.04	0.00	0.00	0.00
LC	2.65	too little			0.00	0.00	0.00
Feeding		23.19	3.68	6.31	3.32	14.71	63.45

Legend: HC Heavy Components, LC Light Components, ρ_L Density of Heavy Media

3.3.4.6 Magnetic Separation with an IFE Permanent Magnetic, Strong Field Drum Separator:

Tab. 52: Data for Mass Percentage, IFE Separator, Barite, MP/NMP, Fig. 49

k = 0.7-1 mm			k = 0.5-0.7 mm		
Product	Mass [g]	Yield [%]	Product	Mass [g]	Yield [%]
Feeding	110.31	100.00	Feeding	104.26	100.00
MP	14.87	13.48	MP	15.76	15.12
NMP	95.44	86.52	NMP	88.50	84.88

k = 0.315-0.5 mm		
Product	Mass [g]	Yield [%]
Feeding	105.39	100.00
MP	16.38	15.54
NMP	89.01	84.46

Legend:

MP = Magnetic Product

NMP = Non Magnetic Product

4.1.3.4 X-Ray Diffractometry

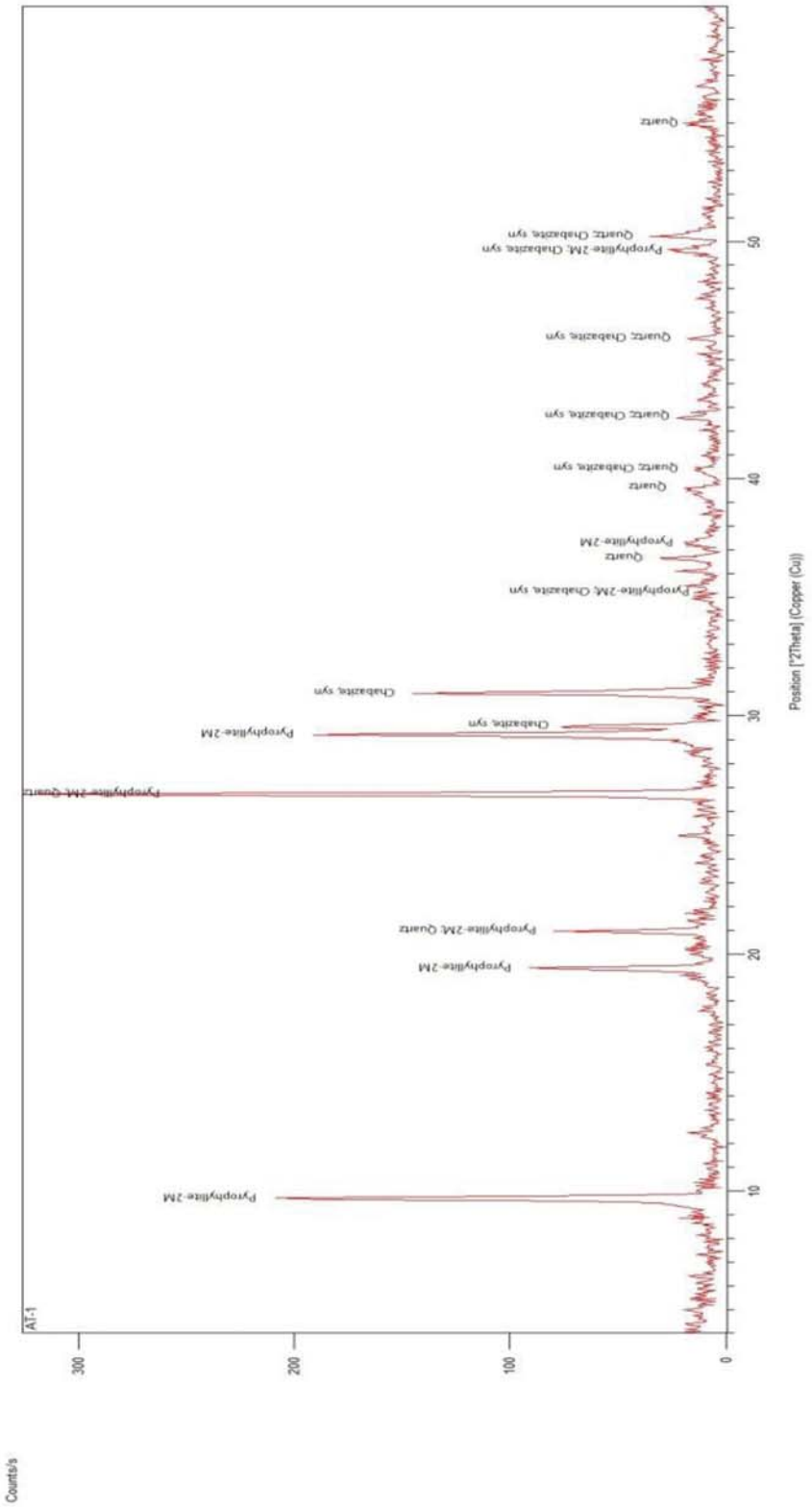

Fig. 71: X-Ray Spectrum AT-1

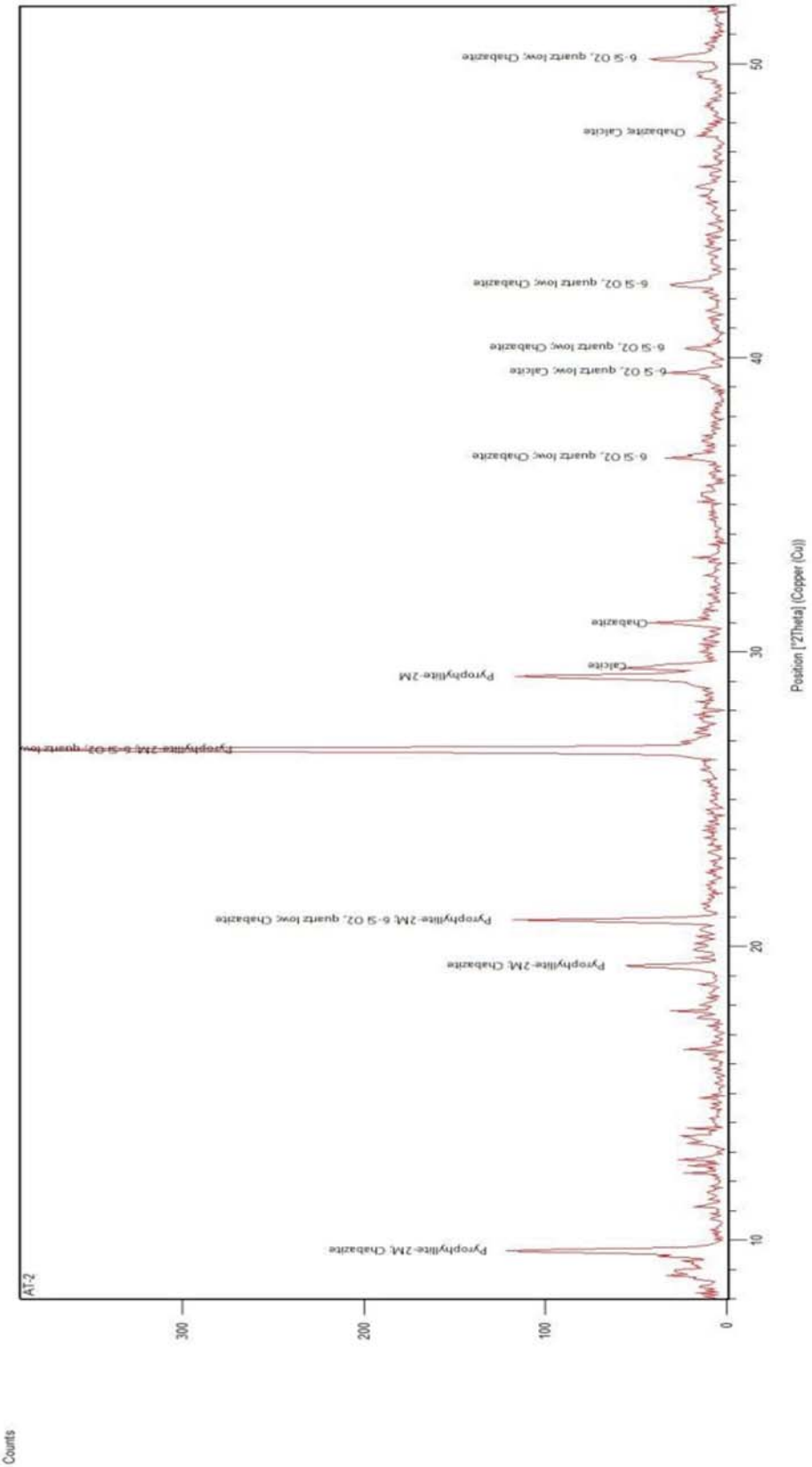

Fig. 72: X-Ray Spectrum AT-2

4.2.4 Results of Mineral Processing

Acid Solubility

Tab. 53: Calculation Table Acid Solubility, Pyrophyllite

Sample	Weight In Sample	Weight Out Sample + Filter	Mass Filter	Weight Out Sample	corr. Value	Soluble Content
	[g]	[g]	[g]	[g]	[g]	m%
AT1 <0.1	1.0203	2.8517	1.9305	0.9212	0.9414	7.73
AT2<0.1	0.9866	2.9575	2.0642	0.8933	0.9135	7.41
FP1-AT1	1.0080	2.9201	2.0090	0.9111	0.9313	7.61
FP1-AT2	0.9925	2.9411	2.0222	0.9189	0.9391	5.38
FP2-AT1	1.0130	2.9068	1.9676	0.9392	0.9594	5.29
FP2-AT2	1.0030	2.8966	1.9534	0.9432	0.9634	3.95
AT1<6	1.0234	2.8730	1.9955	0.8775	0.8977	12.28
AT2<6	1.0093	2.8709	1.9944	0.8765	0.8967	11.15
R-AT1	0.9994	2.8541	2.0600	0.7941	0.8143	18.52
R-AT2	0.9828	2.8696	1.9892	0.8804	0.9006	8.37
AT1>0.1	1.0219	2.8559	2.0379	0.8180	0.8382	17.98
AT2>0.1	0.9991	2.8848	2.0352	0.8496	0.8698	12.94
Blind 1		1.9267	1.9481	-0.0214		
Blind 2		1.9898	2.0049	-0.0151		
Blind 3		2.0242	2.0483	-0.0241		
			Average Loss	**0.2710**		

Loss of Ignition

Tab. 54: Calculation Table Loss of Ignition, Pyrophyllite

Sample	Mass Crucible	Weight In Crucible + Sample	Weight Out Crucible + Sample	LOI
	[g]	[g]	[g]	[m%]
AT1 <0.1	14.0629	18.3040	18.0140	1.58
AT2<0.1	9.4889	13.6623	13.4073	1.87
FP1-AT1	6.5643	11.7510	11.4076	2.92
FP1-AT2	17.3818	22.3136	22.0250	1.29
FP2-AT1	11.1105	14.7058	14.4827	1.52
FP2-AT2	9.2927	14.4887	14.1744	2.17
AT1<6	17.3835	22.4850	22.0591	1.89
AT2<6	9.2946	15.2193	14.7668	2.97
R-AT1	14.0770	18.6219	18.3127	1.66
R-AT2	9.4893	14.7706	14.4347	2.27
AT1>0.1	11.1134	21.7613	20.6041	5.32
AT2>0.1	6.5765	13.1786	12.5720	4.60

4.2.4.1 Crushing

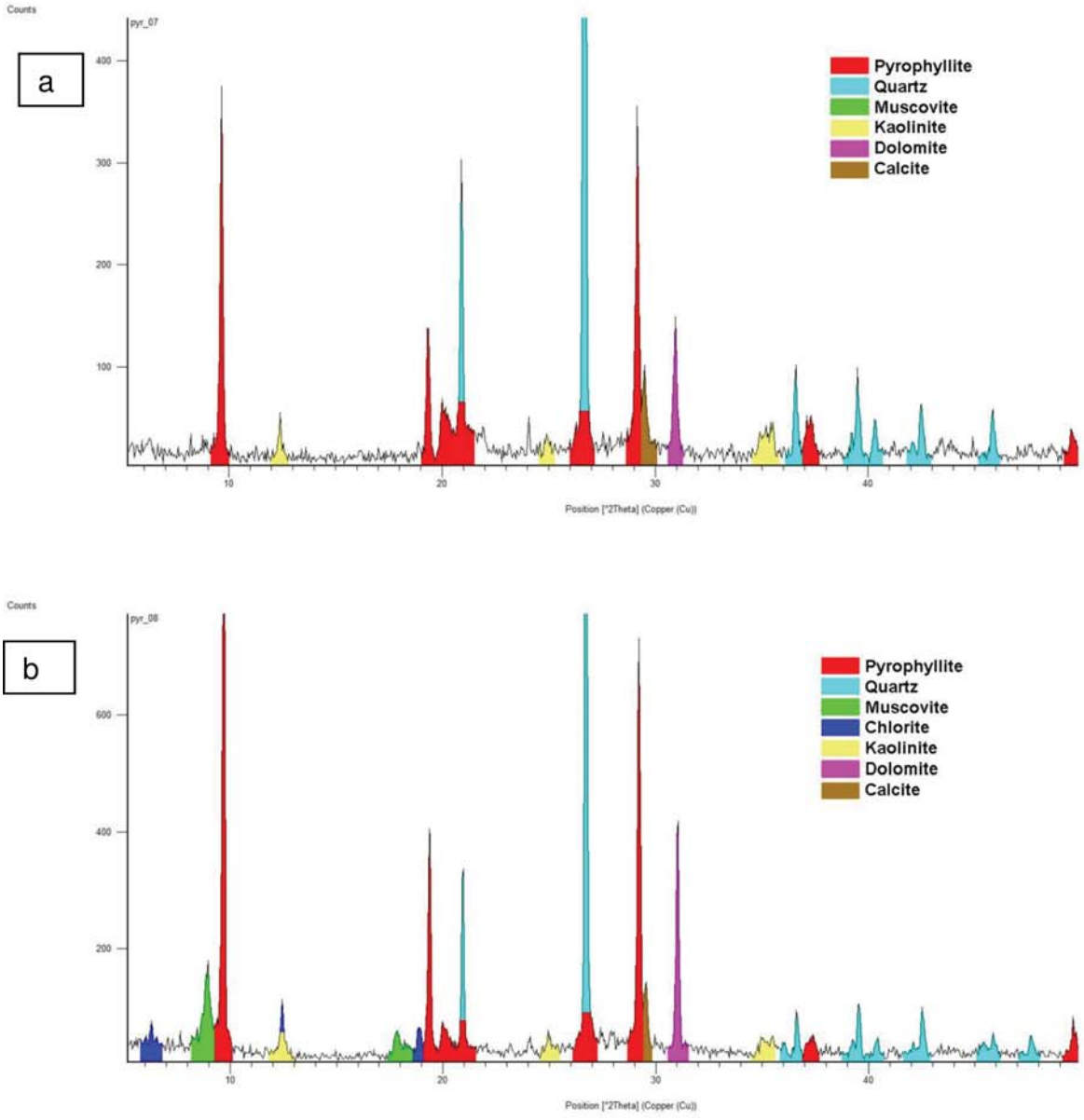

Fig. 73: Crushing Products k < 6 mm: AT-1 (a), AT-2 (b)

4.2.4.2 Attrition

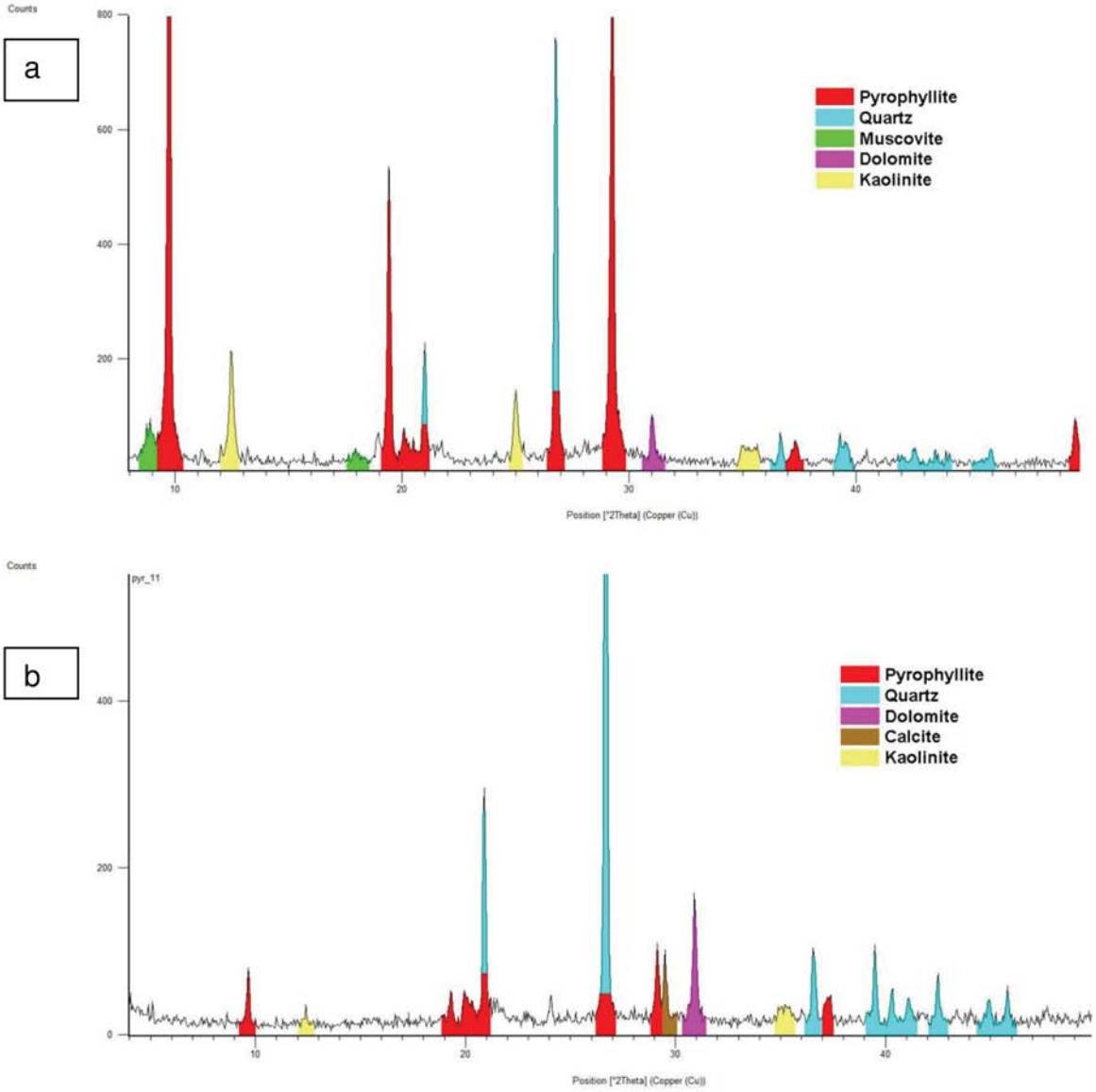

Fig. 74: Attrition Products: AT-1 < 100 µm (a), AT-1 > 100 µm (b)

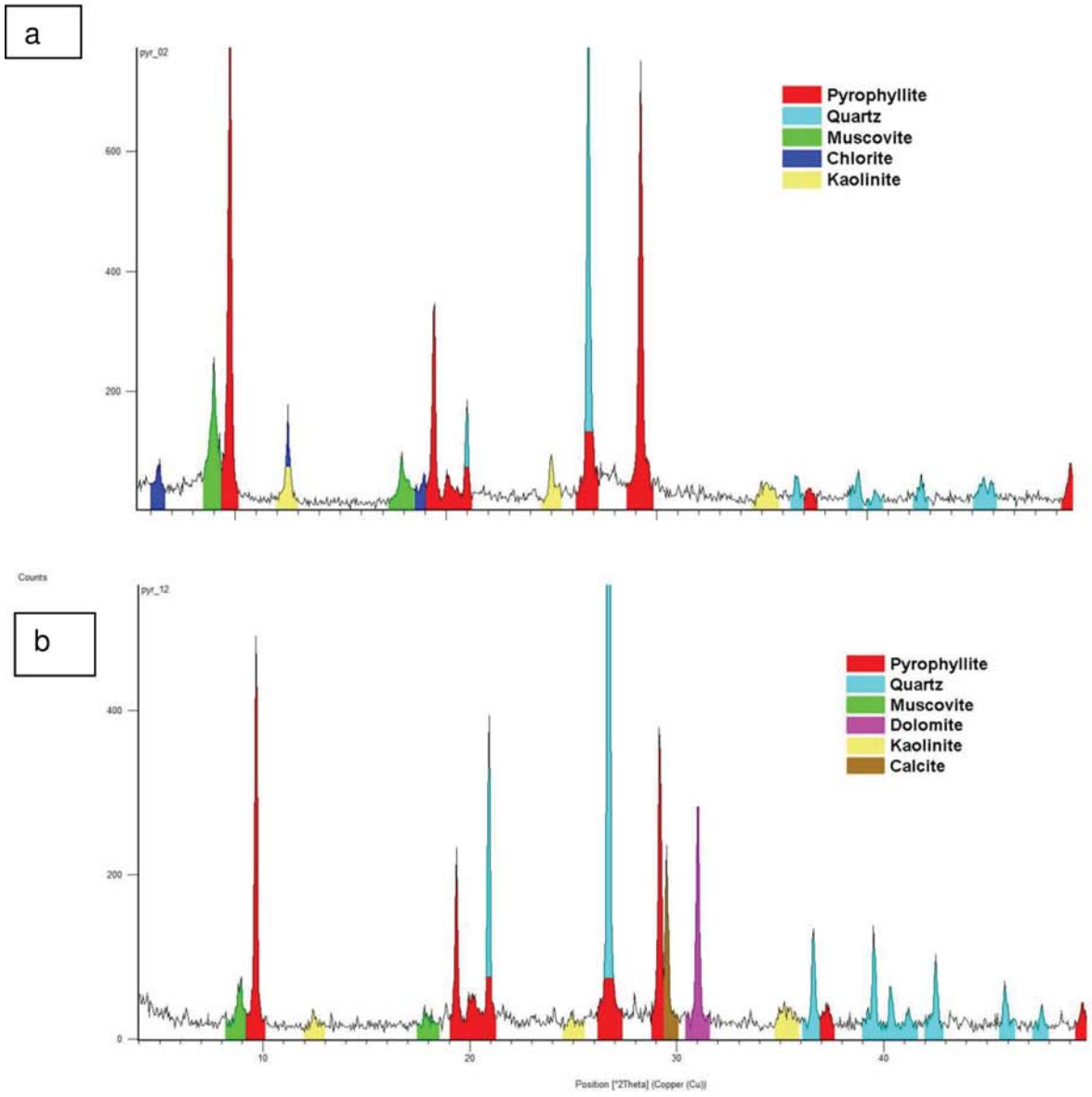

Fig. 75: Attrition Products: AT-2 < 100 µm (a), AT-2 > 100 µm (b)

4.2.4.3 Flotation

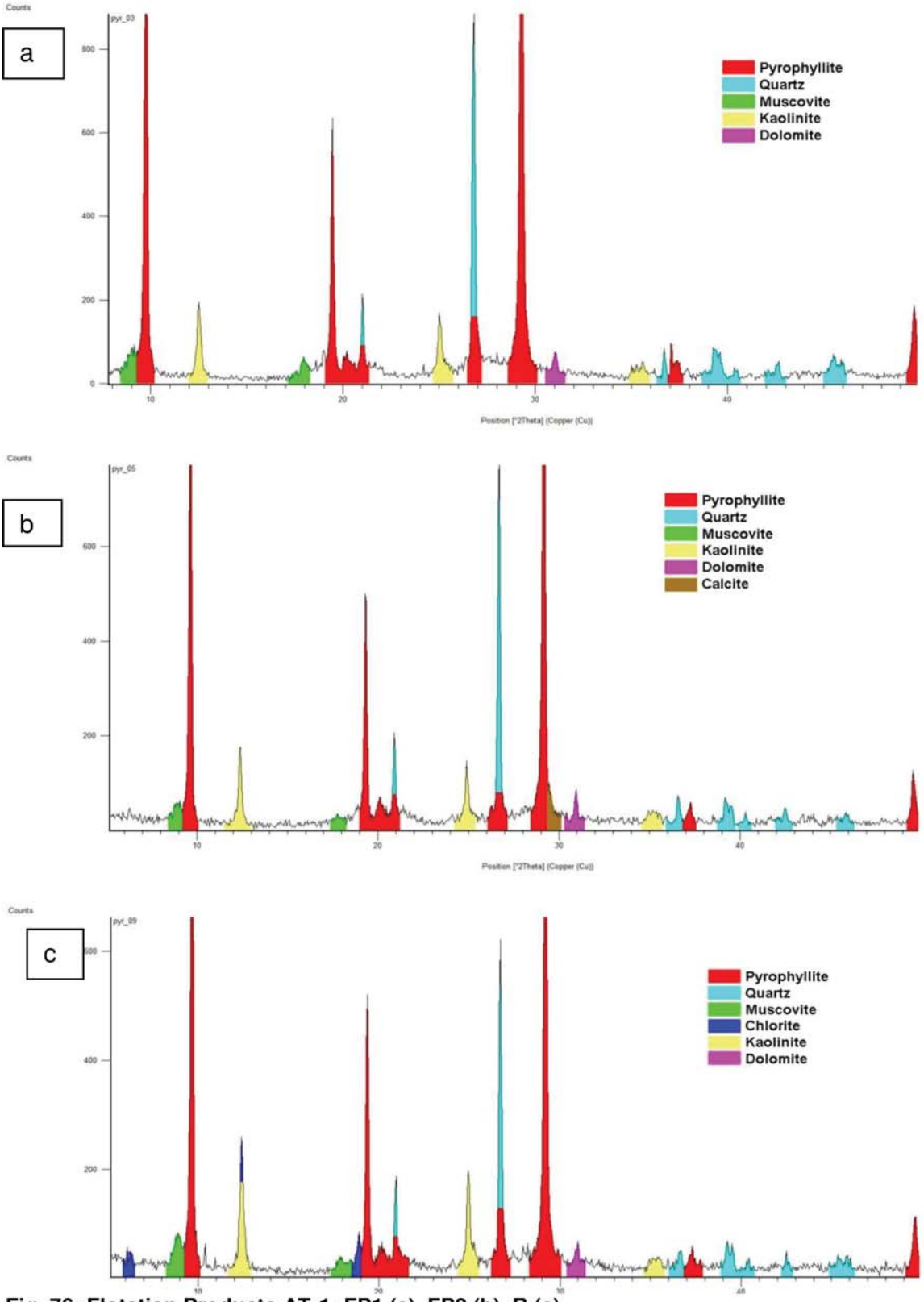

Fig. 76: Flotation Products AT-1: FP1 (a), FP2 (b), R (c)

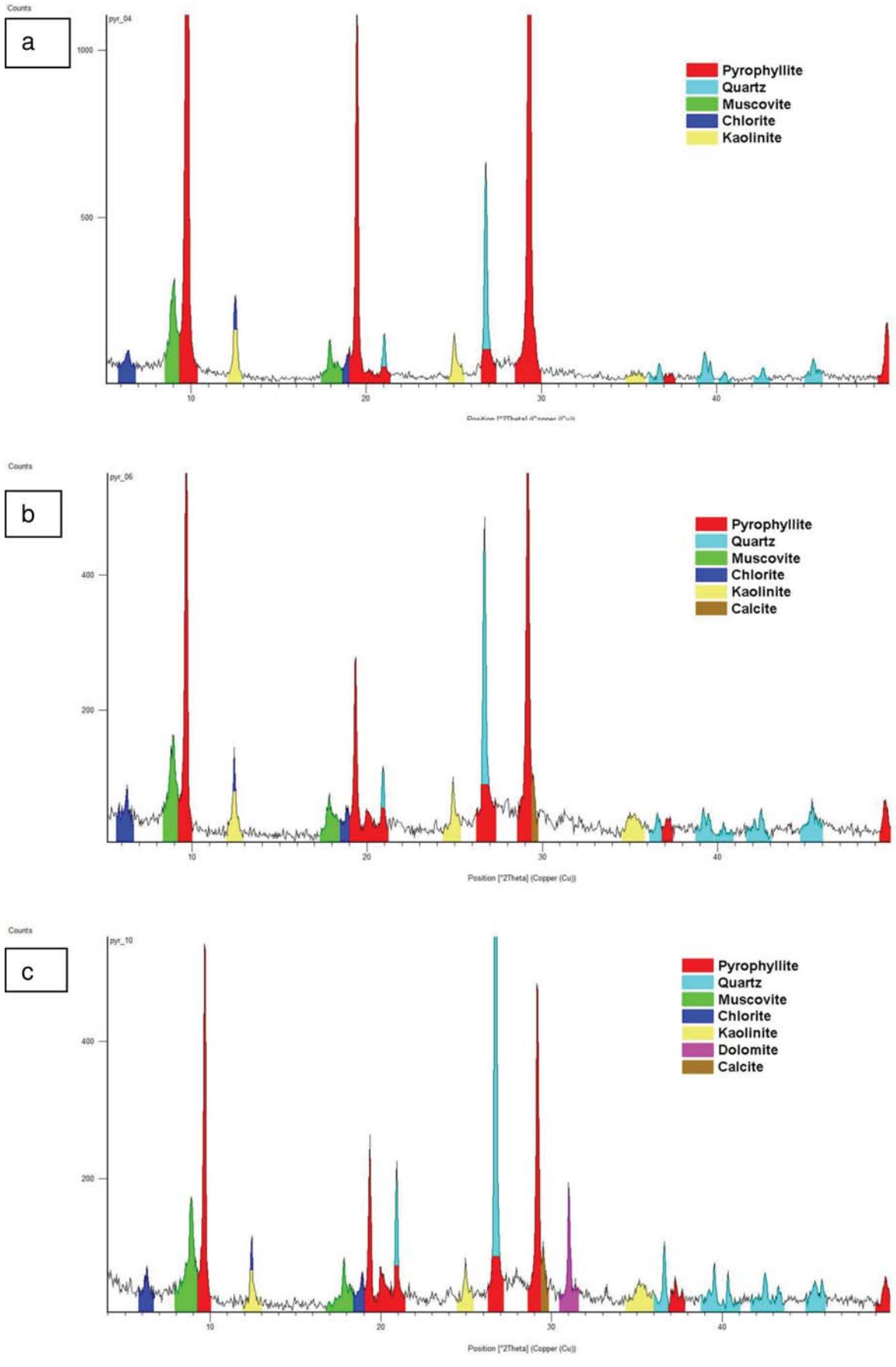

Fig. 77: Flotation Products AT-2: FP1 (a), FP2 (b), R (c)